

# **The Effect of Polymer Modification on Gas Transport Properties and The Synthesis of Poly(ethylene glycol) (PEG) Containing Polymers via Step-Growth Click Coupling Reaction for CO<sub>2</sub> Separation**

**Dissertation with the aim of achieving a doctoral degree  
at the Faculty of Mathematics, Informatics and Natural Sciences  
Department of Chemistry  
of Universität Hamburg**

**submitted by Bahadır Gacal**

2014 in Hamburg

Date of oral defense:

The following evaluators recommend the admission of the dissertation:

1. Gutachter Prof. Dr. Volker Abetz
2. Gutachter Prof. Dr. Patrick Theato

## Declaration

I declare that the submitted thesis has been prepared by me and I have not used any helping material other than cited. This thesis has never been submitted to any University or examining body for evaluation. Some part of dissertation has been published or submitted as mentioned below:

- Gacal, B. N., Filiz, V., Shishatskiy, S., Neumann S., Wind, J., Abetz V., “Effect of Azidation and UV Cross-linking of Poly(epichlorohydrin) and Poly[(ethylene oxide)-*ran*-(epichlorohydrin)] on Gas Transport Properties”, Journal of Membrane Science, 2014, 467, 126-135.
- Gacal, B. N., Shishatskiy, S., Rangou, S., Neumann S., Filiz, V., Abetz V., “Modification of Polyisoprene-block-Poly(vinyl trimethylsilane) Block Copolymers via Hydrosilylation and Hydrogenation, and their Gas Transport Properties”, Journal of Polymer Science Part B: Polymer Physics, 2013, 51, 1252-1261.

The thesis has been prepared maintaining the Rules of Good Scientific Practice of the German Research Foundation.

Geesthacht, 02.12.2013

Bahadir N. Gacal

# Table of Contents

<b>Chapter 1.....</b>	<b>1</b>
1.1. Introduction.....	1
1.2. The Aim of the Thesis.....	3
1.3. References.....	10
<b>Chapter 2. Theoretical Background and State of the Art.....</b>	<b>16</b>
2.1. Membranes.....	16
2.1.1. The Classification of Membranes .....	17
2.1.1.1. <i>Microporous Membranes</i> .....	18
2.1.1.2. <i>Non-Porous (Dense) Membranes</i> .....	19
2.1.2. Membranes for Gas Separation.....	19
2.1.3. Gas Transport through the Membranes.....	21
2.1.3.1. <i>Pore Flow Model</i> .....	21
2.1.3.2. <i>Solution-Diffusion Model</i> .....	22
2.1.4. Common Definitions Describing Membrane Performance.....	23
2.1.5. The Relation between Structure and Gas Transport Properties .....	24
2.1.5.1. <i>Glassy Polymers</i> .....	24
2.1.5.2. <i>Rubbery Polymers</i> .....	26
2.2. Copolymers .....	26
2.3. Hydrosilylation Chemistry.....	30
2.4. Hydrogenation Chemistry .....	31
2.5. Azide Chemistry .....	33
2.6. Click Chemistry .....	34
2.6.1. Copper(I)-Catalyzed Azide-Alkyne Cycloaddition (CuAAC).....	35
2.6.2. Mechanistic Aspect of the Cu(I) Catalysis.....	37
2.7. Benzoxazine Chemistry .....	39
2.7.1. Ring Opening Polymerization of Benzoxazine .....	39
2.8. References.....	42
<b>Chapter 3. Experimental Part.....</b>	<b>55</b>
3.1. Materials .....	55
3.2. Synthesis and Modification.....	56

3.2.1. Synthesis of Polyisoprene- <i>block</i> -Poly(vinyl trimethylsilane) (PI- <i>b</i> -PVTMS).....	56
3.2.2. Modification of PI- <i>b</i> -PVTMS via Hydrosilylation (Hs-PI- <i>b</i> -PVTMS) .....	56
3.2.4. Synthesis of Azidated Poly(epichlorohydrin) Homopolymer (A-H-Hydrin) and Azidated Poly[(ethylene oxide)- <i>ran</i> -(epichlorohydrin)] Copolymer (A-C-Hydrin) .....	58
3.2.5. Synthesis of Bifunctional Poly(ethylene glycol)-Diazide (N <sub>3</sub> -PEG-N <sub>3</sub> ).....	61
3.2.7. General Procedure for CuAAC Step Growth Polymerization .....	64
3.2.8. General Procedure for Catalyst-Free Step Growth Polymerization .....	66
3.3. Characterization .....	66
3.3.1. <sup>1</sup> H, <sup>13</sup> C-NMR & FTIR .....	66
3.3.2. Gel Permeation Chromatography (GPC) .....	66
3.3.3. Thermogravimetric Analysis (TGA).....	67
3.3.4. Transmission Electron Micrographs (TEM) .....	67
3.3.5. Differential Scanning Chromatography (DSC).....	67
3.4. Membrane Formation.....	67
3.5. Gas Transport Properties.....	68
3.6. Density and Fractional Free Volume (FFV) .....	70
3.7. Swelling Experiment.....	70
3.8. References .....	71
<b>Chapter 4. Results and Discussions .....</b>	<b>72</b>
<b>4.1. Modification of Polyisoprene-<i>block</i>-Poly(vinyl trimethylsilane) Block Copolymers via Hydrosilylation and Hydrogenation, and Their Gas Transport Properties.....</b>	<b>72</b>
4.1.1. Brief Introduction.....	72
4.1.2. Synthesis and Characterization of Hydrosilylated Polyisoprene- <i>block</i> -Poly(vinyl trimethylsilane) (Hs-PI- <i>b</i> -PVTMS) .....	72
4.1.4. Gel Permeation Chromatography (GPC) Analysis .....	78
4.1.5. Thermal Characterization.....	80
4.1.6. Morphology.....	81
4.1.7. Gas Transport Properties.....	82
4.1.8. Density and Fractional Free Volume (FFV) .....	87
4.1.9. Conclusions .....	88
4.1.10. References .....	89
<b>4.2. Effect of Azidation and UV Cross-linking of Poly(epichlorohydrin) and Poly[(ethylene oxide)-<i>ran</i>-(epichlorohydrin)] on Gas Transport Properties .....</b>	<b>91</b>
4.2.1. Brief Introduction.....	91

4.2.2. Synthesis and Characterization of Azidated Poly(epichlorohydrin) (A-H-Hydrin) and Poly[(ethylene oxide)- <i>ran</i> -(epichlorohydrin)] (A-C-Hydrin), and their UV Cross-linked (UV-A-H-Hydrin and UV-A-C-Hydrin) Counterparts .....	91
4.2.3. Thermal Characterization.....	99
4.2.4. Gas Transport Properties.....	104
4.2.5. Conclusions.....	109
4.2.6. References.....	110
<b>4.3. The Synthesis of Poly(ethylene glycol) (PEG) Containing Polymers via Step-Growth Click Coupling Reaction for CO<sub>2</sub> Separation .....</b>	<b>112</b>
4.3.1. Brief Introduction.....	112
4.3.2. Synthesis and Characterization of Bifunctional PEG-Diazide (N <sub>3</sub> -PEG-N <sub>3</sub> ).....	113
4.3.3. Synthesis and Characterization of Bifunctional Benzoxazine-Diacetylene Click Monomer..	115
4.3.4. Synthesis and Characterization of Step-Growth Polymers .....	117
4.3.5. Gel Permeation Chromatography (GPC) Analysis .....	121
4.3.6. Thermal Characterization.....	123
4.3.7. Gas Transport Properties.....	126
4.3.8. Conclusions.....	130
4.3.9. References.....	130
<b>Chapter 5. Summary and Outlook .....</b>	<b>133</b>
5.1. Summary and Outlook .....	133
5.2 Zusammenfassung und Ausblick .....	136
<b>Acknowledgement .....</b>	<b>141</b>
<b>Appendix .....</b>	<b>142</b>
<b>List of Publications.....</b>	<b>144</b>
<b>Curriculum Vitae .....</b>	<b>145</b>
<b>Meetings Attended .....</b>	<b>146</b>

# List of Figures

<b>Chapter 1.....</b>	<b>1</b>
FIGURE 1.1. Upper bound correlation between O <sub>2</sub> permeability coefficient and O <sub>2</sub> /N <sub>2</sub> selectivity.. .....	2
FIGURE 1.2. O <sub>2</sub> /N <sub>2</sub> selectivity and O <sub>2</sub> permeability coefficient of PVTMS (▲) compared to other polymers of commercial gas separation membranes (◆) and to the Robeson's present (2008) upper bound.....	4
<b>Chapter 2.....</b>	<b>15</b>
FIGURE 2.1. Schematic draw representing the separation of two phases by membrane.....	17
FIGURE 2.2. Schematic diagram of main types of the membranes. ....	18
FIGURE 2.3. Schematic representation of pore flow model. ....	22
FIGURE 2.4. Schematic representation of solution-diffusion model. ....	23
FIGURE 2.5. Schematic representation of various types of copolymers.....	27
FIGURE 2.6. Morphologies of a diblock copolymer (AB) as function of the volume fraction of the A block. ....	29
FIGURE 2.7. Possible mechanism of hydrosilylation. ....	31
FIGURE 2.8. Thermally activated mechanism of hydrogenation.....	32
FIGURE 2.9. Resonance structures of azide.....	34
FIGURE 2.10. General representation of copper and thermal catalyzed cycloaddition. ....	36
FIGURE 2.11. Proposed mechanism of CuAAC.....	38
FIGURE 2.12. Synthesis of mono-functional 1,3-benzoxazine.....	39
FIGURE 2.13. Thermally induced ring opening polymerization of mono-(A) and bisbenzoxazine (B) monomers. ....	40
FIGURE 2.14. Ring opening initiation of bisbenzoxazine monomer. ....	41
<b>Chapter 3.....</b>	<b>55</b>
FIGURE 3.1. The structure of PI- <i>b</i> -PVTMS for <sup>1</sup> H-NMR-evaluation. ....	56
FIGURE 3.2. The structure of Hs-PI- <i>b</i> -PVTMS for <sup>1</sup> H-NMR-evaluation. ....	57
FIGURE 3.3. The structure of H-PI- <i>b</i> -PVTMS for <sup>1</sup> H-NMR-evaluation.....	58
FIGURE 3.4. The structure of H-Hydrin for <sup>1</sup> H-NMR and <sup>13</sup> C-NMR-evaluation. ....	59
FIGURE 3.5. The structure of A-H-Hydrin for <sup>1</sup> H-NMR and <sup>13</sup> C-NMR-evaluation. ....	59
FIGURE 3.6. The structure of C-Hydrin for <sup>1</sup> H-NMR and <sup>13</sup> C-NMR-evaluation.....	60

FIGURE 3.7. The structure of A-C-Hydrin for $^1\text{H}$ -NMR and $^{13}\text{C}$ -NMR-evaluation. ....	60
FIGURE 3.8. The structure of PEG-Dihydroxyl for $^{13}\text{C}$ -NMR-evaluation. ....	62
FIGURE 3.9. The structure of PEG-Dimesyl for $^{13}\text{C}$ -NMR-evaluation. ....	62
FIGURE 3.10. The structure of PEG-Diazide for $^{13}\text{C}$ -NMR-evaluation. ....	63
FIGURE 3.11. The structure of Bisphenol-A for $^1\text{H}$ -NMR-evaluation. ....	63
FIGURE 3.12. The structure of Benzoxazine-Diacetylene for $^1\text{H}$ -NMR-evaluation. ....	64
FIGURE 3.13. The structure of Step-Polymer for $^1\text{H}$ -NMR-evaluation.....	65
FIGURE 3.14. The structure of Stepbenz-Polymer for $^1\text{H}$ -NMR-evaluation. ....	65
FIGURE 3.15. A typical time lag diagram for the gas transport measurement of membranes. .....	69
<b>Chapter 4.....</b>	<b>66</b>
<b>Chapter 4.1 .....</b>	<b>66</b>
FIGURE 4.1.1. $^1\text{H}$ -NMR spectra of (10 wt. %)PI- <i>b</i> -PVTMS-1 (2) and Hs-(10 wt. %)PI- <i>b</i> - PVTMS-1 (1) in $\text{CDCl}_3$ .....	75
FIGURE 4.1.2. FT-IR spectra of (10 wt. %)PI- <i>b</i> -PVTMS-1 (A) and Hs-(10 wt. %)PI- <i>b</i> - PVTMS-1 (B).....	75
FIGURE 4.1.3. $^1\text{H}$ -NMR spectra of (10 wt. %)PI- <i>b</i> -PVTMS-1 (2) and H-(10 wt. %)PI- <i>b</i> - PVTMS-1 (1) in $\text{CDCl}_3$ .....	77
FIGURE 4.1.4. FT-IR spectra of (10 wt. %)PI- <i>b</i> -PVTMS-1 (A) and H-(10 wt. %)PI- <i>b</i> - PVTMS-1 (B).....	77
FIGURE 4.1.5. Gel permeation chromatograms of (10 wt. %)PI- <i>b</i> -PVTMS-1 (A), (13 wt. %)PI- <i>b</i> -PVTMS-2 (B), (30 wt. %)PI- <i>b</i> -PVTMS-3 (C), and (41 wt. %)PI- <i>b</i> - PVTMS-4 (D) and their modifications.....	79
FIGURE 4.1.6. TGA curves of (10 wt. %)PI- <i>b</i> -PVTMS-1 and its modifications recorded under nitrogen at heating rate 10 K/min.....	80
FIGURE 4.1.7. TEM micrographs of PI- <i>b</i> -PVTMS (A) (Copyright © 2011, Elsevier) and Hs-PI- <i>b</i> -PVTMS (B). The scale bar corresponds to 400 nm. ....	82
FIGURE 4.1.8. Relationship between $\text{O}_2$ and $\text{H}_2$ permeabilities and $\text{O}_2/\text{N}_2$ and $\text{H}_2/\text{N}_2$ selectivities of low isoprene contents (10 and 13 wt. %) PI- <i>b</i> -PVTMS block copolymers and their modified analogues: Hs-PI- <i>b</i> -PVTMS and H-PI- <i>b</i> -PVTMS. ....	85
FIGURE 4.1.9. Relationship between $\text{O}_2$ and $\text{H}_2$ permeabilities and $\text{O}_2/\text{N}_2$ and $\text{H}_2/\text{N}_2$ selectivities of high isoprene contents (30 and 41 wt. %) PI- <i>b</i> -PVTMS block copolymers and their modifications: Hs-PI- <i>b</i> -PVTMS and H-PI- <i>b</i> -PVTMS.....	86



FIGURE 4.1.10. O <sub>2</sub> permeability coefficients of (10, 13 and 30 wt. %) PI- <i>b</i> -PVTMS block copolymers and their modifications as a function of reciprocal fractional free volume (1/FFV).....	88
---	----

## **Chapter 4.2 ..... 91**

FIGURE 4.2.1. <sup>1</sup> H-NMR spectra of H-Hydrin (1), (33 wt. %)A-H-Hydrin (2) and (71 wt. %)A-H-Hydrin (3) in CDCl <sub>3</sub> . ....	94
---	----

FIGURE 4.2.2. <sup>1</sup> H-NMR spectra of C-Hydrin (1), (52 wt. %)A-C-Hydrin (2) and (100 wt. %)A-C-Hydrin (3) in CDCl <sub>3</sub> . ....	95
--	----

FIGURE 4.2.3. <sup>13</sup> C-NMR spectra of H-Hydrin (1), (33 wt. %)A-H-Hydrin (2) and (71 wt. %)A-H-Hydrin (3) in CDCl <sub>3</sub> . ....	96
--	----

FIGURE 4.2.4. <sup>13</sup> C-NMR spectra of C-Hydrin (1), (52 wt. %)A-C-Hydrin (2) and (100 wt. %)A-C-Hydrin (3) in CDCl <sub>3</sub> . ....	96
---	----

FIGURE 4.2.5. FT-IR spectra of H-Hydrin, azidated H-Hydrin homopolymers and their UV cross-linked analogues. ....	98
---	----

FIGURE 4.2.6. FT-IR spectra of C-Hydrin, azidated C-Hydrin copolymers and their UV cross-linked analogues. ....	98
---	----

FIGURE 4.2.7. DSC thermograms of H-Hydrin, azidated H-Hydrin homopolymers and their UV cross-linked counterparts. ....	99
--	----

FIGURE 4.2.8. DSC thermograms of C-Hydrin, azidated C-Hydrin copolymers and their UV cross-linked counterparts.....	100
---	-----

FIGURE 4.2.9. TGA analysis of H-Hydrin, 33 wt. % azidated H-Hydrin and after UV cross-linking (A); C-Hydrin, 52 wt. % azidated C-Hydrin and after UV cross-linking (B); DSC exotherms of 33 wt. % azidated H-Hydrin, its UV cross-linked analogue and 71 wt. % azidated H-Hydrin (C); 52 wt. % azidated C-Hydrin and its UV cross-linked analogue (D)...	103
--	-----

FIGURE 4.2.10. DSC and DTG curve comparisons of 33 wt. % azidated H-Hydrin and its UVcross-linked counterpart. ....	104
---	-----

FIGURE 4.2.11. Relationship between CO <sub>2</sub> and H <sub>2</sub> permeabilities and CO <sub>2</sub> /N <sub>2</sub> , CO <sub>2</sub> /CH <sub>4</sub> , CO <sub>2</sub> /H <sub>2</sub> and H <sub>2</sub> /N <sub>2</sub> selectivities of H-Hydrin and 33 and 71 wt. % azidated H-Hydrin polymers. ....	106
--	-----

FIGURE 4.2.12. Relationship between CO <sub>2</sub> and H <sub>2</sub> permeabilities and CO <sub>2</sub> /N <sub>2</sub> , CO <sub>2</sub> /CH <sub>4</sub> , CO <sub>2</sub> /H <sub>2</sub> and H <sub>2</sub> /N <sub>2</sub> selectivities of C-Hydrin, 52 and 100 wt. % azidated C-Hydrin copolymers and their UV cross-linked analogues.....	107
---	-----

FIGURE 4.2.13. Diffusion coefficient and solubility of CO <sub>2</sub> for C-Hydrin, modified C-Hydrin copolymers and their UV cross-linked analogues. ....	109
---	-----

<b>Chapter 4.3 .....</b>	<b>112</b>
FIGURE 4.3.1. <sup>13</sup> C-NMR spectra of HO-PEG-OH (1), Ms-PEG-Ms (2), and N <sub>3</sub> -PEG-N <sub>3</sub> (3) in CDCl <sub>3</sub> . .....	114
FIGURE 4.3.2. FT-IR spectra of HO-PEG-OH, Ms-PEG-Ms, and N <sub>3</sub> -PEG-N <sub>3</sub> . .....	115
FIGURE 4.3.3. <sup>1</sup> H-NMR spectra of bifunctional benzoxazine-diacetylene monomer (1) and Bisphenol A (2) in DMSO. ....	114
FIGURE 4.3.4. FT-IR spectra of Bisphenol A and bifunctional benzoxazine-diacetylene monomer.....	115
FIGURE 4.3.5. <sup>1</sup> H-NMR spectra of Step-3 in DMSO. ....	118
FIGURE 4.3.6. <sup>1</sup> H-NMR spectra of Step-5 in CDCl <sub>3</sub> . ....	118
FIGURE 4.3.7. FT-IR spectra of bifunctional azide PEG and Step-3. ....	119
FIGURE 4.3.8. Gel permeation chromatograms of Step-Polymers.. ..	119
FIGURE 4.3.9. DSC thermograms of bifunctional benzoxazine-diacetylene monomer and its polymer (Step-5) before and after ring opening polymerization.....	121
FIGURE 4.3.10. TGA curves of Step-(3-5) copolymers, thermally cured Step-5-XL and bifunctional benzoxazine-acetylene monomer (Benz-XL). ....	123
FIGURE 4.3.11. CO <sub>2</sub> , H <sub>2</sub> , O <sub>2</sub> , CH <sub>4</sub> and N <sub>2</sub> permeabilities, and CO <sub>2</sub> /N <sub>2</sub> , H <sub>2</sub> /N <sub>2</sub> , CO <sub>2</sub> /CH <sub>4</sub> , CO <sub>2</sub> /O <sub>2</sub> and O <sub>2</sub> /N <sub>2</sub> selectivities as a function of temperature for Step-5 polymer. ....	126
FIGURE 4.3.12. CO <sub>2</sub> permeability in the heating and cooling cycle as a function of temperature for Step-5 polymer. ....	127

## List of Schemes

<b>Chapter 4.....</b>	<b>66</b>
<b>Chapter 4.1 .....</b>	<b>66</b>
SCHEME 4.1.1. Metal catalyzed hydrosilylation of PI- <i>b</i> -PVTMS .....	74
SCHEME 4.1.2. Noncatalyzed hydrogenation of PI- <i>b</i> -PVTMS.....	78
<b>Chapter 4.2 .....</b>	<b>91</b>
SCHEME 4.2.1. Azidation of H-Hydrin and C-Hydrin.....	92

SCHEME 4.2.2. The mechanism of UV cross-linking of azidated Hydrin polymers .....	92
<b>Chapter 4.3 .....</b>	<b>112</b>
SCHEME 4.3.1. Synthesis of bifunctional PEG-Dimesyl .....	113
SCHEME 4.3.2. Synthesis of bifunctional PEG-Diazide .....	113
SCHEME 4.3.3. Synthesis of bifunctional benzoxazine-diacetylene. ....	113
SCHEME 4.3.4. Step-growth click coupling polyaddition of diethynylbenzene and bifunctional azide PEG in the catalyst and catalyst-free conditions. ....	116
SCHEME 4.3.5. Step-growth click coupling polyaddition of bifunctional benzoxazine- diacetylene and bifunctional PEG-Diazide in the precence of catalyst. ....	117

## List of Tables

<b>Chapter 2.....</b>	<b>15</b>
TABLE 2.1. Classification and Separation Mechanism of Membranes. ....	18
TABLE 2.2. The Permeability Coefficients of Polymers for Commercial Gas Separating Membranes. ....	21
TABLE 2.3. The Effect of the Connector Groups on Polyimides. ....	25
<b>Chapter 4.....</b>	<b>66</b>
<b>Chapter 4.1 .....</b>	<b>66</b>
TABLE 4.1.1. Molecular Weight and Percentage of Modification of the Block Copolymers. .....	73
TABLE 4.1.2. Molecular Weight and Polydispersity of the Block Copolymers Before and After Modification.....	78
TABLE 4.1.3. Thermal Properties of PI- <i>b</i> -PVTMS-1.....	81
TABLE 4.1.4. Gas Permeability Coefficients and Selectivity Values of the Block Copolymers Before and After Modifications. In the brackets is the PI content in wt. % of the block copolymers given.....	84
TABLE 4.1.5. Densities and Fractional Free Volumes of the Block Copolymers Before and After Modifications. ....	87
<b>Chapter 4.2 .....</b>	<b>91</b>

TABLE 4.2.1. Molecular Weight, Polydispersity and Percentage of Modification of Hydrin Polymers.....	93
TABLE 4.2.2. Gel Content Analysis of Cross-linked Hydrin Polymers as Results from Swelling Experiments (%). .....	99
TABLE 4.2.3. Thermal Properties of Initial Hydrin Polymers and the Counterparts after Modification and UV Cross-linking.....	102
TABLE 4.2.4. Gas Permeability Coefficients and Selectivity Values of Homo and Copolymers (H.Hydrin and C-Hydrin), and Their Azidated and UV Cross-linked Counterparts. In the Brackets is the Azidation Degree in wt. % of the Homo and Copolymers Given.....	105
<b>Chapter 4.3 .....</b>	<b>112</b>
TABLE 4.3.1. Step-Growth Click Coupling Polyaddition Conditions.....	116
TABLE 4.3.2. Molecular Weight, Polydispersity (PDI) and Glass Transition Temperature ( $T_g$ ) of Step-(1-5) Polymers. ....	120
TABLE 4.3.3. Thermal Properties of Step-(1-5), Thermally Crosslinked Step-5 (Step-5-XL) and Bifunctional Benzoxazine-Diacetylene Monomer (Benz-XL).....	122
TABLE 4.3.4. Gas Permeability Coefficients and Selectivity Values of Step-5 Polymer in the Temperature Ranging from 30 to 90 °C. . ....	124

# Chapter 1

## 1.1. Introduction

Membrane technology has attracted significant interest for gas separation in particular by polymeric membranes due to their high competitiveness in performance and economics [1-8]. Polymeric membranes have widely been used in various separation processes like microfiltration, ultrafiltration, nanofiltration, pervaporation, dialysis and gas separation. In case of gas separation, air separation ( $O_2/N_2$ ), the removal of carbon dioxide ( $CO_2$ ) from natural gas and hydrogen ( $H_2$ ) separation from nitrogen ( $N_2$ ) or hydrocarbons in petrochemical industry can be taken as examples for the large industrial applications of polymeric membranes [9-11].

The permeability coefficient of a specific component of the gas mixture and the selectivity are the key parameters for gas separation. These two parameters generally shows a trade-off relationship in which the selectivity decreases with increasing permeability coefficient. In 1991, Lloyd M. Robeson plotted a graph describing the selectivity as a function of permeability coefficient on logarithmic scale. This graph is known as Robeson's upper bound and indicates that the polymeric membranes with low permeability coefficient generally possess higher selectivity. In 2008, the revised Robeson's upper bound was reviewed including the data of newly developed polymeric membranes. Figure 1.1 shows the upper bound correlation of  $O_2/N_2$  separation.

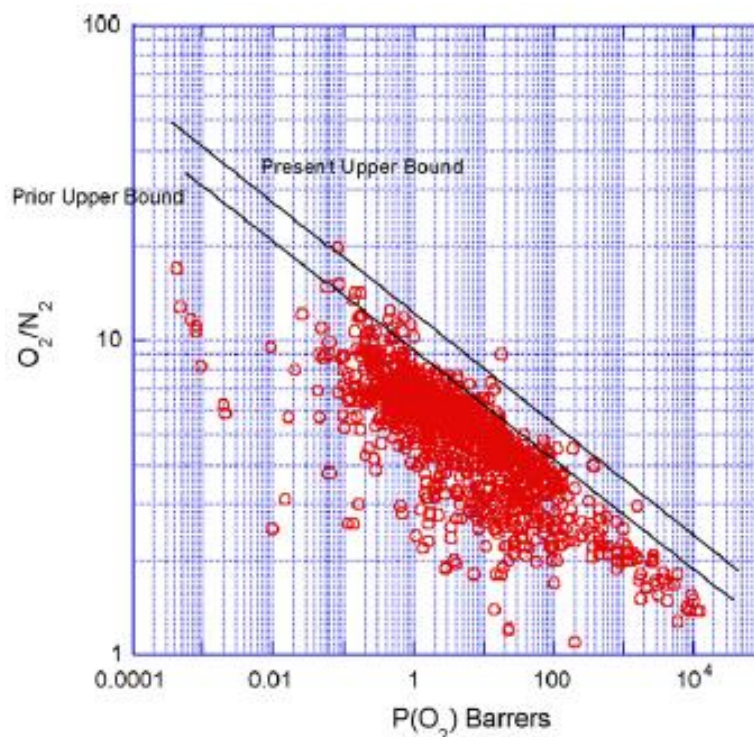


**FIGURE 1.1.** Upper bound correlation between  $O_2$  permeability coefficient and  $O_2/N_2$  selectivity [12].

Until now, hundreds of polymers have been investigated for membrane applications, including polysulfone, polyethersulfone, polyimide, polyepichlorohydrin (Hydrin<sup>®</sup>) and poly(vinyl trimethylsilane) (PVTMS). However, only very few have found use in gas separation membrane industry [13, 14]. It has to be mentioned that despite the fact that numerous polymers were recently synthesized and shifted the Robeson's upper bound curve toward the region of higher permeability and selectivity, other polymer properties such as mechanical stability and ageing, but also the price of precursors prevent their use in large scale membrane production.

Different techniques has been applied to improve gas transport properties of polymeric membranes such as modification of backbone or side chain of conventional polymers, and synthesis of polymers with specific groups for aimed gas separation. The chemical modification methods must be carefully selected according the polymer characteristic in order to obtain a membrane material

with enhanced gas transport properties. The glassy polymers show significant variations on gas transport properties due to their chemical structure. In general, bulky and symmetrical side groups on the main chain of the polymers improve the gas permeability. On the other hand, long linear and asymmetrical side groups on the main chain of the polymers reduce the gas permeability. In the case of rubbery polymers, the most important effect is the mobility of polymer chains. The side groups which decrease the chain mobility result in enhanced permeability coefficients and vice versa. In addition, the polymers with various chemical groups for aimed gas separation can be synthesized. As an example, poly(ethylene glycol) (PEG) and heterocyclic molecules such as triazole, tetrazole and oxazine have favorable interaction with CO<sub>2</sub> leading to higher solubility compared to other gases and so the gas separation improves.

## **1.2. The Aim of the Thesis**

At the first part of the current study, PVTMS, which is a well-known member of the trimethyl silyl (-SiMe<sub>3</sub>) side group family of polymers for distinctive gas transport properties, will be the main focus. Combination of reasonable (not outstanding) gas transport properties of PVTMS ensures a very balanced position of this polymer among other polymers of commercial gas separation membranes on the Robeson plot (Figure 1.2). PVTMS and its block copolymers can be synthesized via anionic polymerization and resulting polymers can be processed to thin film composite membranes (TFCM).

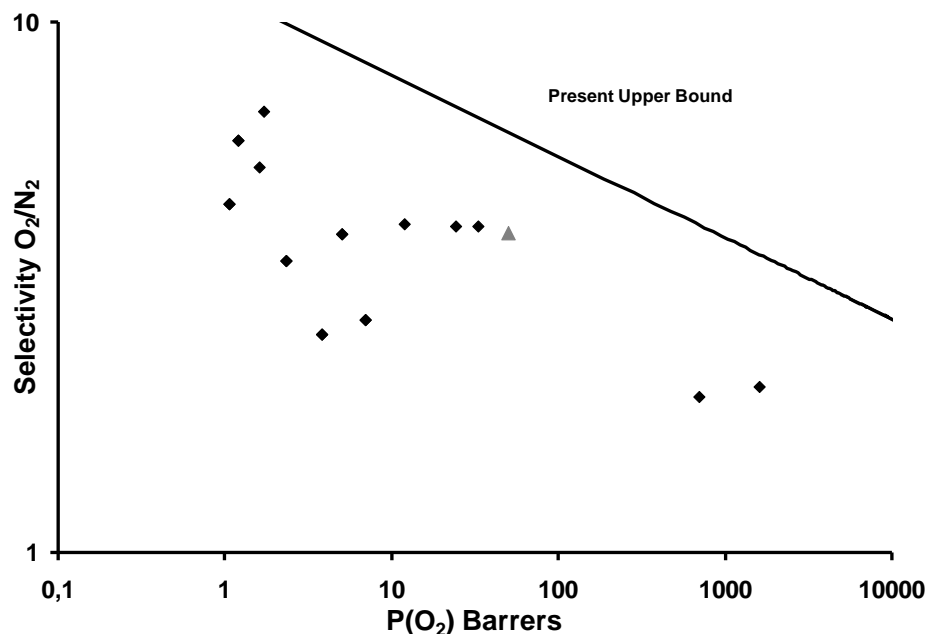


**FIGURE 1.2.**  $O_2/N_2$  selectivity and  $O_2$  permeability coefficient of PVTMS (▲) compared to other polymers of commercial gas separation membranes (♦) and to the Robeson's present (2008) upper bound [12].

PVTMS has been used in industry for air separation (oxygen enrichment and nitrogen generation) with good  $O_2$  permeability and  $O_2/N_2$  selectivity. Not only for air separation, but also for hydrogen separation it has been used as a highly potential polymer with high  $H_2$  permeability and  $H_2/N_2$  selectivity in refineries and petrochemical industry [15, 16]. PVTMS membranes have good properties for gas separation; on the other hand, they have a few deficiencies in membrane formation owing to the polymer characteristics. PVTMS is brittle, with small elongation at break ( $\epsilon = 5\%$ ) [17]. PVTMS is also expensive and excessive consumption of the polymer occurs during integral asymmetric gas separation membrane fabrication. These drawbacks of PVTMS led us to the idea to synthesize block copolymers of PVTMS (hard segment) with polyisoprene (PI, soft segment) and to study their gas transport and membrane formation properties [13]. The block copolymers (PI-*b*-PVTMS) were found to have excellent film forming properties accompanied by



the O<sub>2</sub> permeability and O<sub>2</sub>/N<sub>2</sub> selectivity close to pure PVTMS. However, at high isoprene content in the block copolymer, formation of a lamellar structure because of microphase separation caused a 53% drop in O<sub>2</sub> permeability but no significant difference in O<sub>2</sub>/N<sub>2</sub> selectivity compared to PVTMS-ref. ( $P(O_2) = 48$  Barrer,  $\alpha(O_2/N_2) = 3.9$ ,  $M_w = 650$  kg/mol,  $M_w / M_n = 2.1$ ) [18]. This drawback led us to the idea to modify the isoprene units of PI-*b*-PVTMS chemically to improve the permeability of the rubbery block.

Chemical modification of polymers has been used for many years to improve properties and to add functional groups to polymers if these resulting functional polymers are expensive, difficult or impossible to synthesize in a direct way via conventional polymerization methods [19, 20].

In this part of the current study, our main goal was to modify the polyisoprene block of PI-*b*-PVTMS with suitable components via metal catalyzed hydrosilylation [19] and non-catalyzed hydrogenation [20]. The intent thus is to alter the thermodynamic and repulsive interactions between blocks, resulting in different morphologies, which are directly related to the gas transport properties of the modified block copolymers [21]. In addition, the polymer characteristics were expected to advance from a less permeable and selective, rubbery polyisoprene to a highly permeable, silicon-containing glassy polymer and semicrystalline polyolefin [22]. In this way, we expect to retain the performance of PVTMS homopolymer in terms of its gas transport properties while at the same time decreasing the consumption of PVTMS.

The second part of the current study focuses on the modification of Hydrin<sup>®</sup> polymers via azidation and their gas transport properties. Polymers containing poly(ethylene glycol) (PEG) have been studied as membrane materials for especially CO<sub>2</sub> separation because of its good solubility due to the quadrupole moment resulting in favorable interactions with polar groups in polymers (in the case of PEG, these are polar ether oxygens) [2, 23, 24]. Therefore CO<sub>2</sub> is better soluble in these

polymers compared to non-polar gases (eg. H<sub>2</sub>, N<sub>2</sub>, and CH<sub>4</sub>) leading to enhanced permeability and solubility selectivity. Furthermore, the low glass transition temperature ( $T_g$ ) of amorphous PEG contributes to its high gas diffusivity. Because of these favorable characteristics, PEG has been used in many material platforms for CO<sub>2</sub> based gas separations, such as Hydrin<sup>®</sup> [3], Pebax<sup>®</sup> [25], Polyactive<sup>®</sup> and cross-linked PEG [26, 27].

Poly(epichlorohydrin) homopolymers (H-Hydrin) and poly[(ethylene oxide)-*ran*-(epichlorohydrin)] copolymers (C-Hydrin) under the trade name Hydrin<sup>®</sup> composed of only hard segment and hard and soft segments, respectively, are known to show very high permeability and selectivity towards CO<sub>2</sub> [3]. In the case of C-Hydrin, poly(epichlorohydrin) blocks provide the mechanical strength and give the thermoplastic behavior to the copolymer, whereas PEG as soft segment gives the elastomeric behavior and gas separation property to the copolymer [28]. Additionally, Hydrin polymers can be further modified via the chloride pendent groups. There are two synthetic approaches for the preparation of functional polymers which are direct polymerization or copolymerization of monomers carrying desired functionality and the chemical modification of preformed polymers. In this study, the applied modification method is azidation chemistry which bases on halide ion substitution by azide ( $-N_3$ ) ion [29-36]. Many examples can be found in the literature about azidation of chlorine-containing Hydrin polymers mostly in the direction of enhanced rocketed propellants and plastic bounded explosives due to the presence of energetic azide groups in the polymer side chain [28, 37, 38]. In these studies, one of the most important goals was to decrease the glass transition temperature ( $T_g$ ) of the polymers [28, 37, 38]. This could be a significant advantage to improve the gas transport properties of Hydrin polymers because of the high polymer chain mobility resulting in increased gas diffusivity and then gas permeability. Furthermore, azide groups have the ability to decompose to molecular nitrogen and

highly reactive divalent radical in the presence of UV irradiation or elevated temperature [39]. Therefore, azidated Hydrin polymers are suitable candidates for further UV cross-linking step without using any additional commercial cross-linkers [40]. The cross-linking reaction is an efficient method to produce new gas separation membranes for harsh environmental applications. Owing to the limitation in polymer chain mobility and high packing density, cross-linked polymer membranes exhibit superior dimensional stability; they show better mechanical and environmental resistance, reduced aging, but also reduced permeability [41-44].

This part of the current study focuses on the modification and UV cross-linking of chlorine-containing H-Hydrin and C-Hydrin polymers via azidation chemistry and nitrene reaction, respectively, and their gas transport properties. Moreover, the correlation between  $T_g$  and gas transport properties after azidation and UV cross-linking is reported. In addition, before and after modification and UV cross-linking the thermal decomposition behaviors of H-Hydrin and C-Hydrin polymers are studied and discussed.

At the third part of the current study was the focus on PEG-containing polymers which were synthesized by step-growth click coupling polymerization. Step-growth polymers have been known since the discovery of synthetic polymers as useful polymeric materials within wide application areas [45]. Recently, they have an important role in many industrial applications. Step-growth polymers were introduced with the discovery of the Bakelite resins from the condensation of phenol and formaldehyde by the Belgian chemist BAEKELAND in 1907 [46] and continued with the discovery of the 20<sup>th</sup> century's two most widely used synthetic polymers: nylon and polyester, by WALLACE CAROTHERS and his research group at DuPont [47].

Step-growth click coupling polymerization is a polyaddition type reaction in which monomers react without the elimination of a small molecule. The coupling process bases on azide-alkyne 1,3-

dipolar cycloaddition reaction which was first discovered in 1961 by ROLF HUISGEN [48] and named as “Click” chemistry in 2001 by K.B. SHARPLESS [49]. It is a chemical transformation having advantageous characteristics such as high efficiency, regioselectivity, mild conditions, fast reaction rates and simple product isolation procedures [49]. 1,2,3-Triazoles are formed as linker on the main chain of polymer during step-growth click coupling polymerization. In step-growth polymerizations, high molecular weight polymers are synthesized because any species such as monomers, dimers, trimers etc. can react at any time in consecutive reactions [45]. In our study, the applied coupling process is copper-catalyzed azide-alkyne cycloaddition (CuACC) which is the most progressed example of click chemistry reactions.

In the previous part of the current study, the positive effect of PEG units on CO<sub>2</sub> separation was discussed. In addition, nitrogen containing organic heterocyclic molecules such as triazole which is formed during the step-growth click coupling polymerization have good influence on CO<sub>2</sub> separation as well. This bases on the Lewis acid-Lewis base interactions resulting in hydrogen bonding between heterocyclic molecules and negatively charged oxygen atoms of CO<sub>2</sub>. Therefore, the polymers containing heterocyclic molecules have better interaction with CO<sub>2</sub> leading to higher solubility compared to other gases [50]. Likely, oxazine which is a member of N-containing organic heterocyclic molecules is an effective structure for CO<sub>2</sub> separation. Oxazine ring has the cross-linking ability with thermally induced ring-opening polymerization. Common type of oxazine rings which takes interest of academia and chemical industry is 1-3-benzoxazine. Benzoxazines and their resins have many unique properties such as near zero volumetric change upon curing, no requirement of strong acid catalyst or additives for curing, high thermal stability, low water absorption and high char-yield of the cured products [51]. Another additional property

of the benzoxazine chemistry is easy preparation of monomers which are synthesized from cheap, commercially available phenols, primary amines and formaldehyde [52, 53].

This part of the current study focuses on high molecular weight polymers containing PEG, triazole and benzoxazine rings which are synthesized by step-growth click coupling polymerization, and their gas transport properties. Additionally, the effect of the amount of heterocyclic structures in the polymer and curing of benzoxazine ring on thermal properties was studied.

The present doctoral work is organized as follows: **Chapter 2** sketches the description of membranes and their types. Theoretical background regarding the chemical modification methods enhancing the gas transport properties in gas separation membranes are reported in this chapter. Additionally, the synthesis method of the polymers containing PEG for CO<sub>2</sub> separation is discussed. **Chapter 3** details the experimental procedures employed for different types of polymer modification and step-growth click coupling polymerization, as well as details regarding the characterization of the resulted materials. The results and the discussions are summarized in **Chapter 4**. **Chapter 4** is subdivided in three topics and distributed as follows: (i) **Chapter 4.1** deals with the modification of poly(isoprene)-*block*-poly(vinyl trimethylsilane) (PI-*b*-PVTMS) block copolymers containing four different PI block compositions via diimide hydrogenation and hydrosilylation, and their gas transport properties. (ii) In **Chapter 4.2** the effect of azidation and UV-crosslinking of poly(epichlorohydrin) and pol[(ethylene oxide)-*ran*-(epichlorohydrin)] on gas transport properties is analyzed. (iii) **Chapter 4.3** describes the synthesis of PEG containing polymers via step-growth click coupling polymerization for CO<sub>2</sub> separation. Finally, **Chapter 5** summarizes the conclusions obtained during these investigations.

### 1.3. References

- [1] B.N. Gacal, V. Filiz, S. Shishatskiy, S. Rangou, S. Neumann, V. Abetz, Modification of polyisoprene-block-poly(vinyl trimethylsilane) block copolymers via hydrosilylation and hydrogenation, and their gas transport properties, *Journal of Polymer Science Part B: Polymer Physics*, 51 (2013) 1252-1261.
- [2] H. Lin, E.V. Wagner, J.S. Swinnea, B.D. Freeman, S.J. Pas, A.J. Hill, S. Kalakkunnath, D.S. Kalika, Transport and structural characteristics of crosslinked poly(ethylene oxide) rubbers, *Journal of Membrane Science*, 276 (2006) 145-161.
- [3] C. Charmette, J. Sanchez, P. Gramain, N. Masquelez, Structural characterization of poly(ethylene oxide-co-epichlorohydrin) membranes and relation with gas permeation properties, *Journal of Membrane Science*, 344 (2009) 275-280.
- [4] B.D. Freeman, Basis of permeability/selectivity tradeoff relations in polymeric gas separation membranes, *Macromolecules*, 32 (1999) 375-380.
- [5] S.I. Semenova, Polymer membranes for hydrocarbon separation and removal, *Journal of Membrane Science*, 231 (2004) 189-207.
- [6] C. Staudt-Bickel, W. J. Koros, Improvement of CO<sub>2</sub>/CH<sub>4</sub> separation characteristics of polyimides by chemical crosslinking, *Journal of Membrane Science*, 155 (1999) 145-154.
- [7] M. Khan, V. Filiz, G. Bengtson, S. Shishatskiy, M. Rahman, V. Abetz, Functionalized carbon nanotubes mixed matrix membranes of polymers of intrinsic microporosity for gas separation, *Nanoscale Research Letters*, 7 (2012) 1-12.
- [8] M.M. Khan, V. Filiz, G. Bengtson, S. Shishatskiy, M.M. Rahman, J. Lillepaerg, V. Abetz, Enhanced gas permeability by fabricating mixed matrix membranes of functionalized multiwalled

carbon nanotubes and polymers of intrinsic microporosity (PIM), *Journal of Membrane Science*, 436 (2013) 109-120.

[9] V.I. Bondar, B.D. Freeman, I. Pinnau, Gas transport properties of poly(ether-b-amide) segmented block copolymers, *Journal of Polymer Science Part B: Polymer Physics*, 38 (2000) 2051-2062.

[10] H. Lin, B.D. Freeman, Gas solubility, diffusivity and permeability in poly(ethylene oxide), *Journal of Membrane Science*, 239 (2004) 105-117.

[11] M. Yoshino, K. Ito, H. Kita, K.-I. Okamoto, Effects of hard-segment polymers on CO<sub>2</sub>/N<sub>2</sub> gas-separation properties of poly(ethylene oxide)-segmented copolymers, *Journal of Polymer Science Part B: Polymer Physics*, 38 (2000) 1707-1715.

[12] L.M. Robeson, The upper bound revisited, *Journal of Membrane Science*, 320 (2008) 390-400.

[13] Y. Yampolskii, Polymeric gas separation membranes, *Macromolecules*, 45 (2012) 3298-3311.

[14] R.W. Baker, Future directions of membrane gas separation technology, *Industrial and Engineering Chemistry Research*, 41 (2002) 1393-1411.

[15] Y.M. Baranov, L.V. Stolyarova, M.F. Shopshin, T.K. Melik-Akhnazarov, T.S. Aleksashkina, Modern processes of hydrogen recovery from refinery gas, *Chemistry and Technology of Fuels and Oils*, 27 (1991) 285-287.

[16] A. Tóth, I. Bertóti, V.S. Khotimsky, G. Marletta, J.L. Sullivan, S.O. Saied, Modification of gas separation membranes on a nanometric scale, *Nuclear Instruments and Methods in Physics Research Section B*, 122 (1997) 547-549.

- [17] Y.P. Yampolskii, V.V. Volkov, Studies in gas permeability and membrane gas separation in the Soviet Union, *Journal of Membrane Science*, 64 (1991) 191-228.
- [18] S. Rangou, S. Shishatskiy, V. Filiz, V. Abetz, Poly(vinyl trimethylsilane) and block copolymers of vinyl trimethylsilane with isoprene: Anionic polymerization, morphology and gas transport properties, *European Polymer Journal*, 47 (2011) 723-729.
- [19] X. Guo, R. Farwaha, G.L. Rempel, Catalytic hydrosilylation of diene-based polymers. 1. Hydrosilylation of polybutadiene, *Macromolecules*, 23 (1990) 5047-5054.
- [20] P. Phinyocheep, S. Pasiri, O. Tavichai, Diimide hydrogenation of isoprene–styrene diblock copolymers, *Journal of Applied Polymer Science*, 87 (2003) 76-82.
- [21] Y. Ren, T.P. Lodge, M.A. Hillmyer, Synthesis, characterization, and interaction strengths of difluorocarbene-modified polystyrene–polyisoprene block copolymers, *Macromolecules*, 33 (2000) 866-876.
- [22] W.J. Koros, B.J. Story, S.M. Jordan, K. O'Brien, G.R. Husk, Material selection considerations for gas separation processes, *Polymer Engineering and Science*, 27 (1987) 603-610.
- [23] K. Ghosal, R.T. Chern, B.D. Freeman, W.H. Daly, I.I. Negulescu, Effect of basic substituents on gas sorption and permeation in polysulfone, *Macromolecules*, 29 (1996) 4360-4369.
- [24] A.C. Comer, D.S. Kalika, V.A. Kusuma, B.D. Freeman, Glass-transition and gas-transport characteristics of polymer nanocomposites based on crosslinked poly(ethylene oxide), *Journal of Applied Polymer Science*, 117 (2010) 2395-2405.
- [25] M.M. Rahman, V. Filiz, S. Shishatskiy, C. Abetz, S. Neumann, S. Bolmer, M.M. Khan, V. Abetz, PEBAX<sup>®</sup> with PEG functionalized POSS as nanocomposite membranes for CO<sub>2</sub> separation, *Journal of Membrane Science*, 437 (2013) 286-297.



- [26] H. Lin, E. Van Wagner, B.D. Freeman, L.G. Toy, R.P. Gupta, Plasticization-enhanced hydrogen purification using polymeric membranes, *Science*, 311 (2006) 639-642.
- [27] H. Lin, E. Van Wagner, R. Raharjo, B.D. Freeman, I. Roman, High-performance polymer membranes for natural-gas sweetening, *Advanced Materials*, 18 (2006) 39-44.
- [28] S. Brochu, G. Ampleman, Synthesis and characterization of glycidyl azide polymers using isotactic and chiral poly(epichlorohydrin)s, *Macromolecules*, 29 (1996) 5539-5545.
- [29] T. Cai, K.G. Neoh, E.T. Kang, S.L.M. Teo, Surface-functionalized and surface-functionalizable poly(vinylidene fluoride) graft copolymer membranes via click chemistry and atom transfer radical polymerization, *Langmuir*, 27 (2011) 2936-2945.
- [30] M. Kukut, O. Karal-Yilmaz, Y. Yagci, Synthesis, characterization, and hydrolytic degradation of graft copolymers of polystyrene and aliphatic polyesters, *Designed Monomers and Polymers*, 16 (2012) 233-240.
- [31] S.K. Yadav, H.J. Yoo, J.W. Cho, Click coupled graphene for fabrication of high-performance polymer nanocomposites, *Journal of Polymer Science Part B: Polymer Physics*, 51 (2013) 39-47.
- [32] B.N. Gacal, B. Koz, B. Gacal, B. Kiskan, M. Erdogan, Y. Yagci, Pyrene functional poly(vinyl alcohol) by “click” chemistry, *Journal of Polymer Science Part A: Polymer Chemistry*, 47 (2009) 1317-1326.
- [33] D. Odaci, B.N. Gacal, B. Gacal, S. Timur, Y. Yagci, Fluorescence sensing of glucose using glucose oxidase modified by PVA-Pyrene prepared via “click” chemistry, *Biomacromolecules*, 10 (2009) 2928-2934.
- [34] E.I. Medine, D. Odaci, B.N. Gacal, B. Gacal, S. Sakarya, P. Unak, S. Timur, Y. Yagci, A new approach for in vitro imaging of breast cancer cells by anti-metadherin targeted PVA-Pyrene, *Macromolecular Bioscience*, 10 (2010) 657-663.

- [35] V. Ervithayasuporn, X. Wang, B. Gacal, B.N. Gacal, Y. Yagci, Y. Kawakami, Formation of trimethylsilylated open-cage oligomeric azidophenylsilsesquioxanes, *Journal of Organometallic Chemistry*, 696 (2011) 2193-2198.
- [36] B. Karagoz, Y.Y. Durmaz, B.N. Gacal, N. Bicak, Y. Yagci, Functionalization of poly(divinylbenzene) microspheres by combination of hydrobromination and click chemistry processes: a model study, *Designed Monomers and Polymers*, 12 (2009) 511-522.
- [37] B.S. Min, G. Baek, S.W. Ko, Characterization of polyether-type GAP and PEG blend matrices prepared with varying ratios of different curatives, *Journal of Industrial and Engineering Chemistry*, 13 (2007) 373-379.
- [38] M.B. Frankel, L.R. Grant, J.E. Flanagan, Historical development of glycidyl azide polymer, *Journal of Propulsion and Power*, 8 (1992) 560-563.
- [39] J. Xia, S. Liu, T.-S. Chung, Effect of end groups and grafting on the CO<sub>2</sub> separation performance of poly(ethylene glycol) based membranes, *Macromolecules*, 44 (2011) 7727-7736.
- [40] M.M. Khan, G. Bengtson, S. Shishatskiy, B.N. Gacal, M. Mushfequr Rahman, S. Neumann, V. Filiz, V. Abetz, Cross-linking of polymer of intrinsic microporosity (PIM-1) via nitrene reaction and its effect on gas transport property, *European Polymer Journal*, 49 (2013) 4157-4166.
- [41] P.S. Tin, T.S. Chung, Y. Liu, R. Wang, S.L. Liu, K.P. Pramoda, Effects of cross-linking modification on gas separation performance of Matrimid membranes, *Journal of Membrane Science*, 225 (2003) 77-90.
- [42] D. Montarnal, M. Capelot, F. Tournilhac, L. Leibler, Silica-like malleable materials from permanent organic networks, *Science*, 334 (2011) 965-968.
- [43] C.N. Dudley, B. Schöberl, G.K. Sturgill, H.W. Beckham, M.E. Rezac, Influence of crosslinking technique on the physical and transport properties of ethynyl-terminated

monomer/polyetherimide asymmetric membranes, *Journal of Membrane Science*, 191 (2001) 1-11.

[44] M.S. McCaig, D.R. Paul, Effect of UV crosslinking and physical aging on the gas permeability of thin glassy polyarylate films, *Polymer*, 40 (1999) 7209-7225.

[45] L. Billiet, D. Fournier, F. Du Prez, Step-growth polymerization and ‘click’ chemistry: The oldest polymers rejuvenated, *Polymer*, 50 (2009) 3877-3886.

[46] L.H. Baekeland, US Patent 0942699, in, 1907.

[47] W.H. Carothers, US Patents 2130947 and 2130948, in, 1938.

[48] Proceedings of the Chemical Society. October 1961, Proceedings of the chemical society, (1961) 357-396.

[49] H.C. Kolb, M.G. Finn, K.B. Sharpless, Click chemistry: diverse chemical function from a few good reactions, *Angewandte Chemie International Edition*, 40 (2001) 2004-2021.

[50] N. Du, H.B. Park, G.P. Robertson, M.M. Dal-Cin, T. Visser, L. Scoles, M.D. Guiver, Polymer nanosieve membranes for CO<sub>2</sub>-capture applications, *Nature Materials*, 10 (2011) 372-375.

[51] K. Dogan Demir, B. Kiskan, Y. Yagci, Thermally curable acetylene-containing main-chain benzoxazine polymers via sonogashira coupling reaction, *Macromolecules*, 44 (2011) 1801-1807.

[52] W.J. Burke, 3,4-Dihydro-1,3,2H-Benzoxazines. Reaction of p-substituted phenols with N,N-dimethylolamines, *Journal of the American Chemical Society*, 71 (1949) 609-612.

[53] Y.-L. Liu, C.-Y. Chang, C.-Y. Hsu, M.-C. Tseng, C.-I. Chou, Preparation, characterization, and properties of fluorene-containing benzoxazine and its corresponding cross-linked polymer, *Journal of Polymer Science Part A: Polymer Chemistry*, 48 (2010) 4020-4026.

## **Chapter 2**

### **Theoretical Background and State of the Art**

#### **2.1. Membranes**

Membrane is defined as a permeable or semipermeable barrier between two phases (Figure 2.1). The membrane phenomena has a long history which goes back to eighteenth century to the invention of the term “Osmosis” by ABBE NOLET to describe the permeation of water through a diaphragm in 1748 [1, 2]. At the beginning, membranes were used for an important application in order to test the drinking water at the end of World War II [3]. After that, although significant progress was done in membrane science during 1970s, there were only a few efficient applications in some laboratories as well as small specialized industrial applications. With the simultaneous development of the organic and in particular polymer and material chemistry, membrane science has gained a new perspective in the direction of cheaper and reliable materials which led the membrane processes to be a crucial and irrevocable part of separation and purification technology [3].

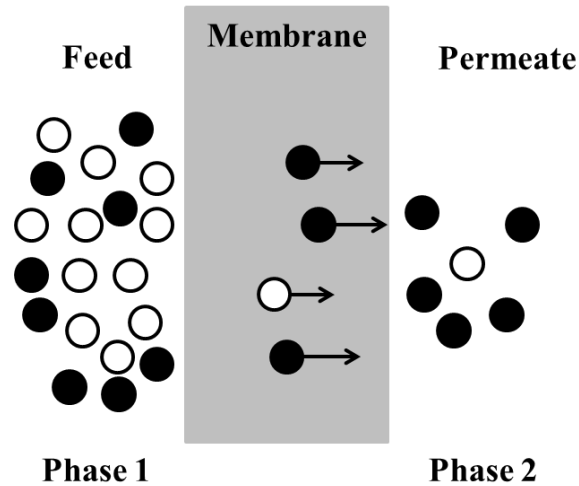


**FIGURE 2.1.** Schematic draw representing the separation of two phases by membrane.

The basic process of membranes is only to some extent similar to normal filters used to separate particular suspensions with particle sizes ranging from 1 to 10  $\mu\text{m}$  [4]. The molecules can pass through the membrane according to principle of active or passive transport. The driving forces of the passive transport are concentration, pressure, temperature and electric potential difference. Membranes are often divided in two main classes concerning their origin which is natural or synthetic [2]. Likely, synthetic membranes can be categorized in two main classes related to the constituents of the membranes, *i.e.* organic and inorganic membranes. The materials for inorganic membranes are glass, ceramic, metal, etc. and for organic membranes all kinds of polymers can be counted [2].

### 2.1.1. The Classification of Membranes

Synthetic membranes can be classified as symmetric (isotropic) and asymmetric (anisotropic) with respect to their cross sectional structure. The classification of the membranes is shown in Figure 2.2 [4]. Additionally, Table 2.1 shows the different processes and separation mechanisms of membranes [2]. Microporous and non-porous (dense) membranes will be in the main focus of this thesis.

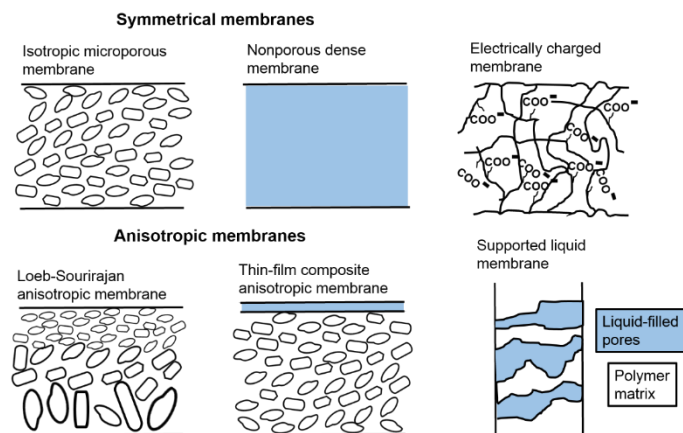


**FIGURE 2.2.** Schematic diagram of main types of the membranes [4].

**TABLE 2.1.** Classification and Separation Mechanism of Membranes.

Process	Size of retained material	Driving force	Separation mechanism
Microfiltration	0.1-10 $\mu\text{m}$ microparticles	Pressure difference (0.2-2 bar)	Sieve effect
Ultrafiltration	1-100 nm macromolecules	Pressure difference (1-5 bar)	Sieve effect
Nanofiltration	0.5-50 nm molecules	Pressure difference (5-20 bar)	Sieve effect, solution-diffusion, exclusion
Reverse osmosis	< 1 nm ions	Pressure difference (10-100 bar)	Solution-diffusion, exclusion
Dialysis	< 1 nm molecules	Concentration difference	Diffusion
Electrodialysis	< 1 nm molecules	Electric potential difference	Exclusion
Pervaporation	< 1 nm molecules	Concentration difference	Solution-diffusion
Gas separation	< 1 nm molecules	Partial pressure difference (10-100 bar)	Sieve effect, solution-diffusion
Membrane distillation	< 1 nm molecules	Temperature and partial pressure difference	Evaporation

#### 2.1.1.1. Microporous Membranes

Microporous membranes have similar properties in structure and function comparing with conventional filters, since they have interconnected and randomly distributed pores in the

structure. The separation mechanism is based on the molecular sieving, where the particles bigger than the membrane pores are rejected in contrast to the smaller particles, which can easily pass through the membrane pores [4]. These membranes find applications in pharmaceutical, food and chemical industries [2].

#### **2.1.1.2. Non-Porous (Dense) Membranes**

Non-porous membranes are formed from a dense film supplying the transportation of the permeate (gases or liquids) under the driving force of pressure, concentration or electrical potential gradient [2]. The separation mechanism is based on the transport rate of different components in the membrane matrix which is strictly correlated to their diffusivity and solubility. Non-porous membranes are generally used for processes like gas separation, pervaporation and reverse osmosis. Due to the slow permeation of the separating mixture through the dense films, the non-porous membranes are commercially applied in the form of composite anisotropic membranes to increase the flux [5].

#### **2.1.2. Membranes for Gas Separation**

GRAHAM and MITCHEL carried out the first studies associated with gas separation membranes [6, 7]. The research of MITCHEL around 1830s started with an observation which is about descending of a hydrogen gas filled in natural rubber balloons after a period of time. This was attributed as a phenomenon to gas release by diffusion through the balloon wall. Then, GRAHAM continued this research for a long time period and measured the permeation rate of a variety of gases with the help of diaphragms available at that time. The first descriptions about the solution-diffusion model in dense membranes and GRAHAM's law of diffusion in porous membranes were introduced by GRAHAM [6, 7].

From 1940 up to 1960, a significant development of modern theories about gas permeation was done by STERN [8], BARRER [9] and MEARES [10]. During that period, the current description of gas transport through the non-porous membranes via the solution and diffusion model was developed. Membrane systems for gas separation were first time commercialized in 1970, for example, hydrogen separation from carbon monoxide was possible with the use of cellulose acetate membranes [11, 12]. The main progress started with the company Monsanto, which applied the new Prism membrane systems on industrial scale [13, 14]. Prism membrane system was a novel approach to gas separations using composite hollow fiber membranes for hydrogen removal from ammonia plants and encouraged other companies to develop their own membrane technologies [14, 15]. For example, the company Cynara (NATCO) has developed the CO<sub>2</sub>/CH<sub>4</sub> gas separation systems for acid gas treatment, Kvarner has developed the H<sub>2</sub>O/hydrocarbon gas separation systems for natural gas dehydration and Permea (Air product) has developed the O<sub>2</sub>/N<sub>2</sub> gas separation systems for nitrogen generation [5].

Polymeric membranes play an important role in the industrial gas separation market with high competitiveness in performance and economics [16]. So far, hundreds of polymers have been investigated for membrane applications, including polysulfone, polyimide and cellulose acetate (Table 2.2) [5]. However, only very few have found use in industrial membrane gas separation. Among the polymers in Table 2.2, only PDMS belongs to the group of rubbery polymers. Glassy polymers are used as materials for gas separation due to their higher selectivity in contrast to the rubbery polymers which have higher permeabilities, but low selectivities. They have permeable nature for all gases at different rates; therefore in order to reach the high purity of permeate from polymer membranes, many separation stages are usually performed. Thus, effective gas separation by polymeric membranes highly depends on the designed system [17].



**TABLE 2.2.** The Permeability Coefficients of Polymers for Commercial Gas Separating Membranes.

Polymers	Permeability		at 30 °C	[Barrer]	[Barrer]
	H <sub>2</sub>	N <sub>2</sub>	O <sub>2</sub>	CH <sub>4</sub>	CO <sub>2</sub>
Polysulfone	14	0.25	1.4	0.25	5.6
Cellulose acetate	2.63	0.21	0.59	0.21	6.3
Polyimide (Matrimid)	28.1	0.32	2.13	0.25	10.7
Polycarbonate, brominated	-	0.18	1.36	0.13	4.3
Polyphenyleneoxide	113	3.81	16.8	11	76
Polymethylpentene	125	6.7	27	14.9	84.6
Polydimethylsiloxane (PDMS)	550	250	500	800	2700

### 2.1.3. Gas Transport through the Membranes

Gas transport is strongly dependent on the structural type of the membranes. Porous and non-porous membranes can be used as barrier for gas separation. Pore flow and solution-diffusion models can be used to explain the gas transport through the porous and non-porous membranes, respectively.

#### 2.1.3.1. Pore Flow Model

In the pore flow model, the relation between the pore size of a porous membrane and the mean free path of the gas molecules is the most important issue. This relation is shown in Figure 2.3 [4]. The transportation of permeants is supplied by pressure driven flow through the membrane pores. If the size of the pores is between 0.1  $\mu\text{m}$  and 10  $\mu\text{m}$ , the gas molecules pass through the membrane with convective flow resulting in no separation. However, if the pore size is smaller than 0.1  $\mu\text{m}$  (equal or smaller than the mean free path of the gas molecules), the gas molecules permeate through the membrane via KNUDSEN diffusion. This diffusion strongly depends on the molecular weight ratios of the gas molecules. Since the molecular weight ratios of most gases are not high enough to have an efficient separation, a high number of separation stages is required. In case of membranes with a pore size between 5  $\text{\AA}$  and 20  $\text{\AA}$ , separation is achieved through molecular

sieving. If the pore sizes of the membrane are between the sizes of the gas molecules, only the smaller gas molecules can easily pass through the pores, leading to a high separation factor [4].

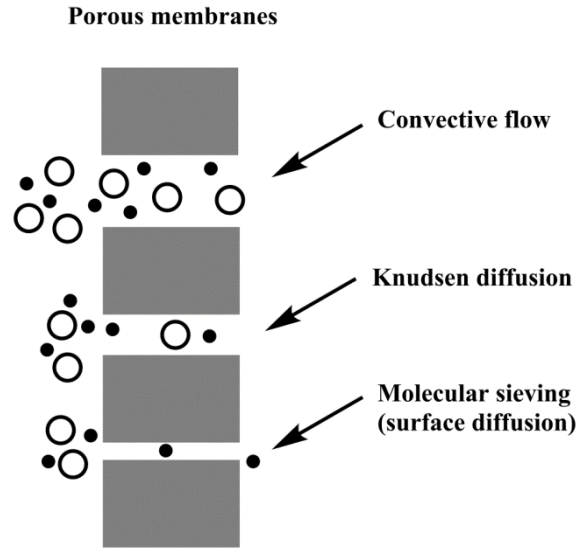


**FIGURE 2.3.** Schematic representation of pore flow model.

#### **2.1.3.2. Solution-Diffusion Model**

The gas transport in non-porous membranes can be explained by the solution-diffusion mechanism (Figure 2.4) [4]. The permeability coefficient ( $P$ ) can be described as the product of two distinctive parameters which are diffusivity ( $D$ ) and solubility ( $S$ ). The most important part is to understand the evaluation of these parameters which give the idea about how the gas molecules are dissolved and how they pass through the membrane. The solution-diffusion mechanism consists of three steps: a-) the gas molecules are adsorbed at the membrane surface on the stream side (feed side), b-) the gas molecules diffuse through the polymer matrix and c-) the gas molecules are desorbed from membrane on the downstream side (permeate side).

## Non-porous membranes

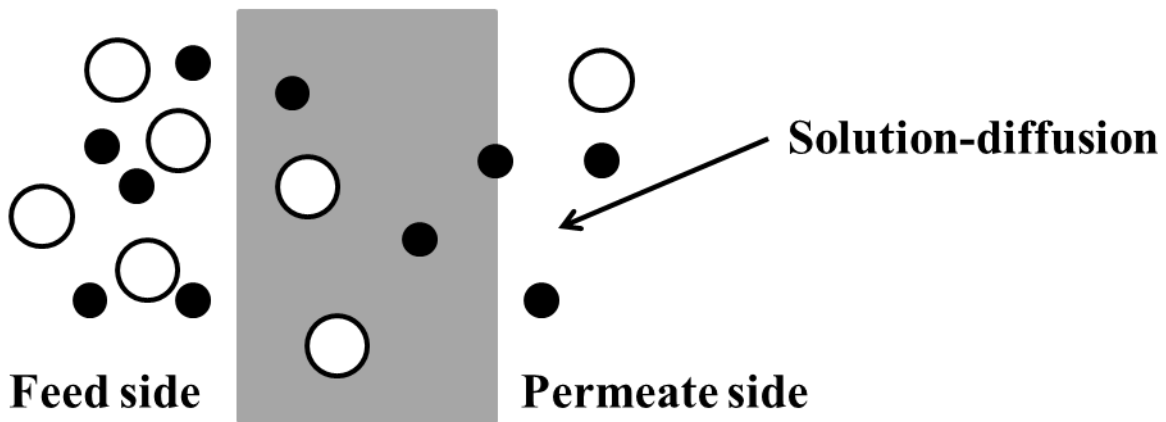


**FIGURE 2.4.** Schematic representation of solution-diffusion model

### 2.1.4. Common Definitions Describing Membrane Performance

The performance of gas separation membranes can be described by two characteristic parameters which are permeability ( $P$ ) and selectivity ( $\alpha$ ). They show the separation ability of the membrane. The permeability describes the amount of the gas molecules which permeate through the membrane per unit of time and surface area (equation 2.1)

$$P = \frac{\text{flow rate} \times \text{thickness}}{\text{area} \times \text{pressure difference}} \quad (2.1)$$

The permeability coefficient is generally given in the barrer unit introduced by RICHARD BARRER in 1951 [9]. Although barrer is a non-SI unit which is defined as  $10^{-10} \text{cm}^3 \cdot \text{cm} \cdot \text{cm}^{-2} \cdot \text{s}^{-1} (\text{cm Hg})^{-1}$ , it is a commonly used unit in the field of gas separation. 1 Barrer corresponds to  $7.5005 \times 10^{-18} \text{m}^2 \cdot \text{s}^{-1} \cdot \text{Pa}^{-1}$  in terms of SI units. The selectivity is the ratio of permeability of two gases “a” and “b” (equation 2.2). It gives a separation factor ( $\alpha_{a/b}$ ) between the gas “a” and “b” depending on their permeability value. The separation factor cannot be smaller than one. If it is equal to 1, no separation can occur.

$$\alpha_{a/b} = \frac{P_a}{P_b} \quad (2.2)$$

The concentration gradient across the membrane is the driving force required for the transport of the gas molecules through the non-porous membrane. The flux ( $J$ ) of gases can be described by FICK`'s first law (equation 2.3) [18].

$$J = -D \frac{dc}{dx} \quad (2.3)$$

where  $D$  is the diffusion coefficient and  $dc/dx$  is the concentration gradient across the membrane. According to HENRY`'s law [19], the concentration ( $c_a$ ) of a gas “a” in a polymer system is proportional to the applied pressure ( $p_a$ ) which assists to describe its solubility ( $S_a$ ) ( $\text{cm}^3(\text{STP})\cdot\text{cm}^{-3}\cdot(\text{cm Hg})^{-1}$ ) (equation 2.4).

$$c_a = S_a \times p_a \quad (2.4)$$

The integration of equation 2.3 over the membrane thickness ( $x_1 = 0$  and  $x_2 = l$ ) and substitution of equation 2.4 yields equation 2.5 under the condition of constant diffusion coefficient ( $D$ ):

$$J_a = \frac{D_a \times (c_{a,0} - c_{a,l})}{l} = \frac{D_a \times S_a (p_{a,0} - p_{a,l})}{l} \quad (2.5)$$

where  $c_{a,0}$ ,  $p_{a,0}$  and  $c_{a,l}$ ,  $p_{a,l}$  are the concentration and pressure, respectively, of gas “a” in the membrane on the upstream and downstream side.

## 2.1.5. The Relation between Structure and Gas Transport Properties

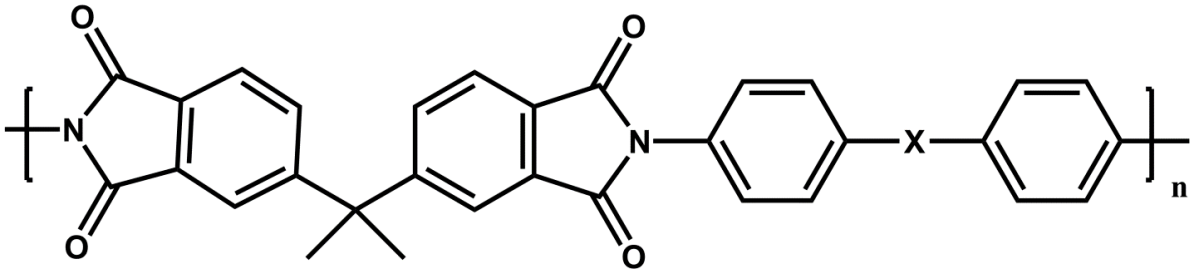
### 2.1.5.1. Glassy Polymers

The effect of chemical structure of glassy polymers on the gas permeation properties is much more significant compared to the rubbery polymers. The glassy polymers containing bulky side groups show crucial changes in gas permeation. The increased bulkiness of the side groups on the main chain of the polymers results in significantly enhanced permeability coefficients [20]. They should

be attached directly to the main chain; otherwise, the attachment via a spacer will not show the same effect. In case of glassy polymers with Si pendent groups, the substituents on the Si have also a significant impact on the gas permeation [20]. The long linear substituents on Si crucially decrease the gas permeability. Moreover, the symmetry between the substituents on Si affects the permeability, and more in detail, Si side group which contains completely symmetric substituents ( $\text{Si}(\text{CH}_3)_3$ ) has a better effect on enhancement of the permeability than non-symmetric ones ( $\text{Si}(\text{Me})_2\text{Et}$ ) [20].

The symmetrical or asymmetrical substitution of the phenylene rings on the polymers with aromatic backbones can influence the permeability [20]. Different substitution groups were used in these studies such as linear or branched alkyls,  $\text{CF}_3$  and Cl. These groups lead the polymers to have less dense chain packing, but higher free volume and permeability. Another way to increase the permeability in aromatic backbone polymers is the use of bulkier connector groups [20]. These groups make the chains of backbone stiffer resulting in dense packing declination, and thus increasing free volume and permeability. Table 2.3 shows a study about aromatic polyimides [20].

**TABLE 2.3.** The Effect of Connector Groups on Polyimides.

		
Connectors (X)	$P(\text{CO}_2)$ , Barrer <sup>a</sup>	$\alpha(\text{CO}_2/\text{CH}_4)$
-O-	23	60.5
-CH <sub>2</sub> -	19.3	44.9
-C(CH <sub>3</sub> ) <sub>2</sub> -	30	42.9
-C(CF <sub>3</sub> ) <sub>2</sub> -	63.9	39.9

<sup>a</sup> 1 barrer =  $10^{-10} \text{ cm}^3 \text{ (STP) cm}/(\text{cm}^2 \text{ s cmHg})$

Additionally, the substituents introduced to the polymer can create some intermolecular interactions between polymer chains or with some penetrants such as dipole-dipole or hydrogen bonding [20]. These interactions have a high impact on gas transport properties. As an example, over 20 wt. % carboxylated (-COOH) poly(vinyltrimethylsilane) (PVTMS) has 2-fold decreased permeability coefficients of hydrocarbon gases but 4.5-fold increased water vapors permeability coefficients [20].

#### **2.1.5.2. Rubbery Polymers**

Rubbery polymers most important characteristic is mobility of polymer chains [20]. If the mobility increases with the modification of the side group, then permeability coefficient simultaneously increases. Generally, rubbers with bulky side groups have higher glass transition temperatures ( $T_g$ ) and less chain mobility, and thus decrease permeability coefficients in contrast with glassy polymers. The bonds such as Si-O located at the main chain or as side group, lead the polymers to have higher chain mobility, gas permeability and decrease in  $T_g$  [20].

## **2.2. Copolymers**

Polymerization of two or more monomers at the same time usually gives either statistical, gradient or alternating copolymers (Figure 2.5). This is a common way to prepare polymers having improved or modified mechanical and physical properties [21-23]. The type of the polymers strongly depends on the reactivity ratio of the monomers. The ideal statistical copolymers can be prepared by choosing the monomers with reactivity ratios close to 1. That allows the radical chain ends react with either type of monomers with the same reactivity. Conventional free radical polymerization can be a useful way to obtain the statistical copolymers. Due to the different reactivity of the monomers which will directly affect their consumption in the system, the polymer chains will have varied monomer composition. Thus, random copolymers refer to a specific type

of copolymers. A wide variety of different compositional statistical copolymers can be obtained according to followed statistics such as BERNOLLI and MARKOVIAN [24-27]. If both reactivity ratios are significantly higher than 1, this will lead to a more blocky structure because of preference of homo-propagation rather than cross-propagation. In all of the common controlled radical polymerization (CRP) methods including atom transfer radical polymerization (ATRP) and nitroxide mediated polymerization (NMP) as well as other living polymerization techniques including anionic addition polymerization and ring-opening polymerization (ROP), the simultaneous growth of the chains at the same rate results in the same chemical composition of the chains. Gradient copolymers, a novel class of polymers, are synthesized by these polymerization methods [27-29]. These copolymers show a gradual change in composition along the chain from mostly one type of monomers to another type of monomer (Figure 2.5) [27]. They are intermediates between statistical and block copolymers. Gradient copolymers show different physical properties compared to random and block copolymers at the same composition [30, 31].

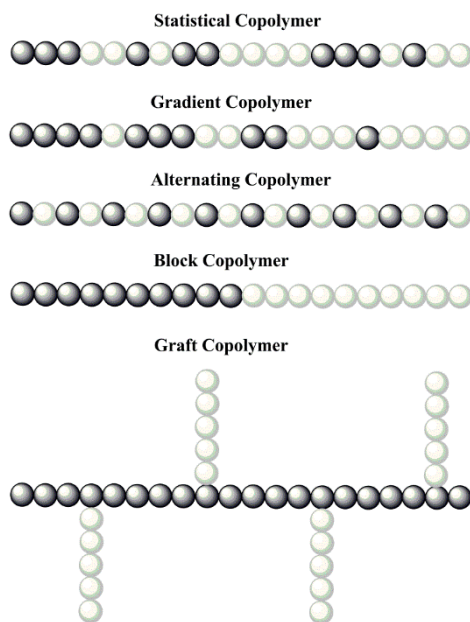


**FIGURE 2.5.** Schematic representation of various types of copolymers.

In case of reactivity ratios much lower than 1, the alternating copolymers are obtained. This indicates that both radicals will prefer to have cross-propagation. As an example, RAFT polymerization of styrene and maleic anhydride gives alternating structure at especially the temperatures below 80 °C [32]. However, when temperature increases from 80 °C to 130 °C, the copolymer type starts to change from alternating structure to random structure [32].

A block copolymer consists of a linear arrangement of blocks which are chemically bound together. The simplest example is the diblock copolymers where two chains are bound together. With an increase of block number they are named as tri-, tetra- or multiblock copolymer.

Living polymerization techniques have been used for many years to prepare block copolymers. Anionic polymerization is one of the most important techniques which provides end group control and allows to have polymers with low polydispersity index [33]. Due to recent progress in the controlled polymerization techniques such as radical, cationic, group transfer and metathesis, polymers with predetermined molecular weights and low polydispersities can be synthesized [34-36].

Block copolymers are most demanded materials because of their diverse copolymer structures [37]. The first important characteristic of block copolymers is their ability to have a combination of desired properties. As an example, a block copolymer containing a minority block with a high melting temperature ( $T_m$ ) and a majority block with a low glass transition temperature ( $T_g$ ) exhibits thermoplastic elastomeric behavior. Another example could be a block copolymer having hard block as major segment accompanied by a minority rubber block resulting in enhanced mechanical and impact properties.



The second and more significant characteristic of block copolymers is their ability to self-assemble [38]. Different polymers having particularly sufficient high molecular weight often do not mix well for enthalpic reasons as the mixing entropy is too low [39]. Therefore, they often show a tendency to form separate phases. Block copolymers have a tendency to self-assemble into a variety of well-ordered nanostructures because of immiscibility of the chemically different blocks (Figure 2.6) [40-42].

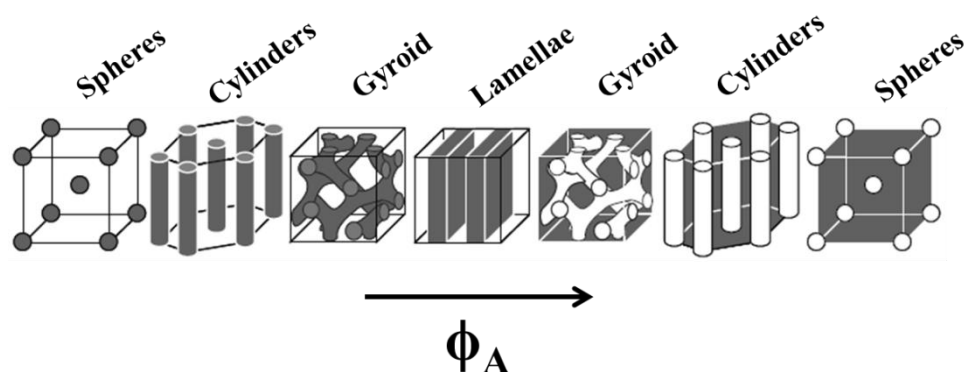


**FIGURE 2.6.** Morphologies of a diblock copolymer (AB) as function of the volume fraction of the A block [40-42].

Phase diagram for A-b-B diblock copolymers having stable microphases of body centered cubic packed spheres, hexagonal closed packed cylinders, double gyroids and alternating lamella was constructed by MATSEN and BATES [43]. With increased number of the chemically different blocks more complicated thermodynamically stable nanostructures are observed [44, 45]. The morphologies formed by diblock copolymers as a function of the volume fraction  $\phi_A$  (Figure 2.6) [46, 47].

### 2.3. Hydrosilylation Chemistry

It is well-known that certain hydrosilanes give addition reaction across the carbon-carbon multiple bonds under metal catalyst conditions. Transition metal complexes have especially been used as the catalytic system and the reaction is referred to as the hydrosilylation [48-51]. NAGAI et al. firstly reported the hydrosilylation reaction in 1972 [51]. The reaction is performed in the presence of homogeneous catalysis. There are several types of hydrosilylation under different reaction conditions which are commonly used for the modification of polyisoprene or polybutadiene rubbers [48, 49], styrene [52, 53] and cyclic olefins [54, 55]. Hydrosilylation has been called as “*the most important application of platinum in homogeneous catalysis*” [56].

Particularly, an electron rich complex of a late metal such as Co(I), Rh(I), Pd(0), or Pt(0) as a pre-catalyst activates both hydrosilanes,  $\text{HSiR}_3$ , a variety of substrates such as alkenes and alkynes. The transition metal complex,  $\text{ML}_n$  (M= metal, L= ligand), for the conventional hydrosilylation is  $\text{H}_2\text{PtCl}_6 \cdot 6\text{H}_2\text{O} / i\text{PrOH}$  (SPEIER catalyst) [57]. The mostly accepted possible mechanism of hydrosilylation was proposed by A.J. CHALK and J.F. HARROD in 1965 (Figure 2.7) [58]. The reaction starts with the oxidative addition of a hydrosilane resulting in hydro-silyl complex which is coordinated with the substrate alkene. Then, it is continuing with the migratory insertion of the alkene into the metallic hydrogen bond (M-H) to give the alkyl-silyl species. At the end, the reaction completes with a reductive elimination of the alkyl and silyl ligands which results in the formation of the hydrosilylation product. The products usually involve anti-MARKOVNIKOV addition [59]. Actually, the mechanism is similar to hydrogenation; therefore same catalysts are sometimes employed for the two catalytic processes [49, 60].

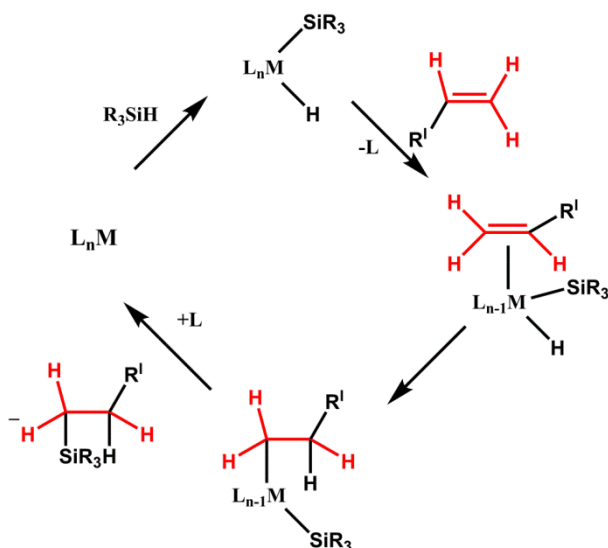


**FIGURE 2.7.** Possible mechanism of hydrosilylation.

## 2.4. Hydrogenation Chemistry

Hydrogenation is one of the most important chemical modification methods to improve the physical, chemical and thermal properties of diene based elastomers. This bases on the replacement of the radical sensitive C=C to saturated hydrocarbon bonds. Polydiene containing polymers can give degradation reaction in the presence of oxygen and UV irradiation, making them unsuitable for many applications [61, 62]. As an example, cis-1,4-polyisoprene main-chain double bonds can be saturated to a strictly alternating ethylene-propylene copolymer using diimide reduction.

There are two general methods for the hydrogenation of unsaturated polymers that are catalytic and non-catalytic. Due to the high amount production ability, catalytic hydrogenation methods are favored on the industrial scale. The hydrogenation can be performed in heterogeneous [63, 64] or homogeneous [65, 66] catalyst systems. The effect of the catalytic process toward the selective hydrogenation of unsaturated polymers bases on the catalyst activity and hydrogenation conditions [67]. Although heterogeneous catalysis had been highly effective for PI hydrogenation, it usually requires harsh conditions that can result in polymer degradation and branching [68]. In addition,

most of heterogeneous catalysts can lose the effectivity over time because of the absorption of the polymer chains onto the catalyst [63]. On the other hand, homogeneous catalysts such as WILKINSON'S catalyst [69] and Ni/Al [70] require mild reaction conditions that highly decrease the possibility of side reactions. At the same time, they are more selective and tolerant toward the presence of functional groups [67, 71]. However, particularly in case of homogeneous catalytic hydrogenations by WILKINSON'S catalyst, high pressure autoclaves [72] and long reaction times [66, 72] are required.

Non-catalytic hydrogenation approach "Diimide Hydrogenation" has milder reaction conditions and in the meantime it does not require high pressures like catalytic hydrogenation methods [66, 69]. The diimide hydrogenation starts with a thermal decomposition of *p*-toluenesulphonylhydrazide (PTSH) to *p*-toluenesulphinic acid and diimide (Figure 2.8 (1)). The diimide gives then highly specific syn-hydrogen addition to double bonds (Figure 2.8 (2)). In the hydrogenation reaction, excess amount of PTSH is used to give the quantitative modification due to the disproportionation of the diimide molecules which gives unreactive nitrogen and hydrazine (Figure 2.8 (3)).

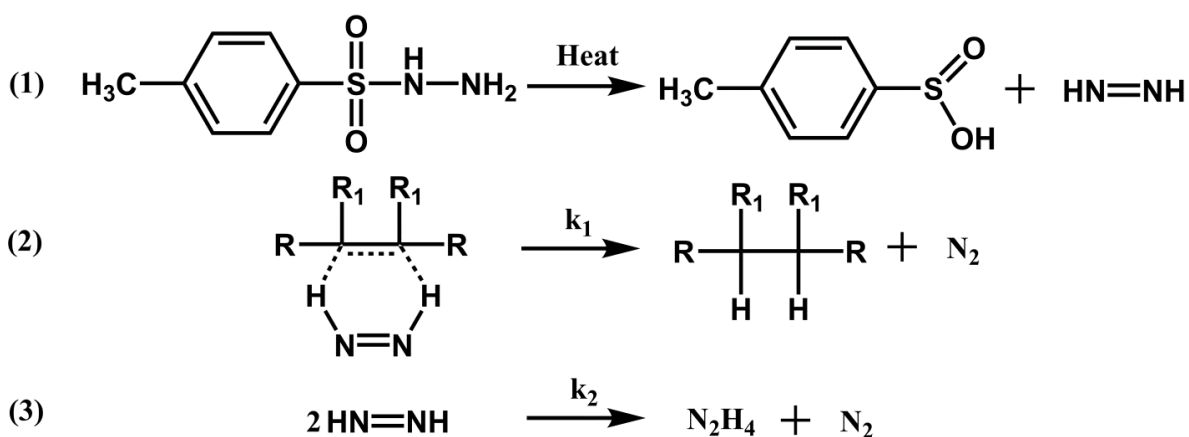


**FIGURE 2.8.** Thermally activated mechanism of hydrogenation.

## 2.5. Azide Chemistry

The first organic azide, phenyl azide, was synthesized in 1984 by PETER GRIEB [73-75]. These energy-rich and flexible intermediates have gained a crucial interest by some researchers, particularly THEODOR CURTIUS, who developed the first aliphatic diazo compound, ethyl diazoacetate, alkyl azides and acyl azides [74]. The rearrangement of acyl azides to the corresponding isocyanates was also discovered by THEODOR CURTIUS and has been known as CURTIUS rearrangement [76]. Due to the new applications in the chemistry of acyl, aryl and alkyl azides, organic azides took attention in 1950s and 1960s [73]. With the synthesis of heterocycles from azide compounds such as triazoles and tetrazoles, industrial interest started to increase to the organic azides, especially in case of their use as blowing agents and functional groups in pharmaceuticals [73].

The azide substances decompose with release of nitrogen under a slight effect of the external energy such as heat and pressure. Therefore, most of them are known as explosive compounds. Especially, the heavy-metal azides are used for the technology of explosives as detonators [77]. In spite of their explosive features, particularly organic azides are useful intermediates in the synthesis of organic compounds such as anilines [78], triazoles [79], and nitrenes [80].

The first structural proposal of azides was done by CURTIUS and HANTZSCH [73]. They suggested a cyclic 1*H*-triazirine structure, however; it was revised in the favor of the linear structure. The stabilization of the aromatic azides is supplied by the conjugation of the aromatic system (Figure 2.9) [73]. The mesomeric structure **d** explains the regioselectivity of their electrophilic (electrophiles are attacked by negative charged N) and nucleophilic (nucleophiles attack on positive charged N) reactions. Additionally, the dipolar structures of **c** and **d** clarify the decomposition ability and the reactivity.

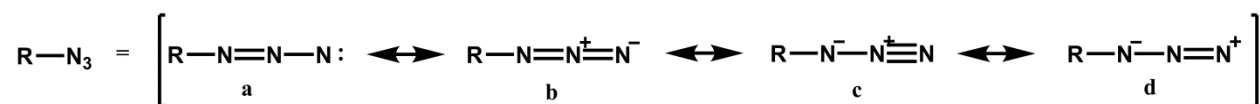


**FIGURE 2.9.** Resonance structures of azide.

There are several methods to synthesize the organic azides such as insertion of the  $\text{N}_3$  group by substitution reaction [81], insertion of  $\text{N}_2$  group by diazo transfer [82], insertion of nitrogen atom by diazotization [83] and rearrangement of azides. The classic nucleophilic substitution is one of the most applied methods to synthesize alkyl azides. The process bases on the halide displacement by azide ion. The mostly used azide source is sodium azide ( $\text{NaN}_3$ ). The reaction is commonly performed in DMF under thermal conditions [84, 85].

## 2.6. Click Chemistry

Click chemistry is a chemical term which describes the chemistry to obtain the substances rapidly and reliably by joining small units together [86]. The term was introduced by SHARPLESS in 2001 [86]. Click chemistry is a powerful strategy to synthesize new molecules and can be summarized only in one sentence: “*all searches must be restricted to molecules that are easy to make*” [86]. Furthermore, there are several criteria introduced by SHARPLESS to fulfill the requirements as reactions that: are stereospecific, high yielding, wide in scope, are modular, do not create offensive by-products, are simple to perform and require the organic solvents that have low boiling point. Nowadays, several reaction processes have been defined under this term owing to these criteria such as thiol additions to carbon-carbon multiple bonds (thiol-ene and thiol-yne); cycloaddition reactions; and nucleophilic ring opening reactions. Particularly, copper(I)-catalyzed azide-alkyne (CuAAC) reactions have gained much interest among the synthetic and polymer chemists.

### 2.6.1. Copper(I)-Catalyzed Azide-Alkyne Cycloaddition (CuAAC)

1,3-dipolar cycloaddition reactions were first introduced in 1963 by ROLF HUISGEN [87]. Afterwards, he and his co-workers reported lots of new studies between 1950 and 1970 clarifying the formulation of the general concepts of 1,3-dipolar cycloaddition reactions [88-90]. The process is intensely thermodynamically favored ( $\Delta H^\circ = -45$  to  $-55$  kcal/mol) because of the high potential energy content of the two reaction components. However, it has a relatively high kinetic energy barrier such as ca. 26 kcal/mol for methyl azide and propyne [91]. Due to these properties of the process, 1,3-cycloaddition reactions have found widespread applications in organic and polymer synthesis and have been the subject of several reviews [92-94].

TORNØE and MELDAL introduced Cu(I) catalysis for the HUISGEN 1,3-dipolar cycloaddition reaction of organic azides and alkynes in 2001 [95]. Cu(I) catalysis turned this cycloaddition reaction into a fundamentally quantitative and regioselective click reaction. The first studies were carried out by the MELDAL and the SHARPLESS laboratories [94, 96-98].

With the addition of Cu(I) catalysis to the 1,3-dipolar cycloaddition, the reaction between azide and alkyne components dramatically accelerated (Figure 2.10). This CuAAC reaction is very insensitive, general, robust and orthogonal to most other chemistries used in polymer synthesis [99].

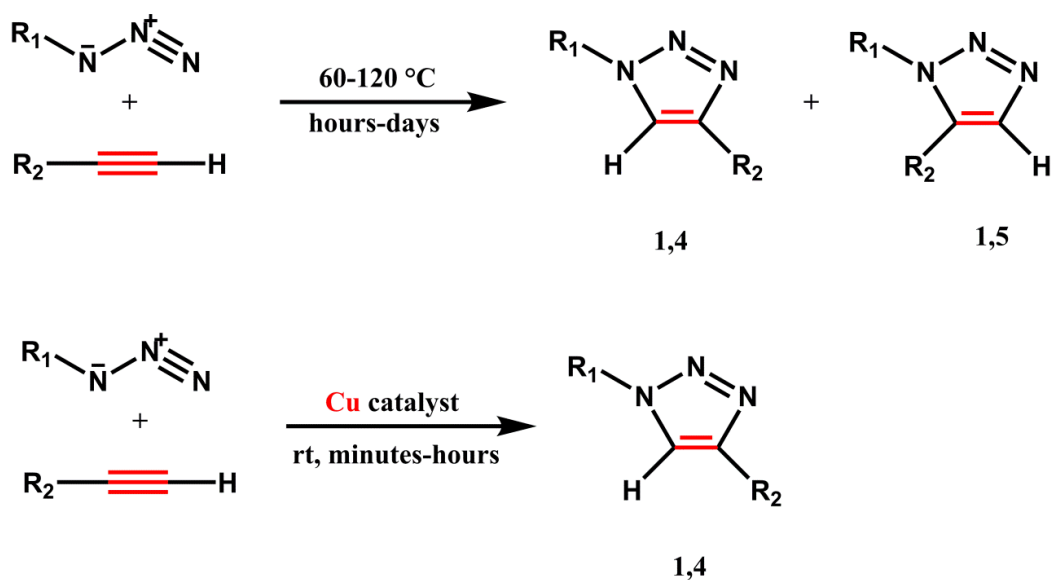


**FIGURE 2.10.** General representation of copper and thermal catalyzed cycloaddition [100].

The thermal cycloaddition of azides and alkynes requires long reaction time and high reaction temperature resulting in mixtures of the 1,4- and 1,5-disubstituted regioisomers. On the other hand, CuAAC gives as product only 1,4-disubstituted-1,2,3-triazoles at room temperature in high yields (Figure 2.10). The properties and advantages of CuAAC can be summarized as follows: a) Steric and electronic properties of the neighboring groups attached to the azide and alkyne reactive centers have not significant impact on the reaction [100]; b) Reaction is not affected by water or by most organic and inorganic groups [100]; c) Cu(I)-catalyzed process has approximately  $10^7$  times more reaction rate than that of the un-catalyzed version that makes the reaction conveniently fast in the temperature range of 0 to 25 °C. Moreover, ligand effects on the catalyst resulting in enhanced reaction rates are also significant [100, 101]; d) 1,2,3-triazole units have several advantageous properties such as high chemical stability, strong dipole moment (5.2-5.6 D), aromatic character and good hydrogen-bond-accepting ability [102].



### 2.6.2. Mechanistic Aspect of the Cu(I) Catalysis

The first mechanism for the copper catalyzed reaction was proposed by MELDAL [96], SHARPLESS [97] and their co-workers. Later, it was also verified by computational methods [103, 104].

The first proposal about the intermediacy of copper acetylides in CuAAC was based on the lack of reactivity of internal alkynes. Afterwards, some computational studies about the elementary steps of the sequence was performed which initially focused on the possible reaction pathways between copper acetylides and organic azides [103]. The proposed mechanistic cycle can be seen in Figure 2.11. The formation of the copper acetylide 2 (Step A) is an exothermic process (11.7 kcal/mol) which leads to have the intermediacy of a  $\pi$ -alkyne-copper complex. The calculations of an alkyne  $\pi$  coordination to copper showed that the pKa of the alkyne terminal proton decreases 10 times bringing it into a proper range to be deprotonated in an aqueous medium. Due to the high potential energy barrier (23.7 kcal/mol) of the concerted 1,3-dipolar cycloaddition of the azide to the copper acetylide, the metal must play an additional role. The activation of the azide is supplied by coordination to copper which forms intermediate 3 (Figure 2.11). This ligand exchange step is a nearly thermoneutral process that is, for example, 2 kcal/mol (computational calculation) for a water molecule as a ligand. The main bond-forming process starts with Step C with the transformation of 3 to the unusual 6-membered copper metallacycle 4 (Figure 2.11). This is an endothermic step (12.6 kcal/mol) with a calculated barrier of 18.7 kcal/mol which is significantly lower than the barrier for the uncatalyzed reaction (26 kcal/mol) [100]. The regiospecificity of the copper catalyzed 1,3-dipolar cycloaddition can be explained by the binding of both azide and alkyne to the copper prior for the formation of the C-C bond. Intermediate 4 has a quite low energy barrier (3.2 kcal/mol) for the ring contraction leading to the triazolyl-copper derivative 5 (Figure

2.11). With the proteolysis of intermediate 5 the triazole product is obtained and the catalytic cycle completed with Step E [100].

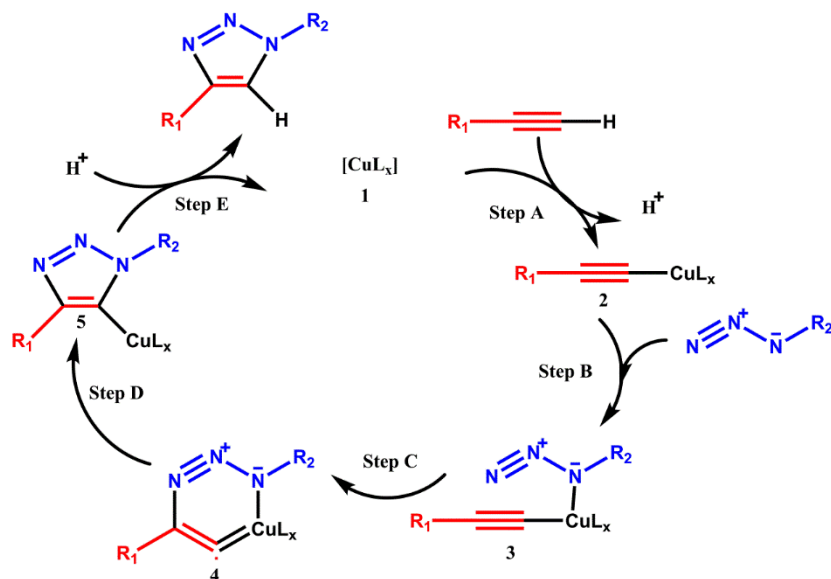


**FIGURE 2.11.** Proposed mechanism of CuAAC.

The proposed mechanism was investigated by an examination of the kinetics of the copper mediated reaction between benzyl azide and phenylacetylene described above using the density functional theory (DFT) [105]. The study revealed that the reaction was second-order in copper with the effect of catalytic Cu(I) concentrations under saturation conditions that are rate independent of the alkyne concentration [100, 106]. The high aggregation of most copper acetylides is making reasonable the second order dependence on Cu(I) [107]. In fact, the second copper atom is required for the metallacycle step (Step C) that is also suggested by recent DFT studies [99, 108].

$$rate = [alkyne]^0 [azide]^{0.2 \pm 0.1} [Cu]^{2.0 \pm 0.1} \quad (2.6)$$

## 2.7. Benzoxazine Chemistry

The benzoxazines, which are one of the most famous members of phenolic resins, were first synthesized in 1944 by COPE and HOLLY [109]. Although, in the beginning researchers paid no attention, recently there is immense interest particularly in the field of polymer research due to their excellent thermal and mechanical properties and molecular design flexibility [110]. Benzoxazine monomers are typically synthesized using phenol, formaldehyde and aliphatic or aromatic amines as starting materials in solvent or solvent-free systems [111, 112]. Various types of benzoxazine monomer can be synthesized using different types of phenols and amines with varied substitution groups. These substituting groups can act as an additional polymerizable site and also have impact on the curing process. These newly developed benzoxazine resins have unique properties such as low water absorption, near zero volumetric change during the curing process, high char-yield, no harsh conditions required for curing and no by-products [113]. An example reaction for benzoxazine formation can be seen in Figure 2.12.

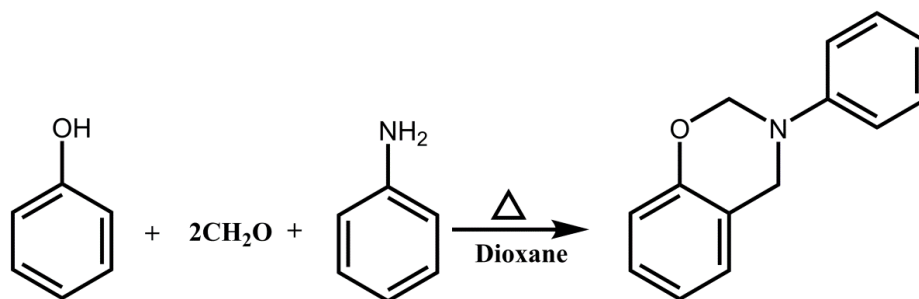


**FIGURE 2.12.** Synthesis of mono-functional 1,3-benzoxazine.

### 2.7.1. Ring Opening Polymerization of Benzoxazine

The chemical structure of the oxazine ring has the most important impact on the polymerization mechanism. According to a single crystal X-ray crystallographic study, a distorted semi-chair structure is the preferential conformation of a mono-oxazine ring of benzoxazine, in which the nitrogen and the carbon between the oxygen and the nitrogen are placed on the oxazine ring with

the benzene ring plane below and above [114]. The ring strain of such six- membered rings usually helps to give the ring opening reaction under specific conditions. The oxygen and the nitrogen on the oxazine ring have high basicity regarding to Lewis definition that lead them to be a suitable initiation site for cationic polymerization [114-116]. The prediction of the electron charge calculations after energy minimization showed that the oxygen might play an important role as the preferred polymerization site over the nitrogen due to high negative charge distribution ( $O = -0.311$ ;  $N = -0.27$ ) [117]. The thermal curing is the typical method of ring opening polymerization of benzoxazine monomers without using any catalyst (Figure 2.13) [118].

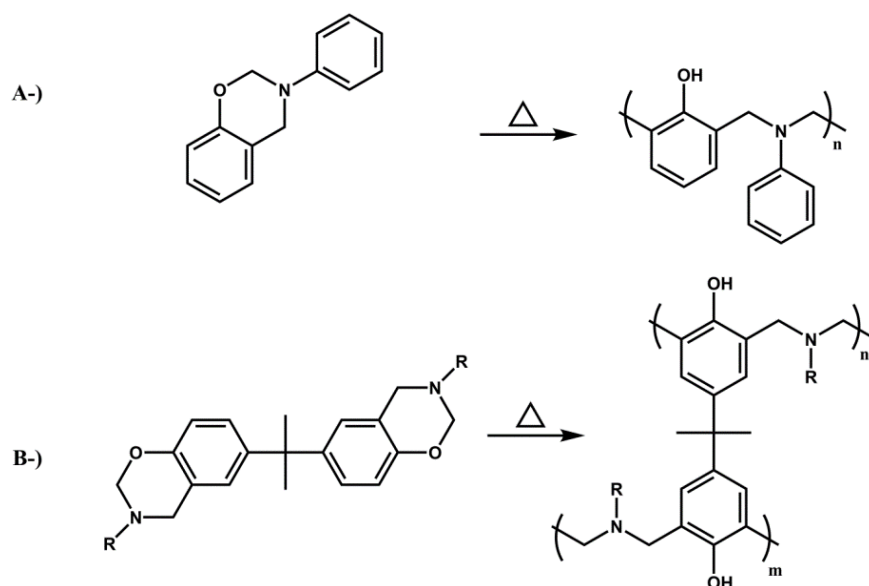


**FIGURE 2.13.** Thermally induced ring opening polymerization of mono-(A) and bisbenzoxazine (B) monomers.

One of the other polymerization methods is acid catalyzed polymerization [117, 119]. It should be emphasized that the polymerization mechanism of benzoxazines is still not well established. It has been proposed that the ring opening initiation of benzoxazine results in the formation of a carbocation and an iminium ion which exist in equilibrium (Figure 2.14) [120]. The progress of the polymerization occurs with the electrophilic substitution of the carbocation to the benzene ring.

The free *ortho* and *para* positions of the phenol group are the preferred transfer sites for the substitution reaction. The carbocation is responsible for propagation, thus the stability of the iminium ion has a crucial impact on the polymerization of benzoxazines. Moreover, the basicity of the amine groups plays an important role in the reactivity of the equilibrium pair. The increased basicity indicates to have more free-electron density of the nitrogen which provides capability to stabilize more positive charge of the iminium ion. The increase of the iminium ion stability leads to the shift in the equilibrium toward it, which directly points out the lowering in propagation rate. On contrary, the decreased stability will make the equilibrium shift toward the carbocation, so a higher propagation rate is achieved [120]. Additionally, the temperature has also an important effect on the propagation since the reaction involves the chain transfer to a benzene ring. According to the kinetic studies, at early stages of polymerization there is relatively less dependency on the the cure temperature, however, in the further stages of propagation the importance of the temperature becomes more evident in the reaction kinetics.

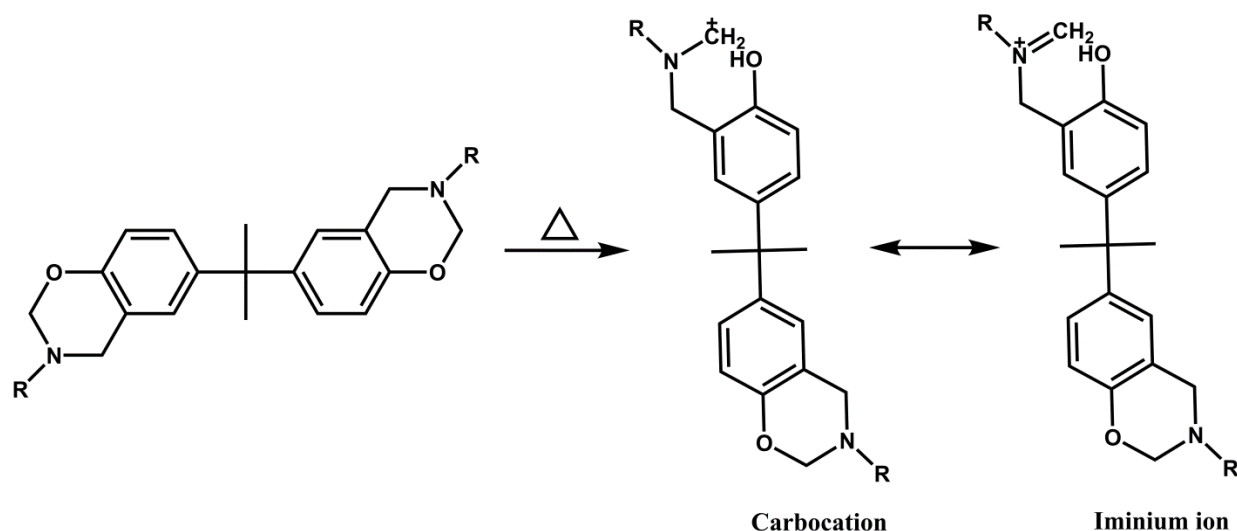


**FIGURE 2.14.** Ring opening initiation of bisbenzoxazine monomer.

## 2.8. References

- [1] J. Glater, The early history of reverse osmosis membrane development, *Desalination*, 117 (1998) 297-309.
- [2] M. Mulder, *Basic Principles of Membrane Technology* Second Edition, Kluwer Academic Pub, 1996.
- [3] R. Baker, *Membrane technology and applications*, John Wiley & Sons, 2012.
- [4] R.W. Baker, Overview of membrane science and technology, *Membrane Technology and Applications*, Second Edition, (2004) 1-14.
- [5] S.P. Nunes, K.-V. Peinemann, *Membrane technology: in the chemical industry*, John Wiley & Sons, 2006.
- [6] T. Graham, LV. On the absorption and dialytic separation of gases by colloid septa, *The London, Edinburgh, and Dublin Philosophical Magazine and Journal of Science*, 32 (1866) 401-420.
- [7] M. Kelly, John Kearsley Mitchell (1793–1858) and the neurogenic theory of arthritis, *Journal of the History of Medicine and Allied Sciences*, 20 (1965) 151-156.
- [8] S. Stern, W. Walawender Jr, Analysis of membrane separation parameters, *Separation Science and Technology*, 4 (1969) 129-159.
- [9] R.M. Barrer, *Diffusion in and through solids*, University Press Cambridge, 1951.
- [10] P. Meares, The diffusion of gases through polyvinyl acetate, *Journal of the American Chemical Society*, 76 (1954) 3415-3422.
- [11] W.J. Schell, Gas separation membranes, in, *Google Patents*, 1979.
- [12] A. Coady, J. Davis, CO<sub>2</sub> recovery by gas permeation, *Chemical Engineering Progress*, 78 (1982) 43.

- [13] A. Tabe-Mohammadi, A review of the applications of membrane separation technology in natural gas treatment, *Separation Science and Technology*, 34 (1999) 2095-2111.
- [14] A. Fouda, Y. Chen, J. Bai, T. Matsuura, Wheatstone bridge model for the laminated polydimethylsiloxane/polyethersulfone membrane for gas separation, *Journal of Membrane Science*, 64 (1991) 263-271.
- [15] W. Koros, G. Fleming, Membrane-based gas separation, *Journal of Membrane Science*, 83 (1993) 1-80.
- [16] S. Alexander Stern, Polymers for gas separations: the next decade, *Journal of Membrane Science*, 94 (1994) 1-65.
- [17] K. Ghosal, B.D. Freeman, Gas separation using polymer membranes: an overview, *Polymers for Advanced Technologies*, 5 (1994) 673-697.
- [18] A. Fick, V. On liquid diffusion, *The London, Edinburgh, and Dublin Philosophical Magazine and Journal of Science*, 10 (1855) 30-39.
- [19] S. Stern, H. Frisch, The selective permeation of gases through polymers, *Annual Review of Materials Science*, 11 (1981) 523-550.
- [20] Y. Yampolskii, Polymeric gas separation membranes, *Macromolecules*, 45 (2012) 3298-3311.
- [21] S. Rangou, S. Shishatskiy, V. Filiz, V. Abetz, Poly(vinyl trimethylsilane) and block copolymers of vinyl trimethylsilane with isoprene: Anionic polymerization, morphology and gas transport properties, *European Polymer Journal*, 47 (2011) 723-729.
- [22] N. Gladkova, S. Durgar'yan, Synthesis of the AB type block copolymers (polyvinyltrimethylsilane-polydimethylsiloxane), *Polymer Science USSR*, 26 (1984) 1642-1648.

- [23] S. Durgar'yan, V. Filippova, Synthesis and properties of three-block copolymers poly (dimethylsiloxane)-poly (vinyltrimethylsilane)-poly (dimethylsiloxane), *Polymer Science USSR*, 28 (1986) 364-370.
- [24] J. Kasperczyk, M. Bero, Coordination polymerization of lactides, 4. The role of transesterification in the copolymerization of L,L-lactide and  $\epsilon$ -caprolactone, *Die Makromolekulare Chemie*, 194 (1993) 913-925.
- [25] H. Cheng, Markovian statistics and simplex algorithm for carbon-13 nuclear magnetic resonance spectra of ethylene-propylene copolymers, *Analytical Chemistry*, 54 (1982) 1828-1833.
- [26] Y. Feng, J. Hay, The characterisation of random propylene-ethylene copolymer, *Polymer*, 39 (1998) 6589-6596.
- [27] K. Matyjaszewski, M.J. Ziegler, S.V. Arehart, D. Greszta, T. Pakula, Gradient copolymers by atom transfer radical copolymerization, *Journal of Physical Organic Chemistry*, 13 (2000) 775-786.
- [28] K. Davis, K. Matyjaszewski, Statistical, gradient, block, and graft copolymers by controlled/living radical polymerizations, in: Springer Berlin Heidelberg, 2002, pp. 1-13.
- [29] M.M. Mok, J. Kim, J.M. Torkelson, Gradient copolymers with broad glass transition temperature regions: Design of purely interphase compositions for damping applications, *Journal of Polymer Science Part B: Polymer Physics*, 46 (2008) 48-58.
- [30] T. Pakula, K. Matyjaszewski, Copolymers with controlled distribution of comonomers along the chain, 1. Structure, thermodynamics and dynamic properties of gradient copolymers. Computer simulation, *Macromolecular Theory and Simulations*, 5 (1996) 987-1006.



- [31] K. Karaky, E. Péré, C. Pouchan, J. Desbrières, C. Dérail, L. Billon, Effect of the synthetic methodology on molecular architecture: from statistical to gradient copolymers, *Soft Matter*, 2 (2006) 770-778.
- [32] M.-Q. Zhu, L.-H. Wei, M. Li, L. Jiang, F.-S. Du, Z.-C. Li, F.-M. Li, A unique synthesis of a well-defined block copolymer having alternating segments constituted by maleic anhydride and styrene and the self-assembly aggregating behavior thereof, *Chemical Communications*, (2001) 365-366.
- [33] M. Szwarc, Termination of anionic polymerization, in: *Fortschritte Der Hochpolymeren-Forschung*, Springer, 1960, pp. 275-306.
- [34] B. Novak, W. Risse, R. Grubbs, The development of well-defined catalysts for ring-opening olefin metathesis polymerizations (ROMP), in: *Polymer synthesis oxidation processes*, Springer, 1992, pp. 47-72.
- [35] K. Matyjaszewski, T.P. Davis, *Handbook of radical polymerization*, Wiley Online Library, 2002.
- [36] T. Pernecker, J.P. Kennedy, B. Ivan, Living carbocationic polymerization. 48. Poly (isobutylene-*b*-methyl vinyl ether), *Macromolecules*, 25 (1992) 1642-1647.
- [37] A. Noshay, J.E. McGrath, *Block copolymers: overview and critical survey*, Academic Press New York, 1977.
- [38] G.M. Whitesides, J.P. Mathias, C.T. Seto, Molecular self-assembly and nanochemistry: a chemical strategy for the synthesis of nanostructures, in, *DTIC Document*, 1991.
- [39] A.-V. Ruzette, L. Leibler, Block copolymers in tomorrow's plastics, *Nature Materials*, 4 (2005) 19-31.

- [40] L. Leibler, Theory of microphase separation in block copolymers, *Macromolecules*, 13 (1980) 1602-1617.
- [41] M. Li, C.K. Ober, Block copolymer patterns and templates, *Materials Today*, 9 (2006) 30-39.
- [42] F.S. Bates, G.H. Fredrickson, Block copolymer thermodynamics: theory and experiment, *Annual Review of Physical Chemistry*, 41 (1990) 525-557.
- [43] M. Matsen, F. Bates, Unifying weak-and strong-segregation block copolymer theories, *Macromolecules*, 29 (1996) 1091-1098.
- [44] Y. Bohbot-Raviv, Z.-G. Wang, Discovering new ordered phases of block copolymers, *Physical Review Letters*, 85 (2000) 3428.
- [45] H. Elbs, C. Drummer, V. Abetz, G. Krausch, Thin film morphologies of ABC triblock copolymers prepared from solution, *Macromolecules*, 35 (2002) 5570-5577.
- [46] C.A. Tyler, J. Qin, F.S. Bates, D.C. Morse, SCFT study of nonfrustrated ABC triblock copolymer melts, *Macromolecules*, 40 (2007) 4654-4668.
- [47] V. Raman, R. Sharma, T.A. Hatton, B.D. Olsen, Magnet field induced morphological transitions in block copolymer/superparamagnetic nanoparticle composites, *ACS Macro Letters*, 2 (2013) 655-659.
- [48] B.N. Gacal, V. Filiz, S. Shishatskiy, S. Rangou, S. Neumann, V. Abetz, Modification of polyisoprene-block-poly(vinyl trimethylsilane) block copolymers via hydrosilylation and hydrogenation, and their gas transport properties, *Journal of Polymer Science Part B: Polymer Physics*, 51 (2013) 1252-1261.
- [49] X. Guo, R. Farwaha, G.L. Rempel, Catalytic hydrosilylation of diene-based polymers. 1. Hydrosilylation of polybutadiene, *Macromolecules*, 23 (1990) 5047-5054.

- [50] B. Marciniec, Hydrosilylation Polymerisation, in: B. Marciniec (Ed.) Hydrosilylation, Springer Netherlands, 2009, pp. 191-214.
- [51] I. Ojima, M. Nihonyanagi, Y. Nagai, Rhodium complex catalysed hydrosilylation of carbonyl compounds, *Journal of the Chemical Society, Chemical Communications*, (1972) 938a-938a.
- [52] A. Onopchenko, E.T. Sabourin, D.L. Beach, Rhodium(I)-catalyzed hydrosilylation of styrene, *The Journal of Organic Chemistry*, 48 (1983) 5101-5105.
- [53] W.R. Cullen, N. Fong Han, Polymer supported ferrocene derivatives. Catalytic hydrosilylation of olefins by supported palladium and platinum complexes, *Journal of Organometallic Chemistry*, 333 (1987) 269-280.
- [54] L.F. Kelly, A.S. Narula, A.J. Birch, Organometallic compounds in organic synthesis : electrophilic reactions of some tricarbonylcyclohexadienyl-iron complexes with allyltrimethyl silanes, *Tetrahedron Letters*, 21 (1980) 871-874.
- [55] Y. Uozumi, T. Hayashi, Asymmetric hydrosilylation of dihydrofurans by use of palladium-MOP catalyst, *Tetrahedron Letters*, 34 (1993) 2335-2338.
- [56] H. Renner, G. Schlamp, I. Kleinwächter, E. Drost, H.M. Lüscho, P. Tews, P. Panster, M. Diehl, J. Lang, T. Kreuzer, A. Knödler, K.A. Starz, K. Dermann, J. Rothaut, R. Drieselmann, C. Peter, R. Schiele, Platinum group metals and compounds, in: *Ullmann's Encyclopedia of Industrial Chemistry*, Wiley-VCH Verlag GmbH & Co. KGaA, 2000.
- [57] J.L. Speier, Homogeneous catalysis of hydrosilation by transition metals, in: F.G.A. Stone, W. Robert (Eds.) *Advances in Organometallic Chemistry*, Academic Press, 1979, pp. 407-447.
- [58] A.J. Chalk, J.F. Harrod, Homogeneous catalysis. II. The mechanism of the hydrosilation of olefins catalyzed by group VIII metal complexes, *Journal of the American Chemical Society*, 87 (1965) 16-21.

- [59] B. Marciniec, Hydrosilylation of alkenes and their derivatives, in: B. Marciniec (Ed.) Hydrosilylation, Springer Netherlands, 2009, pp. 3-51.
- [60] A.J. Birch, D.H. Williamson, Homogeneous hydrogenation catalysts in organic Synthesis, in: Organic Reactions, John Wiley & Sons, Inc., 2004.
- [61] L.A. Mango, R.W. Lenz, Hydrogenation of unsaturated polymers with diimide, *Die Makromolekulare Chemie*, 163 (1973) 13-36.
- [62] P. Phinyocheep, S. Pasiri, O. Tavichai, Diimide hydrogenation of isoprene–styrene diblock copolymers, *Journal of Applied Polymer Science*, 87 (2003) 76-82.
- [63] M.D. Gehlsen, F.S. Bates, Heterogeneous catalytic hydrogenation of polystyrene: thermodynamics of poly(vinylcyclohexane)-containing diblock copolymers, *Macromolecules*, 26 (1993) 4122-4127.
- [64] M.D. Watson, K.B. Wagener, Tandem homogeneous metathesis/heterogeneous hydrogenation: preparing model ethylene/CO<sub>2</sub> and ethylene/CO copolymers, *Macromolecules*, 33 (2000) 3196-3201.
- [65] L. Stahl, The handbook of homogeneous hydrogenation, Volumes 1–3 Edited by Johannes G. de Vries (DSM Pharmaceutical Products, Geleen, The Netherlands) and Cornelis J. Elsevier (Universiteit van Amsterdam, The Netherlands), *Journal of the American Chemical Society*, 129 (2007) 10297-10298.
- [66] H. Schmalz, A. Böker, R. Lange, G. Krausch, V. Abetz, Synthesis and properties of ABA and ABC triblock copolymers with glassy (A), elastomeric (B), and crystalline (C) blocks, *Macromolecules*, 34 (2001) 8720-8729.
- [67] N.A. Mohammadi, G.L. Rempel, Homogeneous selective catalytic hydrogenation of C=C in acrylonitrile-butadiene copolymer, *Macromolecules*, 20 (1987) 2362-2368.

- [68] V. Balsamo, A.J. Müller, F. von Gyldenfeldt, R. Stadler, Ternary ABC block copolymers based on one glassy and two crystallizable blocks: polystyrene-block-polyethylene-block-poly( $\epsilon$ -caprolactone), *Macromolecular Chemistry and Physics*, 199 (1998) 1063-1070.
- [69] U. Breiner, U. Krappe, V. Abetz, R. Stadler, Cylindrical morphologies in asymmetric ABC triblock copolymers, *Macromolecular Chemistry and Physics*, 198 (1997) 1051-1083.
- [70] S. Smeds, D. Murzin, T. Salmi, Kinetics of ethylbenzene hydrogenation on Ni/Al<sub>2</sub>O<sub>3</sub>, *Applied Catalysis A: General*, 125 (1995) 271-291.
- [71] J.M. Yu, Y. Yu, P. Dubois, P. Teyssié, R. Jérôme, Synthesis and characterization of hydrogenated poly[alkylmethacrylate(-b-styrene)-b-butadiene-b-(styrene-b-) alkylmethacrylate] triblock and pentablock copolymers, *Polymer*, 38 (1997) 3091-3101.
- [72] C. Auschra, R. Stadler, Synthesis of block copolymers with poly(methyl methacrylate): P(B-b-MMA), P(EB-b-MMA), P(S-b-B-b-MMA) and P(S-b-EB-b-MMA), *Polymer Bulletin*, 30 (1993) 257-264.
- [73] S. Bräse, C. Gil, K. Knepper, V. Zimmermann, Organic azides: an exploding diversity of a unique class of compounds, *Angewandte Chemie International Edition*, 44 (2005) 5188-5240.
- [74] S. Bräse, K. Banert, *Organic azides: syntheses and applications*, Wiley, 2010.
- [75] J. Boyer, F. Canter, Alkyl and aryl azides, *Chemical Reviews*, 54 (1954) 1-57.
- [76] T. Curtius, 20. Hydrazide und azide organischer säuren I. Abhandlung, *Journal für Praktische Chemie*, 50 (1894) 275-294.
- [77] J.O. Wear, CXX. Azide hazards with automatic blood cell counters, *Journal of Chemical Education*, 52 (1975) A23.

- [78] T.Y. Liang, G.B. Schuster, Photochemistry of 3-and 4-nitrophenyl azide: detection and characterization of reactive intermediates, *Journal of the American Chemical Society*, 109 (1987) 7803-7810.
- [79] V.V. Rostovtsev, L.G. Green, V.V. Fokin, K.B. Sharpless, A stepwise huisgen cycloaddition process: copper (I)-catalyzed regioselective “ligation” of azides and terminal alkynes, *Angewandte Chemie*, 114 (2002) 2708-2711.
- [80] A. Reiser, G. Bowes, R. Horne, Photolysis of aromatic azides. Part 1.—Electronic spectra of aromatic nitrenes and their parent azides, *Transactions of the Faraday Society*, 62 (1966) 3162-3169.
- [81] B.N. Gacal, B. Koz, B. Gacal, B. Kiskan, M. Erdogan, Y. Yagci, Pyrene functional poly(vinyl alcohol) by “click” chemistry, *Journal of Polymer Science Part A: Polymer Chemistry*, 47 (2009) 1317-1326.
- [82] P.B. Alper, S.-C. Hung, C.-H. Wong, Metal catalyzed diazo transfer for the synthesis of azides from amines, *Tetrahedron Letters*, 37 (1996) 6029-6032.
- [83] R. Butler, Diazotization of heterocyclic primary amines, *Chemical Reviews*, 75 (1975) 241-257.
- [84] A.P. Vogt, B.S. Sumerlin, An efficient route to macromonomers via ATRP and click chemistry, *Macromolecules*, 39 (2006) 5286-5292.
- [85] X. Zhang, Z. Zhong, R. Zhuo, Preparation of azido polycarbonates and their functionalization via click chemistry, *Macromolecules*, 44 (2011) 1755-1759.
- [86] H.C. Kolb, M.G. Finn, K.B. Sharpless, Click chemistry: diverse chemical function from a few good reactions, *Angewandte Chemie International Edition*, 40 (2001) 2004-2021.

- [87] R. Huisgen, 1,3-Dipolare cycloadditionen rückschau und ausblick, *Angewandte Chemie*, 75 (1963) 604-637.
- [88] R.S. Clegg, S.M. Reed, R.K. Smith, B.L. Barron, J.A. Rear, J.E. Hutchison, The interplay of lateral and tiered interactions in stratified self-organized molecular assemblies, *Langmuir*, 15 (1999) 8876-8883.
- [89] P.A. Lewis, R.K. Smith, K.F. Kelly, L.A. Bumm, S.M. Reed, R.S. Clegg, J.D. Gunderson, J.E. Hutchison, P.S. Weiss, The role of buried hydrogen bonds in self-assembled mixed composition thiols on Au{111}, *The Journal of Physical Chemistry B*, 105 (2001) 10630-10636.
- [90] R.K. Smith, P.A. Lewis, P.S. Weiss, Patterning self-assembled monolayers, *Progress in Surface Science*, 75 (2004) 1-68.
- [91] R.K. Smith, S.M. Reed, P.A. Lewis, J.D. Monnell, R.S. Clegg, K.F. Kelly, L.A. Bumm, J.E. Hutchison, P.S. Weiss, Phase separation within a binary self-assembled monolayer on Au{111} driven by an amide-containing alkanethiol, *The Journal of Physical Chemistry B*, 105 (2001) 1119-1122.
- [92] F. Amblard, J.H. Cho, R.F. Schinazi, Cu(I)-catalyzed huisgen azide–alkyne 1,3-dipolar cycloaddition reaction in nucleoside, nucleotide, and oligonucleotide chemistry, *Chemical Reviews*, 109 (2009) 4207-4220.
- [93] N. Karousis, N. Tagmatarchis, D. Tasis, Current progress on the chemical modification of carbon nanotubes, *Chemical Reviews*, 110 (2010) 5366-5397.
- [94] M. Meldal, C.W. Tornøe, Cu-catalyzed azide–alkyne cycloaddition, *Chemical Reviews*, 108 (2008) 2952-3015.

- [95] C. Tornøe, M. Meldal, Peptidotriazoles: Copper (I)-catalyzed 1, 3-dipolar cycloadditions on solid-phase, in: PEPTIDES-AMERICAN SYMPOSIUM-, Kluwer Academic Publishers, 2001, pp. 263-264.
- [96] C.W. Tornøe, C. Christensen, M. Meldal, Peptidotriazoles on solid phase: [1,2,3]-triazoles by regiospecific copper(I)-catalyzed 1,3-dipolar cycloadditions of terminal alkynes to azides, *The Journal of Organic Chemistry*, 67 (2002) 3057-3064.
- [97] V.V. Rostovtsev, L.G. Green, V.V. Fokin, K.B. Sharpless, A stepwise Huisgen cycloaddition process: copper(I)-catalyzed regioselective “ligation” of azides and terminal alkynes, *Angewandte Chemie International Edition*, 41 (2002) 2596-2599.
- [98] F. Himo, T. Lovell, R. Hilgraf, V.V. Rostovtsev, L. Noodleman, K.B. Sharpless, V.V. Fokin, Copper(I)-catalyzed synthesis of azoles. DFT study predicts unprecedented reactivity and intermediates, *Journal of the American Chemical Society*, 127 (2004) 210-216.
- [99] M. Meldal, Polymer “clicking” by CuAAC reactions, *Macromolecular Rapid Communications*, 29 (2008) 1016-1051.
- [100] P. Wu, V.V. Fokin, Catalytic azide-alkyne cycloaddition: reactivity and applications, *Aldrichimica Acta*, 40 (2007) 7-17.
- [101] N.V. Tsarevsky, B.S. Sumerlin, K. Matyjaszewski, Step-growth “click” coupling of telechelic polymers prepared by atom transfer radical polymerization, *Macromolecules*, 38 (2005) 3558-3561.
- [102] V.P. Krivopalov, O.P. Shkurko, 1, 2, 3-Triazole and its derivatives. Development of methods for the formation of the triazole ring, *Russian Chemical Reviews*, 74 (2005) 339.



- [103] F. Himo, T. Lovell, R. Hilgraf, V.V. Rostovtsev, L. Noodleman, K.B. Sharpless, V.V. Fokin, Copper (I)-catalyzed synthesis of azoles. DFT study predicts unprecedented reactivity and intermediates, *Journal of the American Chemical Society*, 127 (2005) 210-216.
- [104] W.H. Binder, R. Sachsenhofer, 'Click'chemistry in polymer and materials science, *Macromolecular Rapid Communications*, 28 (2007) 15-54.
- [105] J.E. Hein, V.V. Fokin, Copper-catalyzed azide-alkyne cycloaddition (CuAAC) and beyond: new reactivity of copper(i) acetylides, *Chemical Society Reviews*, 39 (2010) 1302-1315.
- [106] V.O. Rodionov, V.V. Fokin, M. Finn, Mechanism of the ligand-free CuI-catalyzed azide-alkyne cycloaddition reaction, *Angewandte Chemie*, 117 (2005) 2250-2255.
- [107] A.J. Link, M.K. Vink, D.A. Tirrell, Presentation and detection of azide functionality in bacterial cell surface proteins, *Journal of the American Chemical Society*, 126 (2004) 10598-10602.
- [108] M. Sawa, T.-L. Hsu, T. Itoh, M. Sugiyama, S.R. Hanson, P.K. Vogt, C.-H. Wong, Glycoproteomic probes for fluorescent imaging of fucosylated glycans in vivo, *Proceedings of the National Academy of Sciences*, 103 (2006) 12371-12376.
- [109] F.W. Holly, A.C. Cope, Condensation products of aldehydes and ketones with o-aminobenzyl alcohol and o-hydroxybenzylamine, *Journal of the American Chemical Society*, 66 (1944) 1875-1879.
- [110] J. Liu, H. Ishida, J. Salamone, *The polymeric materials encyclopedia*, Salamone, JC, Ed, (1996) 484.
- [111] T. Takeichi, T. Kano, T. Agag, Synthesis and thermal cure of high molecular weight polybenzoxazine precursors and the properties of the thermosets, *Polymer*, 46 (2005) 12172-12180.

- [112] A. Chernykh, T. Agag, H. Ishida, Effect of polymerizing diacetylene groups on the lowering of polymerization temperature of benzoxazine groups in the highly thermally stable, main-chain-type polybenzoxazines, *Macromolecules*, 42 (2009) 5121-5127.
- [113] C. Nair, Advances in addition-cure phenolic resins, *Progress in Polymer Science*, 29 (2004) 401-498.
- [114] Y.-X. Wang, H. Ishida, Cationic ring-opening polymerization of benzoxazines, *Polymer*, 40 (1999) 4563-4570.
- [115] C. Liu, D. Shen, R.M.a. Sebastián, J. Marquet, R. Schönfeld, Mechanistic studies on ring-opening polymerization of benzoxazines: a mechanistically based catalyst design, *Macromolecules*, 44 (2011) 4616-4622.
- [116] P. Chutayothin, H. Ishida, Cationic ring-opening polymerization of 1, 3-benzoxazines: mechanistic study using model compounds, *Macromolecules*, 43 (2010) 4562-4572.
- [117] Y.-X. Wang, H. Ishida, Synthesis and properties of new thermoplastic polymers from substituted 3, 4-dihydro-2 H-1, 3-benzoxazines, *Macromolecules*, 33 (2000) 2839-2847.
- [118] H. Ishida, Y. Rodriguez, Curing kinetics of a new benzoxazine-based phenolic resin by differential scanning calorimetry, *Polymer*, 36 (1995) 3151-3158.
- [119] R. Andreu, J. Reina, J. Ronda, Carboxylic acid-containing benzoxazines as efficient catalysts in the thermal polymerization of benzoxazines, *Journal of Polymer Science Part A: Polymer Chemistry*, 46 (2008) 6091-6101.
- [120] Y. Yagci, B. Kiskan, N.N. Ghosh, Recent advancement on polybenzoxazine—a newly developed high performance thermoset, *Journal of Polymer Science Part A: Polymer Chemistry*, 47 (2009) 5565-5576.

## Chapter 3

### Experimental Part

#### 3.1. Materials

*p*-Toluenesulfonyl hydrazide (*p*-TSH, 97 %, Aldrich), Wilkinson's catalyst, tris(triphenylphosphine)rhodium(I) chloride ( $\text{RhCl}(\text{PPh}_3)_3$ ), Aldrich), triethylsilane (99 %, Aldrich), toluene (for analysis, Merck), ethanol (absolute for analysis, Merck), *o*-xylene ( $\geq 99$  %, Sigma-Aldrich), poly(epichlorohydrin) and poly[(ethylene oxide)-*ran*-(epichlorohydrin)] (HYDRIN H-55, and HYDRIN C-70CG (65 % ethylene oxide), ZEON Chemicals), sodium azide ( $\text{NaN}_3$ ,  $\geq 99$  %, Sigma-Aldrich), tetrabutylammonium iodide (TBAI,  $\geq 99$  %, Aldrich), *N,N*-dimethylformamide ( $\geq 99$  %, Merck), bifunctional hydroxyl poly(ethylene glycol) (HO-PEG-OH) (400 and 600 g/mol, Merck), methanesulfonyl chloride ( $\text{MsCl}$ ,  $\geq 99.7$  %, Sigma-Aldrich), dichloromethane ( $\geq 99.8$  %, anhydrous, Sigma-Aldrich), magnesium sulfate ( $\text{MgSO}_4$ ,  $\geq 99.8$  %, anhydrous, Sigma-Aldrich), triethylamine (TEA,  $\geq 99.8$  % GC, Fluka), hydrochloric acid ( $\text{HCl}$ , 37 %, Merck), sodium hydroxide ( $\text{NaOH}$ ,  $\geq 98$  %, Sigma-Aldrich), sodium chloride ( $\text{NaCl}$ ,  $\geq 99.5$  %, Merck), 1,4-diethynylbenzene (96 %, Aldrich), copper(I) bromide ( $\text{CuBr}$ , 98 %, Aldrich), 4-ethynylaniline (97 %, Aldrich), bisphenol A ( $\geq 99$  %, Aldrich), *N,N,N',N'',N'''*-pentamethyldiethylenetriamine (PMDETA, 99 %, Aldrich), paraformaldehyde (95 %, Aldrich) and xylenes ( $\geq 98.5$  %, Aldrich), tetrahydrofuran (THF,  $\geq 99.9$  %, Sigma-Aldrich), diethyl ether ( $\geq 99.9$  %, Sigma-Aldrich) were used as received.

Argon with purity 99.999 % was purchased from Linde AG and used as received.

## 3.2. Synthesis and Modification

### 3.2.1. Synthesis of Polyisoprene-*block*-Poly(vinyl trimethylsilane) (PI-*b*-PVTMS)

PI-*b*-PVTMS block copolymers were synthesized by Dr. Sofia Rangou from Helmholtz-Zentrum Geesthacht (HZG) as described elsewhere [1].

### 3.2.2. Modification of PI-*b*-PVTMS via Hydrosilylation (Hs-PI-*b*-PVTMS)

Hydrosilylation of isoprene units was carried out under argon atmosphere in a three-necked round-bottomed flask with an argon inlet and outlet, a reflux condenser and a magnetic bar at 110 °C in toluene. Triethylsilane (1:1; in terms of double bond moieties) was added dropwise to a solution of PI-*b*-PVTMS (2 g, 29.21 mmol) and additionally Wilkinson's catalyst ( $\text{RhCl}(\text{PPh}_3)_3$  ( $29.21 \times 10^{-3}$  mmol)). The mixture was stirred for one day. The modified polymer was precipitated in ethanol (5 times excess) and dissolved in toluene three times, filtered and dried under vacuum.

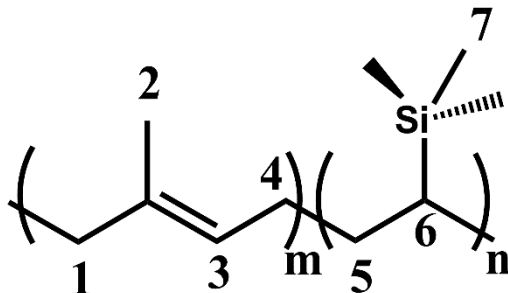


**FIGURE 3.1.** The structure of PI-*b*-PVTMS for  $^1\text{H}$ -NMR-evaluation.

$^1\text{H}$ -NMR ( $\text{CDCl}_3$ , 20 °C, 300 MHz):

$\delta[\text{ppm}] = 5.2\text{-}4.6$  (m, 1H, H-3),  $2.50\text{-}1.75$  (m, 4H, H-1, H-4),  $1.70\text{-}1.05$  (m, 4H, H-2, H-6),  $1.02\text{-}0.27$  (m, 2H, H-5), 0.0 (m, 9H, H-7).

IR (20 °C):

$\nu[\text{cm}^{-1}] = 2954$  (s), 2891 (s), 2844 (m), 1716 (m), 1455 (w), 1408 (w), 1376 (w), 1331 (w), 1246 (vs), 1059 (s), 826 (vs), 741 (vs), 678 (vs).

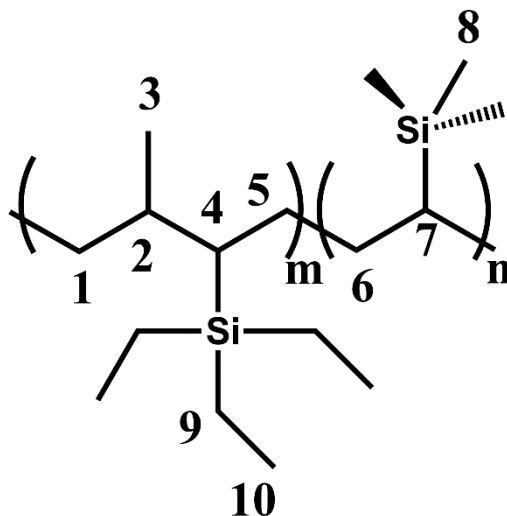


**FIGURE 3.2.** The structure of Hs-PI-*b*-PVTMS for  $^1\text{H}$ -NMR-evaluation.

$^1\text{H}$ -NMR ( $\text{CDCl}_3$ , 20 °C, 300 MHz):

$\delta[\text{ppm}] = 1.75\text{-}1.04$  (m, 7H, H-1, H-2, H-4, H-5, H-7), 1.03-0.26 (m, 10H, H-3, H-6, H-9, H-10), 0.0 (m, 9H, H-8).

IR (20 °C):

$\nu[\text{cm}^{-1}] = 2951$  (s), 2887 (s), 2843 (m), 1457 (w), 1402 (w), 1329 (w), 1245 (vs), 1055 (s), 827 (vs), 745 (vs), 680 (vs).

### 3.2.3. Modification of PI-*b*-PVTMS via Hydrogenation (H-PI-*b*-PVTMS)

Hydrogenation of isoprene units was carried out under nitrogen atmosphere using magnetic stirring in a three-neck round-bottom flask with a nitrogen inlet and outlet and a reflux condenser at 135 °C in *o*-xylene. *p*-Toluenesulfonylhydrazide (*p*-TSH; 2:1; in terms of double bond moieties) was added to a solution of 2 % (w/v) PI-*b*-PVTMS. The mixture was stirred for one day. The modified polymer was precipitated three times in ethanol (5 times excess) and dissolves in toluene three times, filtered and dried under vacuum.

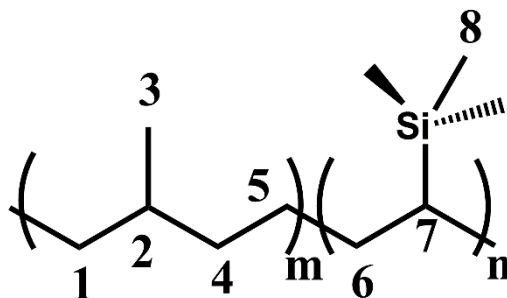


**FIGURE 3.3.** The structure of H-PI-*b*-PVTMS for  $^1\text{H}$ -NMR-evaluation.

$^1\text{H}$ -NMR ( $\text{CDCl}_3$ , 20 °C, 300 MHz):

$\delta[\text{ppm}] = 1.76\text{--}1.04$  (m, 8H, H-1, H-2, H-4, H-5, H-7),  $1.02\text{--}0.24$  (m, 5H, H-3, H-6), 0.0 (m, 9H, H-8).

IR (20 °C):

$\nu[\text{cm}^{-1}] = 2955$  (s), 2883 (s), 2849 (m), 1451 (w), 1399 (w), 1334 (w), 1244 (vs), 1057 (s), 825 (vs), 749 (vs), 681 (vs).

#### 3.2.4. Synthesis of Azidated Poly(epichlorohydrin) Homopolymer (A-H-Hydrin) and Azidated Poly[(ethylene oxide)-*ran*-(epichlorohydrin)] Copolymer (A-C-Hydrin)

Caution! This modification reaction should be performed behind a protective shield. Azidation of chloride units was carried out in a two-necked round-bottomed flask with nitrogen balloon to protect the system during nitrogen formation and a magnetic bar at 60 °C in DMF. Sodium azide ( $\text{NaN}_3$ ) (1:1 and 1:2; in terms of chloride moieties) and tetrabutylammonium iodide (TBAI) were added sequentially. The reaction solution was kept at 4 % (w/v) of polymer because of possible cross-linking at higher concentrations. The mixture was stirred for one day. After the reaction was completed, the mixture was allowed to cool to room temperature, the salts were filtered. The filtered mixture was precipitated drop wise in ten times excess ethanol, filtered and dried under vacuum.

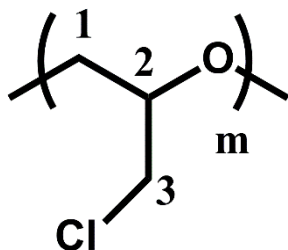


**FIGURE 3.4.** The structure of H-Hydrin for  $^1\text{H}$ -NMR and  $^{13}\text{C}$ -NMR-evaluation.

**$^1\text{H}$ -NMR** ( $\text{CDCl}_3$ , 20 °C, 300 MHz, TMS):

$\delta[\text{ppm}] = 3.76\text{--}3.55$  (m, 5H, H-1, H-2, H-3).

**$^{13}\text{C}$ -NMR** ( $\text{CDCl}_3$ , 20 °C, 300 MHz, TMS):

$\delta[\text{ppm}] = 79.4$  (m, 1C, C-2), 69.8 (m, 1C, C-1), 44.1 (m, 1C, C-3).

**IR** (20 °C):

$\nu[\text{cm}^{-1}] = 2956$  (m), 2924 (m), 2866 (m), 1461 (s), 1429 (s), 1346 (w), 1294 (w), 1249 (w), 1197 (w), 1088 (vs), 972 (w), 901 (w), 836 (w), 746 (s), 701 (m), 630 (w).

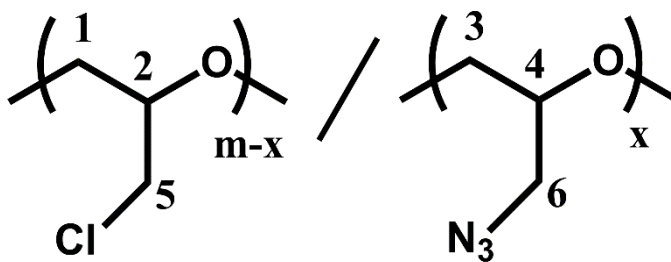


**FIGURE 3.5.** The structure of A-H-Hydrin for  $^1\text{H}$ -NMR and  $^{13}\text{C}$ -NMR-evaluation.

**$^1\text{H}$ -NMR** ( $\text{CDCl}_3$ , 20 °C, 300 MHz, TMS):

$\delta[\text{ppm}] = 3.76\text{--}3.55$  (m, 8H, H-1, H-2, H-3, H-4, H-5), 3.47–3.28 (m, 2H, H-6).

**$^{13}\text{C}$ -NMR** ( $\text{CDCl}_3$ , 20 °C, 300 MHz, TMS):

$\delta[\text{ppm}] = 79.2$  (m, 2C, C-2, C-4), 69.6 (m, 2C, C-1, C-3), 52.2 (m, 1C, C-6), 44.2 (m, 1C, C-5).

**IR** (20 °C):

$\nu[\text{cm}^{-1}] = 2955 \text{ (m)}, 2922 \text{ (m)}, 2869 \text{ (m)}, 2097 \text{ (vs)}, 1461 \text{ (s)}, 1441 \text{ (s)}, 1346 \text{ (w)}, 1275 \text{ (s)}, 1197 \text{ (w)}, 1088 \text{ (vs)}, 971 \text{ (w)}, 905 \text{ (w)}, 831 \text{ (w)}, 743 \text{ (s)}, 703 \text{ (m)}, 625 \text{ (w)}.$

**IR after UV-cross-linking (20 °C):**

$\nu[\text{cm}^{-1}] = 2957 \text{ (m)}, 2919 \text{ (m)}, 2875 \text{ (m)}, 2099 \text{ (w)}, 1667 \text{ (vs)}, 1526 \text{ (w)}, 1435 \text{ (w)}, 1346 \text{ (w)}, 1249 \text{ (w)}, 1069 \text{ (vs)}, 888 \text{ (w)}, 836 \text{ (w)}, 740 \text{ (m)}, 701 \text{ (w)}, 617 \text{ (w)}.$

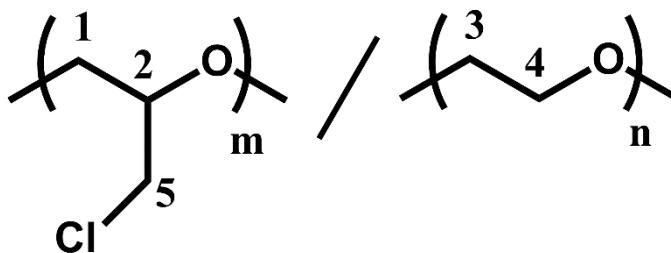


**FIGURE 3.6.** The structure of C-Hydrin for  $^1\text{H}$ -NMR and  $^{13}\text{C}$ -NMR-evaluation.

**$^1\text{H}$ -NMR** ( $\text{CDCl}_3$ , 20 °C, 300 MHz, TMS):

$\delta[\text{ppm}] = 3.81\text{-}3.55 \text{ (m, 9H, H-1, H-2, H-3, H-4, H-5)}.$

**$^{13}\text{C}$ -NMR** ( $\text{CDCl}_3$ , 20 °C, 300 MHz, TMS):

$\delta[\text{ppm}] = 79.3 \text{ (m, 1C, C-2)}, 72.2 \text{ (m, 2C, C-3, C-4)}, 69.9 \text{ (m, 1C, C-1)}, 44.3 \text{ (m, 1C, C-3)}.$

**IR** (20 °C):

$\nu[\text{cm}^{-1}] = 2911 \text{ (m)}, 2871 \text{ (m)}, 1425 \text{ (s)}, 1429 \text{ (s)}, 1345 \text{ (w)}, 1292 \text{ (w)}, 1251 \text{ (w)}, 1084 \text{ (vs)}, 950 \text{ (w)}, 876 \text{ (w)}, 836 \text{ (w)}, 749 \text{ (m)}, 689 \text{ (w)}, 629 \text{ (w)}, 488 \text{ (m)}.$

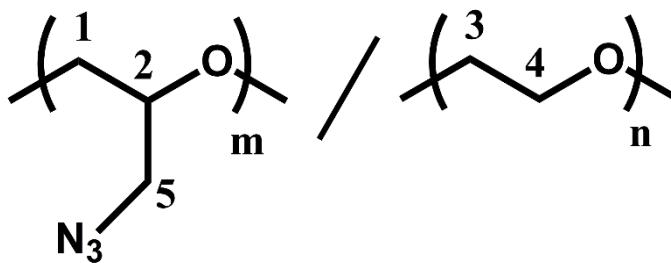




**FIGURE 3.7.** The structure of A-C-Hydrin for  $^1\text{H}$ -NMR and  $^{13}\text{C}$ -NMR-evaluation.

**$^1\text{H}$ -NMR** ( $\text{CDCl}_3$ , 20 °C, 300 MHz, TMS):

$\delta[\text{ppm}] = 3.79\text{--}3.56$  (m, 7H, H-1, H-2, H-3, H-4), 3.44–3.25 (m, 2H, H-5).

**$^{13}\text{C}$ -NMR** ( $\text{CDCl}_3$ , 20 °C, 300 MHz, TMS):

$\delta[\text{ppm}] = 79.1$  (m, 1C, C-2), 72.1 (m, 2C, C-3, C-4), 69.8 (m, 1C, C-1), 52.6 (m, 1C, C-5).

**IR** (20 °C):

$\nu[\text{cm}^{-1}] = 2917$  (m), 2870 (m), 2096 (vs), 1445 (m), 1351 (w), 1284 (s), 1090 (vs), 930 (w), 736 (w), 629 (w), 555 (w), 481 (m).

**IR after UV-cross-linking** (20 °C):

$\nu[\text{cm}^{-1}] = 2904$  (m), 2871 (m), 2094 (vs), 1639 (w), 1451 (m), 1351 (w), 1278 (s), 1091 (vs), 937 (w), 743 (w), 622 (w), 475 (m).

### 3.2.5. Synthesis of Bifunctional Poly(ethylene glycol)-Diazide ( $\text{N}_3\text{-PEG-N}_3$ )

To a stirred solution of the PEG600-dihydroxyl (15 g, 0.025 mol) in 130 mL methylene chloride, anhydrous magnesium sulfate ( $\text{MgSO}_4$ ) was added for drying. After filtration to remove the  $\text{MgSO}_4$ , the solution was cooled to 0 °C. Triethylamine (TEA) (13.9 mL, 0.1 mol) and methanesulfonyl chloride ( $\text{MsCl}$ ) (7.8 mL, 0.1 mol) were added sequentially. The flask was kept at room temperature for one day. During the reaction, the colour of the solution turned yellowish and some solid precipitated out. The reaction solution first was filtrated to remove the solid and then washed consequently with 400 mL of 1 M hydrochloric acid ( $\text{HCl}$ ), 400 mL of 1 M sodium hydroxide ( $\text{NaOH}$ ), and 300 mL of 1 M sodium chloride ( $\text{NaCl}$ ) solutions. The organic layer was dried over anhydrous  $\text{MgSO}_4$  overnight, and the solvent was removed in vacuum. The bifunctional mesyl PEG was obtained with the yield of 14.2 g (75 %) and was characterized by FT-IR and  $^{13}\text{C}$ -NMR. The PEG-dimesyl (14 g, 0.018 mol) was dissolved in 100 mL *N,N*-dimethylformamide

(DMF). Sodium azide (4.8 g, 0.072 mol) and 0.53 g tetrabutylammonium iodide (TBAI) were added sequentially. The reaction solution was stirred at 50 °C for 1 day, and DMF was removed by rotary evaporation. The resulting viscous liquid was dissolved in methylene chloride to remove undissolved solids by filtration. The organic layer was washed twice with water and dried overnight over MgSO<sub>4</sub>. Methylene chloride was evaporated to give the PEG-diazide (9.5 g, 81 %) as a yellow viscous liquid. The same protocol was applied for PEG400.

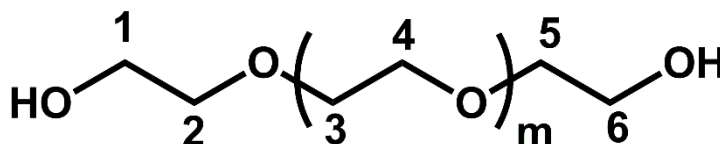


**FIGURE 3.8.** The structure of PEG-Dihydroxyl for <sup>13</sup>C-NMR-evaluation.

<sup>13</sup>C-NMR (CDCl<sub>3</sub>, 20 °C, 300 MHz, TMS):

δ[ppm] = 70.85 (s, 2C+2mC, C-2, C-3, C-4, C-5), 61.89 (s, 2C, C-1, C-6)

IR (20 °C):

ν[cm<sup>-1</sup>] = 3456 (b), 2869 (vs), 1448 (w), 1352 (w), 1303 (w), 1246 (w), 1093 (vs), 948 (m), 833 (w), 526 (m).

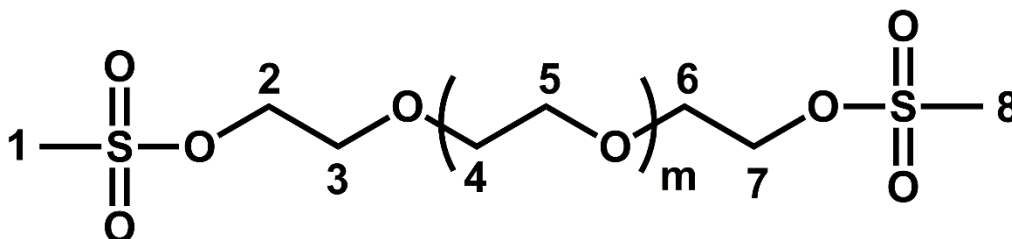


**FIGURE 3.9.** The structure of PEG-Dimesyl for <sup>13</sup>C-NMR-evaluation.

<sup>13</sup>C-NMR (CDCl<sub>3</sub>, 20 °C, 300 MHz, TMS):

δ[ppm] = 70.83 (s, 4C+2mC, C-2, C-3, C-4, C-5, C-6, C-7), 38.03 (s, 2C, C-1, C-8)

**IR** (20 °C):

$\nu[\text{cm}^{-1}] = 2859$  (vs), 1457 (w), 1342 (vs), 1236 (w), 1178 (m), 1083 (vs), 1015 (w), 920 (vs), 795 (s), 718 (s), 516 (s).

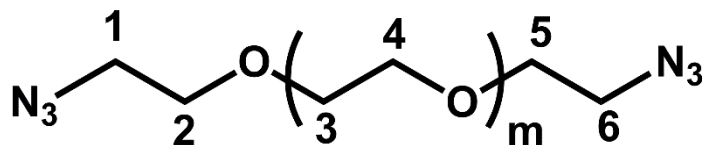


**FIGURE 3.10.** The structure of PEG-Diazide for  $^{13}\text{C}$ -NMR-evaluation.

$^{13}\text{C}$ -NMR ( $\text{CDCl}_3$ , 20 °C, 300 MHz, TMS):

$\delta[\text{ppm}] = 70.73$  (s, 2C+2mC, C-2, C-3, C-4, C-5), 50.62 (s, 2C, C-1, C-6)

**IR** (20 °C):

$\nu[\text{cm}^{-1}] = 2869$  (vs), 2098 (vs), 1448 (w), 1342 (w), 1284 (m), 1246 (w), 1092 (vs), 948 (s), 823 (s), 641 (w), 535 (w).

### 3.2.6. Synthesis Benzoxazine-Diacetylene Monomer

4-Ethynylaniline (1.75 g, 15 mmol), bisphenol A (1.71 g, 7.5 mmol), and paraformaldehyde (0.9 g, 30 mmol) and 15 mL of xylenes were mixed into a 50 mL flask. The solution was stirred at 120 °C for 6 h. After cooling, the crude product was recrystallized from the reaction solvent which behaves also as a crystallization solvent, filtered, and dried under vacuum to have beige powder (3.43 g, 88 %).

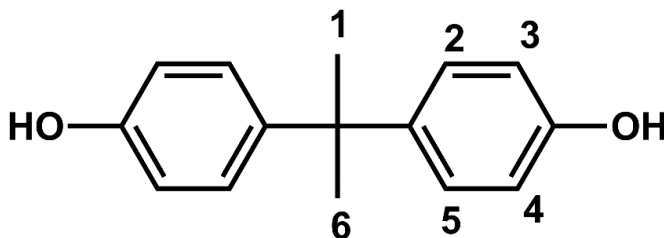


**FIGURE 3.11.** The structure of Bisphenol-A for  $^1\text{H}$ -NMR-evaluation.

**<sup>1</sup>H-NMR** (DMSO, 20 °C, 300 MHz, TMS):

δ[ppm] = 7.1-6.55 (8H, aromatic protons (H-2, H-3, H-4, H-5)), 1.51 (s, 6H, H-1, H-6)

**IR** (20 °C):

ν[cm<sup>-1</sup>] = 3303 (b), 2964 (m), 1594 (s), 1507 (vs), 1438 (s), 1369 (s), 1291 (w), 1213 (vs), 1065 (w), 1004 (w), 813 (vs), 761 (w), 631 (w), 544 (vs).

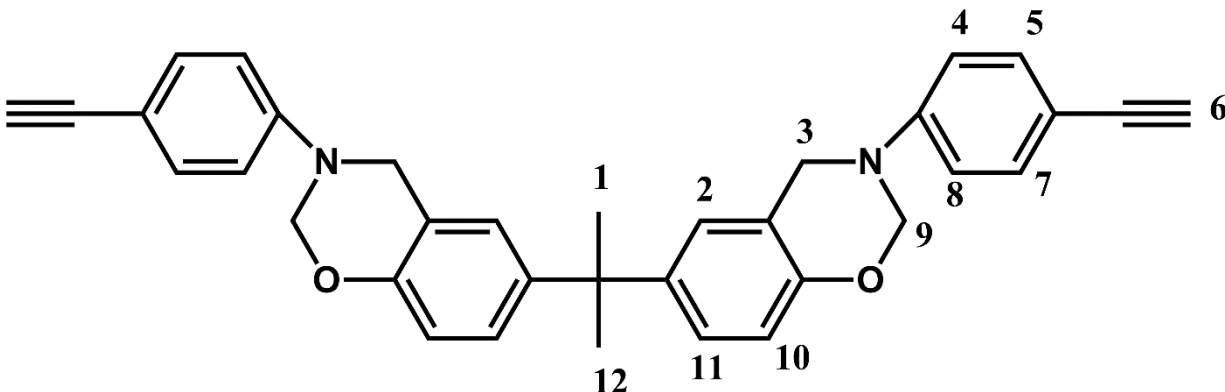


**FIGURE 3.12.** The structure of benzoxazine-biacetylene for <sup>1</sup>H-NMR-evaluation.

**<sup>1</sup>H-NMR** (DMSO, 20 °C, 300 MHz, TMS):

δ[ppm] = 7.39-6.58 (14H, aromatic protons (H-2, H-4, H-5, H-7, H-8, H-10, H-11)), 5.43 (s, 4H, H-9), 4.64 (s, 4H, H-3), 3.97 (s, 2H, H-6), 1.52 (s, 6H, H-1, H-12).

**IR** (20 °C):

ν[cm<sup>-1</sup>] = 3276 (s), 2973 (m), 2105 (m), 1608 (s), 1506 (vs), 1372 (m), 1220 (vs), 1178 (s), 1102 (m), 1026 (w), 934 (vs), 824 (vs), 748 (w), 638 (w), 613 (m), 529 (m).

### 3.2.7. General Procedure for CuAAC Step Growth Polymerization

The solvent (20 mL), and click monomer with diacetylene end groups (5 mmol) were introduced to a polymerization flask containing PEG-diazide (5 mmol), CuBr (50 mg, 5 mol %) and *N,N,N',N'',N'''*-Pentamethyldiethylenetriamine (PMDETA) under nitrogen atmosphere. The resulting mixture was stirred at 100 °C. Mixture was filtrated through a short alumina column to remove the

copper salt and the polymer was precipitated twice in diethyl ether (200 mL) and dried under vacuum.

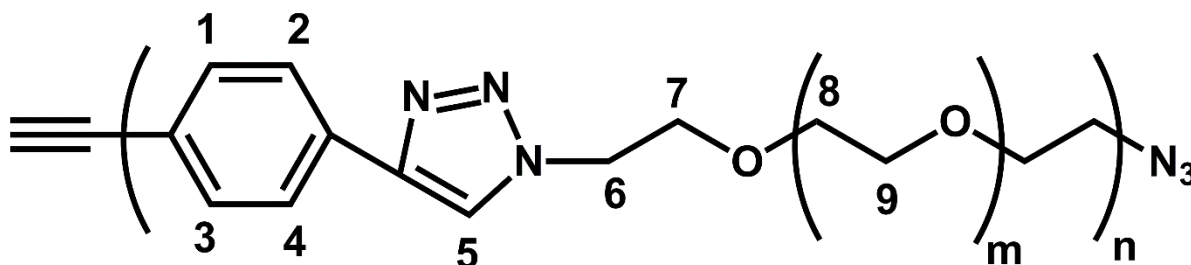


**FIGURE 3.13.** The structure of step-polymer for  $^1\text{H}$ -NMR-evaluation.

**$^1\text{H}$ -NMR** (DMSO, 20 °C, 300 MHz, TMS):

$\delta[\text{ppm}] = 8.75\text{--}8.50$  (s, 1H, H-5),  $8.03\text{--}7.63$  (4H, aromatic protons (H-1, H-2, H-3, H-4)),  $4.52$  (d, 2H, H-6),  $3.85$  (d, 2H, H-7),  $3.6\text{--}3.3$  (4mH, H-8, H-9,  $\text{H}_2\text{O}$ ).

**IR** (20 °C):

$\nu[\text{cm}^{-1}] = 2867$  (s),  $1462$  (m),  $1347$  (m),  $1301$  (w),  $1233$  (w),  $1099$  (vs),  $931$  (s),  $843$  (s),  $540$  (m).

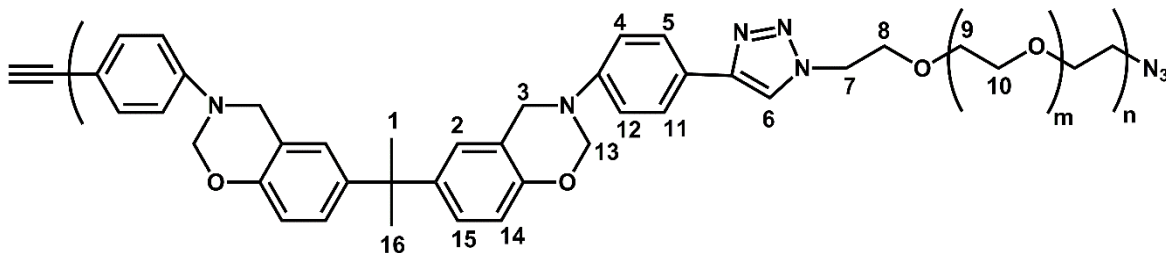


**FIGURE 3.2.14.** The structure of stepbenz-polymer for  $^1\text{H}$ -NMR-evaluation.

**$^1\text{H}$ -NMR** ( $\text{CDCl}_3$ , 20 °C, 300 MHz, TMS):

$\delta[\text{ppm}] = 8.0\text{--}6.5$  (15H, aromatic protons (H-2, H-4, H-5, H-6, H-11, H-12, H-14, H-15), chloroform),  $5.37$  (s, 4H, H-13),  $4.75\text{--}4.50$  (m, 6H, H-3, H-7),  $4.15\text{--}3.40$  (m,  $2\text{H}+4\text{mH}$ , H-8, H-9, H-10),  $1.56$  (6H, H-1, H-16).

### 3.2.8. General Procedure for Catalyst-Free Step Growth Polymerization

DMF (20 mL), and 1,4-diethynylbenzene (0.63 g, 5 mmol) were introduced to a polymerization flask containing PEG600-diazide (3 g, 5 mmol) under nitrogen atmosphere. The resulting mixture was stirred at 100 °C. After stirring for 10 days, the mixture was precipitated twice in diethyl ether (200 mL) and dried under vacuum.

## 3.3. Characterization

### 3.3.1. $^1\text{H}$ , $^{13}\text{C}$ -NMR & FTIR

$^1\text{H}$  and  $^{13}\text{C}$ -NMR spectra were recorded using a Bruker Advance 300 NMR spectrometer at 300 resp. 75 MHz. Fourier transform infrared (FT-IR) spectra were recorded on a Bruker Equinox 55. The transmission measurements were carried out in a spectral range of 400–4000  $\text{cm}^{-1}$  with a spectral resolution of 4  $\text{cm}^{-1}$  and 64 scans.

### 3.3.2. Gel Permeation Chromatography (GPC)

Gel permeation chromatography (GPC) measurements were performed at room temperature in THF using 5  $\mu$  PSS SDV gel columns (102, 103, 104, 105 Å, 8x300 mm each, PSS GmbH, Mainz, Germany) at a flow rate of 1.0 mL/min (VWR-Hitachi 2130 pump). A Waters 2410 refractive index detector ( $\lambda = 930$  nm) and a Waters UV-photometer (typically operated at  $\lambda = 254$  nm) were used for concentration detection. Samples were injected employing a Waters 717 autosampler (injection volume 50  $\mu\text{L}$ ). To compensate for flow-rate fluctuations 20 ppm 2,6-di-*t*-butyl-hydroxytoluene (BHT) was added as internal standard to each sample. Raw data were processed using the PSS WinGPC Unity software package. Elugrams are corrected for flow-rate; polystyrene calibration was used to calculate the apparent molecular weight distribution and the corresponding averages.

### **3.3.3. Thermogravimetric Analysis (TGA)**

Thermogravimetric analysis (TGA) was performed on an Iris TG 209 F1 instrument (Netzsch), at a linear heating rate of 10 K/min, up to 900 °C under nitrogen atmosphere and processed with the Proteus<sup>®</sup> software.

### **3.3.4. Transmission Electron Micrographs (TEM)**

Transmission electron micrographs were taken with a Tecnai G2 F20 (FEI) operated at 200 kV in the bright field mode. Approximately 50 nm thick sample films were obtained by microtoming epoxy embedded membrane films at room temperature. The films were then stained with OsO<sub>4</sub> to visualize polyisoprene domains.

### **3.3.5. Differential Scanning Chromatography (DSC)**

All DSC runs were performed on a DSC 1 (Star system) from Mettler Toledo using a nitrogen purge gas stream (60 mL/min) at a scan rate of 10 K/min. Heating and cooling scans were performed by initially heating the sample up to 100 °C and holding it at that temperature for 5 minutes in order to erase the thermal history, then the sample was cooled down to -100 °C. Finally a second heating scan up to 250 °C and a second cooling scan down to -100 °C were applied. The DSC thermograms presented here correspond to the second heating and second cooling.

## **3.4. Membrane Formation**

The synthesized polymers were dissolved in tetrahydrofuran (THF), determined as the best solvent for poly(vinyl trimethylsilane) (PVTMS), polyisoprene, modified polyisoprene, poly(epichlorohydrin) homopolymer, poly[(ethylene oxide)-*ran*-(epichlorohydrin)] copolymer and step-growth polymers. The polymer concentration was maintained below 4 wt% in order to work with polymer solutions of low viscosity and to have enough solvent for filling the membrane casting setup with the layer of solution being thick enough for slow (at least 48 h) evaporation.

The membrane casting setup consisted of an 80 mm diameter aluminum ring with polished upper and bottom sides, a glass plate coated with Teflon<sup>®</sup>, and a levelled table. The polymer solution was filtered through a fine cotton filter and poured into the aluminum ring placed on the Teflon<sup>®</sup> surface. The ring was covered with a glass lid having openings for the gas connection and ventilation. A nitrogen gas stream (10 mL/min) was used to remove solvent vapor from the casting setup. Solvent evaporation was carried out at room temperature. When the presence of THF was no longer indicated, the obtained membrane was mechanically removed from the Teflon<sup>®</sup> surface and placed into the vacuum oven where it was evacuated for at least 4 h at 100 °C in vacuum provided by a turbo molecular pumping unit. The membrane thicknesses varied from 100 to 200  $\mu\text{m}$ . Only membranes with a thickness deviation less than 5  $\mu\text{m}$  as determined by a Fischer Deltascope<sup>®</sup> FMP10 instrument were used for the characterization of gas transport properties. A photoreactor (Helios Italquartz) equipped with a 500 W high-pressure mercury lamp (through a Pyrex glass filter,  $k > 300 \text{ nm}$ ) was used for UV irradiation. The UV irradiation time for each film was 90 min.

### 3.5. Gas Transport Properties

Pure gas permeability measurements were performed by the time lag (constant volume, variable pressure) method. The order of pure gas permeability was He, H<sub>2</sub>, CH<sub>4</sub>, N<sub>2</sub>, O<sub>2</sub>, and CO<sub>2</sub> in the gas transport tests and repeated at least 4 times for each gas. Measurements were carried out at 30 °C and 1 bar. Only results with errors less than  $\pm 3 \%$  were taken into account.

Gas permeability (P), diffusion coefficient (D), solubility (S) and ideal selectivity of the membranes for pure gases ( $\alpha_{A/B}$ ) were obtained from time-lag measurements using the following equations:



$$P = D.S = \frac{V_p.l}{A.R.T.\Delta t} \ln \frac{p_f - p_{p1}}{p_f - p_{p2}} \quad (3.1)$$

$$D = \frac{l^2}{6\theta} \quad (3.2)$$

$$\alpha_{A,B} = \frac{P_A}{P_B} \quad (3.3)$$

where,  $V_p$  is the permeate volume,  $l$  is the membrane thickness,  $A$  is the membrane area,  $R$  is the gas constant,  $\Delta t$  is the time difference between two points (1 and 2) on the pressure curve,  $p_f$  is the feed pressure considered to be constant in the time range  $\Delta t$ ,  $p_{p1}$  and  $p_{p2}$  are permeate pressures at time moment 1 and 2, and  $\theta$  is the time lag, respectively (Figure 3.1).

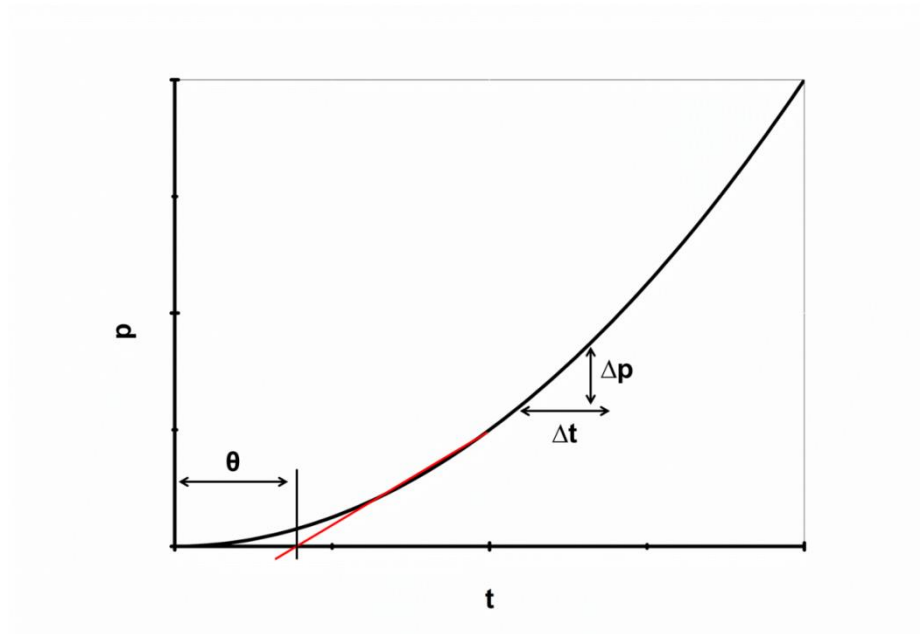


**FIGURE 3.15.** A typical time lag diagram for the gas transport measurement of membranes.

### 3.6. Density and Fractional Free Volume (FFV)

Polymer density was characterized using a Mettler Toledo Balance (Model XP105) with a density determination kit. The polymer density was calculated as follows:

$$\rho = \frac{M_A}{M_A - M_B}(\rho_0 - \rho_L) + \rho_L \quad (3.4)$$

where  $M_A$  is the film weight in air,  $M_B$  is the film weight in the auxiliary liquid,  $\rho$  is the film density,  $\rho_0$  is the density of the auxiliary liquid used, and  $\rho_L$  is air density (0.0012 g/cm<sup>3</sup>). A high density auxiliary liquid was used for two reasons: to decrease the sorption of the auxiliary liquid in polymer and to increase the difference between the densities of the polymer sample and the auxiliary liquid. The perfluoro liquid FC-770, purchased from 3M, has a density of 1.776 g/cm<sup>3</sup> at 25 °C.

The fractional free volume in the polymer matrix is an important parameter effecting gas transport properties and it is defined as:

$$FFV = \frac{V - V_0}{V} \approx \frac{V - 1.3V_w}{V} \quad (3.5)$$

where  $V$  is the specific volume at the temperature of interest, and  $V_0$  is the occupied volume of polymer at 0 K, which is 1.3 times the VAN-DER-WAALS volume ( $V_w$ ) calculated following the BONDI's method [2].

### 3.7. Swelling Experiment

The gel content of cross-linked membrane was determined by soaking the relevant membranes in THF (solvent for film casting) for 24 h [3]. The solvent was then decanted and the

membranes were washed several times with THF. The insoluble membrane portion was dried under high vacuum at room temperature for 24 h to remove the residual solvent before weighing. The gel content was calculated as follows:

$$GC(\%) = \frac{M_1}{M_o} \times 100 \quad (3.6)$$

where  $M_o$  and  $M_1$  are the weights of the cross-linked membrane before and after soaking in THF, respectively.

### 3.8. References

- [1] S. Rangou, S. Shishatskiy, V. Filiz, V. Abetz, Poly(vinyl trimethylsilane) and block copolymers of vinyl trimethylsilane with isoprene: Anionic polymerization, morphology and gas transport properties, *European Polymer Journal*, 47 (2011) 723-729.
- [2] A. Weiss, Arnold Bondi: Physical properties of molecular crystals, liquids, and glasses. John Wiley and Sons, New York, London, Sydney 1968. 502 Seiten. Preis: 175 s, *Berichte der Bunsengesellschaft für Physikalische Chemie*, 72 (1968) 1242-1243.
- [3] M.M. Khan, G. Bengtson, S. Shishatskiy, B.N. Gacal, M. Mushfequr Rahman, S. Neumann, V. Filiz, V. Abetz, Cross-linking of Polymer of iIntrinsic mMicroporosity (PIM-1) via nitrene reaction and its effect on gas transport property, *European Polymer Journal*, 49 (2013) 4157-4166.

## Chapter 4

### Results and Discussions

#### 4.1. Modification of Polyisoprene-*block*-Poly(vinyl trimethylsilane) Block Copolymers via Hydrosilylation and Hydrogenation, and Their Gas Transport Properties

##### 4.1.1. Brief Introduction

In this study, our main goal was to modify the polyisoprene block of PI-*b*-PVTMS with suitable components via metal catalyzed hydrosilylation [1] and noncatalyzed hydrogenation [2]. The intent thus is to alter the thermodynamic and repulsive interactions between blocks, resulting in different morphologies, which are directly related to the gas transport properties of the modified block copolymers [3]. In addition, the polymer characteristics were expected to advance from a less permeable and selective, rubbery polyisoprene polymer to a highly permeable, silicon-containing glassy polymer and semicrystalline polyolefin [4]. In this way, we expect to retain the performance of PVTMS homopolymer in terms of its gas transport properties while at the same time decreasing the consumption of PVTMS.

##### 4.1.2. Synthesis and Characterization of Hydrosilylated Polyisoprene-*block*-Poly(vinyl trimethylsilane) (Hs-PI-*b*-PVTMS)

Polyisoprene is an unsaturated polymer and ideal for further modification due to good accessibility of the double bond. In this study, we report on two different polymer modification methods: a) to

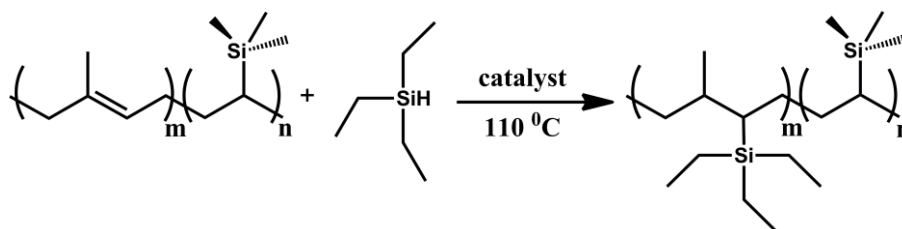
add a new side group (triethylsilane) to the double bonds and b) to saturate unsaturated double bonds of polyisoprene block of PI-*b*-PVTMS carried out by two simple one-step reactions which are based on metal catalyzed hydrosilylation and non-catalytic hydrogenation, respectively.

Hydrosilylation is an efficient synthetic route to introduce silane side group units to the main chain of unsaturated polymers. The reaction was carried out in the presence of Wilkinson's catalyst under mild conditions with a high selectivity toward double bonds [1]. Hydrosilylation of 4 PI-*b*-PVTMS block copolymers (Table 4.1.1) with triethylsilane was performed as described in the experimental section to obtain Hs-PI-*b*-PVTMS (Scheme 4.1.1).

**TABLE 4.1.1.** Molecular Weight and Percentage of Modification of the Block Copolymers.

Polymers	$M_w^a$ (kg/mol)	PI $M_w$ (kg/mol)	PI % <sup>b</sup>	Hs % <sup>c</sup>	H % <sup>d</sup>
PI- <i>b</i> -PVTMS-1	96	9.6	10	80	100
PI- <i>b</i> -PVTMS-2	166	21.6	13	80	100
PI- <i>b</i> -PVTMS-3	118	35.4	30	67	100
PI- <i>b</i> -PVTMS-4	160	65.6	41	15	100
PVTMS ref.	650	-	-	-	-

<sup>a</sup> Molecular weights were determined by GPC; <sup>b</sup> PI content (wt. %) of the block copolymers was determined by <sup>1</sup>H-NMR analysis; <sup>c</sup> Molar percentage of hydrosilylated double bonds in PI blocks of the block copolymers was determined by <sup>1</sup>H-NMR analysis; <sup>d</sup> Molar percentage of hydrogenated double bonds in PI blocks of the block copolymers was determined by <sup>1</sup>H-NMR analysis.



**SCHEME 4.1.1.** Metal catalyzed hydrosilylation of PI-*b*-PVTMS

The extent of the modification was determined using area integration of  $^1\text{H}$ -NMR spectra. The signal intensity of the vinyl proton between 4.6 ppm and 5.2 ppm and neighbouring protons at 1.67 and 2.03 ppm decreased after modification with respect to trimethylsilyl protons of the polymer. Additionally, the appearance of new signals corresponding to resonances of the methylene and methyl protons of the triethylsilyl groups at 0.57 and 0.94 ppm indicate successful modification (Figure 4.1.1). FT-IR spectra of Hs-PI-*b*-PVTMS also show decreases in the intensity of characteristic bands of polyisoprene at  $1716\text{ cm}^{-1}$  and  $1376\text{ cm}^{-1}$  which are assigned to C=C stretching and the methyl group, respectively (Figure 4.1.2) [2, 5, 6].

The composition of the polymers can be calculated using the following equation:

$$\text{HsDb}_{\text{block}}\% = \text{Db}_{\text{before}}\% - (9/\text{Db}_{\text{after}}100/I3\text{CH}_3) \text{ and} \quad (4.1.1)$$

$$\text{HsDb}_{\text{PI}}\% = \text{HsDb}_{\text{block}}\% \cdot 100/\text{Db}_{\text{before}}\% \quad (4.1.2)$$

where  $\text{HsDb}_{\text{block}}\%$ ,  $\text{HsDb}_{\text{PI}}\%$ , and  $\text{Db}_{\text{before}}\%$  represent the percentage of hydrosilylated double bonds in the block copolymer, only in the polyisoprene block, and the percentage of double bonds before modification in the block copolymer, respectively.  $I\text{Db}_{\text{after}}$  and  $I3\text{CH}_3$  represent the intensities of the integrals corresponding to the double bond proton after modification and the methyl protons of the trimethylsilyl pendant group, respectively. The percentages of hydrosilylation of all four block copolymers are presented in Table 4.1.1.

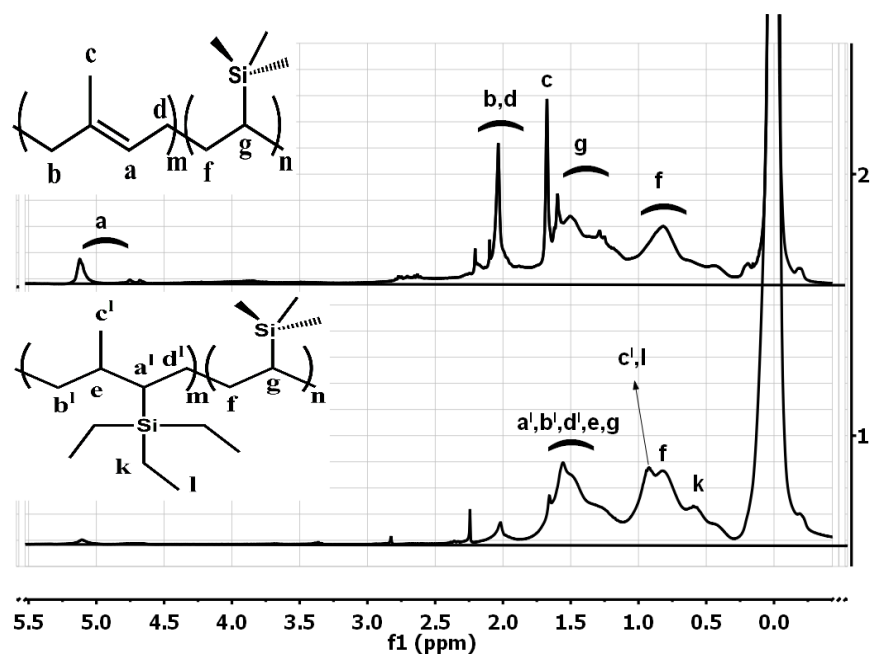


**FIGURE 4.1.1.**  $^1\text{H}$ -NMR spectra of (10 wt. %)PI-*b*-PVTMS-1 (2) and Hs-(10 wt. %)PI-*b*-PVTMS-1 (1) in  $\text{CDCl}_3$ .

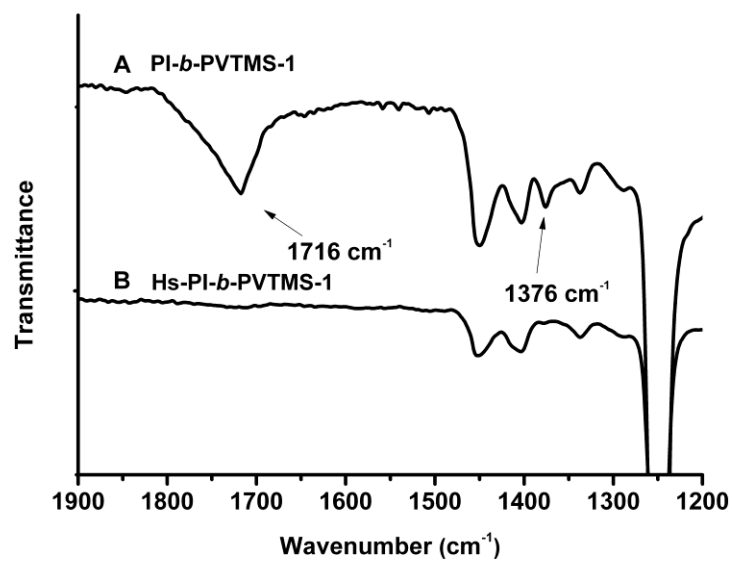
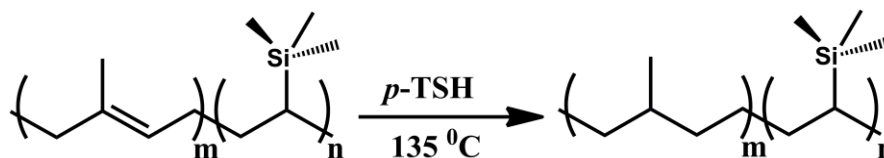


**FIGURE 4.1.2.** FT-IR spectra of (10 wt. %)PI-*b*-PVTMS-1 (A) and Hs-(10 wt. %)PI-*b*-PVTMS-1 (B).

#### 4.1.3. Synthesis and Characterization of Hydrogenated Polyisoprene-*block*-Poly(vinyl trimethylsilane) (H-PI-*b*-PVTMS)

Noncatalyzed hydrogenation is known as diimide ( $N_2H_2$ ) hydrogenation and starts with thermal decomposition of *p*-toluenesulfonylhydrazide (*p*-TSH) to *p*-toluenesulphonic acid and diimide. After thermal decomposition, the diimide saturates the double bonds. It is a homogeneous reaction which is used to hydrogenate diene-containing polymers such as polybutadiene and polyisoprene under nitrogen [2]. Noncatalyzed hydrogenation of the four PI-*b*-PVTMS polymers with *p*-TSH was performed as described in the experimental section to obtain H-PI-*b*-PVTMS (Scheme 4.1.2).



**SCHEME 4.1.2.** Noncatalyzed hydrogenation of H-PI-*b*-PVTMS

In the  $^1H$ -NMR spectrum of H-PI-*b*-PVTMS, the disappearance of the vinyl proton signals and the signals of neighbouring protons gives reliable evidence of hydrogenation (Figure 4.1.3). FT-IR spectra of H-PI-*b*-PVTMS show the disappearance of characteristic bands of polyisoprene at 1716  $cm^{-1}$  and 1376  $cm^{-1}$  which are assigned to C=C stretching and the methyl group, respectively (Figure 4.1.4).



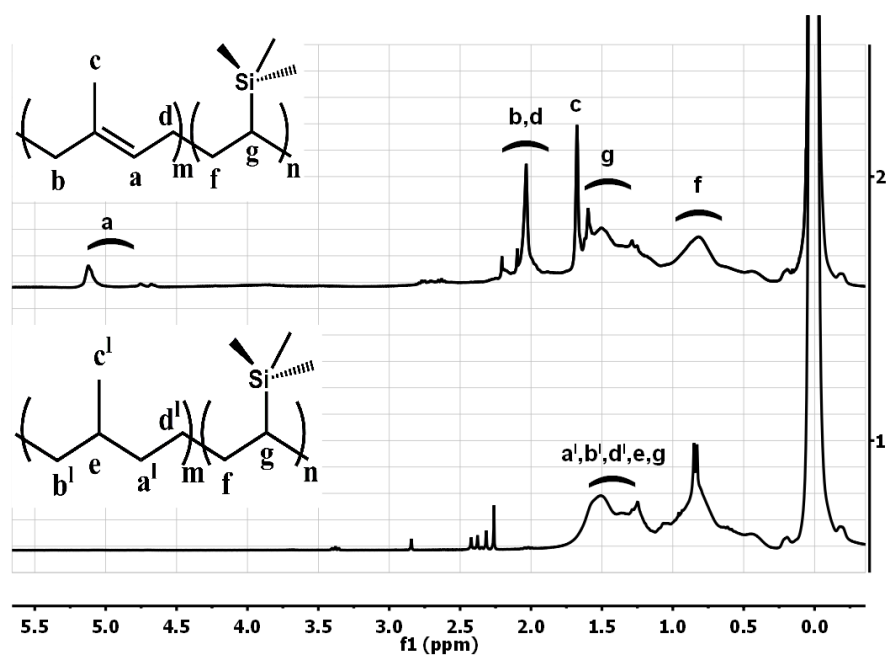


**FIGURE 4.1.3.**  $^1\text{H}$ -NMR spectra of (10 wt. %)PI-*b*-PVTMS-1 (2) and H-(10 wt. %)PI-*b*-PVTMS-1 (1) in  $\text{CDCl}_3$ .

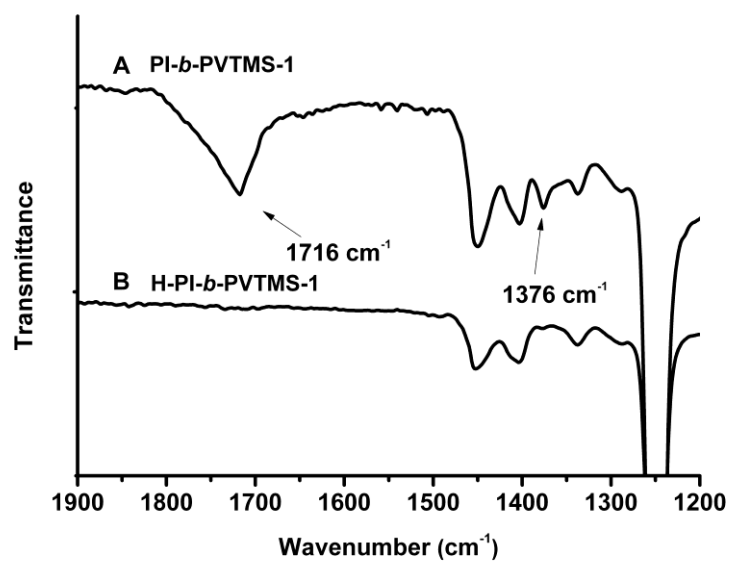


**FIGURE 4.1.4.** FT-IR spectra of (10 wt. %)PI-*b*-PVTMS-1 (A) and H-(10 wt. %)PI-*b*-PVTMS-1 (B).

#### 4.1.4. Gel Permeation Chromatography (GPC) Analysis

GPC results of four different PI-*b*-PVTMS block copolymers before and after post modification are shown in Table 4.1.2.

**TABLE 4.1.2.** Molecular Weight and Polydispersity of the Block Copolymers Before and After Modification.

Polymers	$M_w^a$ (kg/mol)	$M_w/M_n^a$	Polymers	$M_w^a$ (kg/mol)	$M_w/M_n^a$
(10%)PI- <i>b</i> -PVTMS-1	96	2.3	(13%)PI- <i>b</i> -PVTMS-2	166	1.9
Hs-PI- <i>b</i> -PVTMS-1	85	1.8	Hs-PI- <i>b</i> -PVTMS-2	141	2.3
H-PI- <i>b</i> -PVTMS-1	93	2.2	H-PI- <i>b</i> -PVTMS-2	138	2.4
(30%)PI- <i>b</i> -PVTMS-3	118	1.7	(41%)PI- <i>b</i> -PVTMS-4	160	1.6
Hs-PI- <i>b</i> -PVTMS-3	121	1.7	Hs-PI- <i>b</i> -PVTMS-4	51	5.5
H-PI- <i>b</i> -PVTMS-3	110	2.1	H-PI- <i>b</i> -PVTMS-4	50	5.7

<sup>a</sup> Molecular weights and polydispersities were determined with GPC.

In the same molecular weight range, polymers with 10 wt. % (9.6 kg/mol), 13 wt. % (21.6 kg/mol), and 30 wt. % (35.4 kg/mol) isoprene demonstrated a unimodal distribution which shows successful modification without degradation (Figure 4.1.5 a-c). A slight decrease in the apparent molecular weight of the polymer was observed after modification in GPC. This observation can be explained by the different behaviors of unsaturated regions of the polymer and the newly formed hydrogenated and hydrosilylated blocks in GPC because the hydrodynamic volumes may change due to the chemical modification of PI-*b*-PVTMS [2, 7, 8]. On the other hand, the appearance of two shoulders for lower molecular weight fraction (instead of a unimodal curve) as well as the

shift of the whole GPC curve towards lower molecular weight after both types of modifications of 41 wt. % (65.6 kg/mol) isoprene containing PI-*b*-PVTMS indicates the degradation of PI main chain during modification (Figure 4.1.5 d). This is likely due to the relatively high reaction temperature or oxidative degradation of residual unsaturation [2].

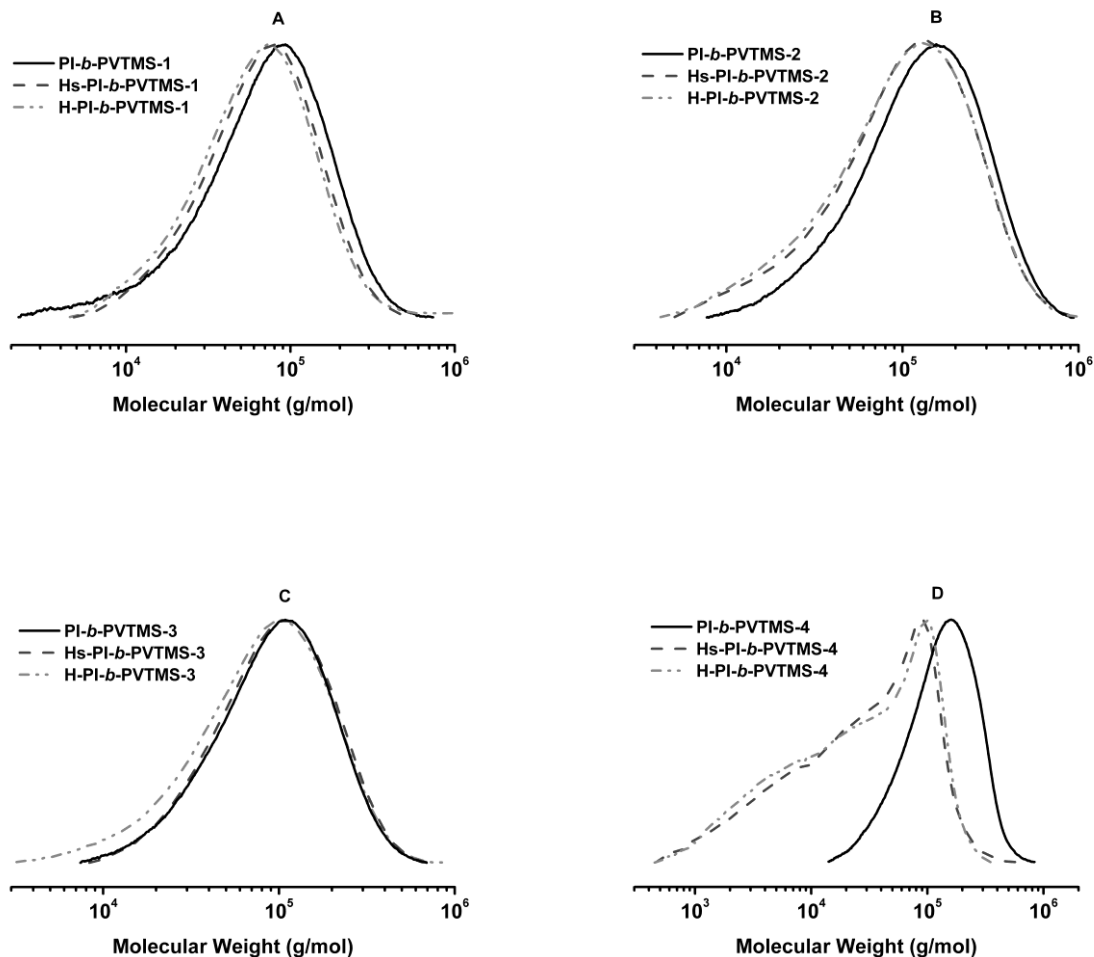


**FIGURE 4.1.5.** Gel permeation chromatograms of (10 wt. %)PI-*b*-PVTMS-1 (A), (13 wt. %)PI-*b*-PVTMS-2 (B), (30 wt. %)PI-*b*-PVTMS-3 (C), and (41 wt. %)-PI-*b*-PVTMS-4 (D) and their modifications.

These results suggest that the efficiency of the chosen chemical modifications depends on the content of polyisoprene in the block copolymer, which is directly correlated to the length of the polyisoprene block. The modified block copolymers easily dissolve before and after modifications in solvents such as tetrahydrofuran (THF), toluene and chloroform ( $\text{CHCl}_3$ ). Thus, we concluded that no gel or crosslink formation occurred during modifications.

#### 4.1.5. Thermal Characterization

The thermal stability increases with modification similarly to double bonds hydrogenation of the unsaturated main chain of diene polymers [9]. The thermal stability of the Hs-PI-*b*-PVTMS and H-PI-*b*-PVTMS was investigated by thermogravimetric analysis (TGA) and compared with PI-*b*-PVTMS. The TGA curves are presented in Figure 4.1.6 and weight loss behaviours of the species are given in Table 4.1.3. The starting temperatures for 5 and 10 % weight losses were much higher than for the initial block copolymer which shows the enhanced thermal stability after modification.

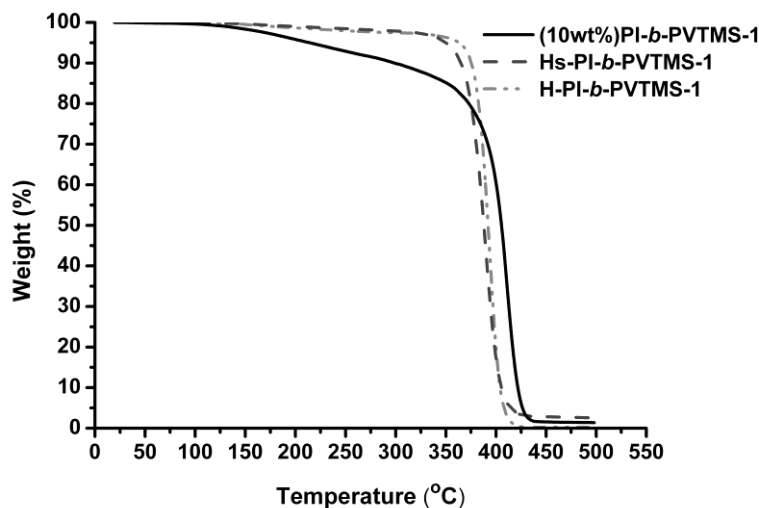


**FIGURE 4.1.6.** TGA curves of (10 wt. %)PI-*b*-PVTMS-1 and its modifications recorded under nitrogen at heating rate 10 K/min.

**TABLE 4.1.3.** Thermal Properties of PI-*b*-PVTMS-1.

<b>Polymer</b>	<b>T<sub>5%</sub><sup>a</sup></b> <b>(°C)</b>	<b>T<sub>10%</sub><sup>b</sup></b> <b>(°C)</b>	<b>T<sub>d max</sub><sup>c</sup></b> <b>(°C)</b>	<b>Y<sub>c</sub><sup>d</sup> at</b> <b>500 °C</b> <b>(%)</b>
(10wt%)PI- <i>b</i> -PVTMS-1	214	298	394	1.38
Hs-PI- <i>b</i> -PVTMS-1	350	365	372	0.25
H-PI- <i>b</i> -PVTMS-1	363	375	381	2.53

<sup>a</sup> T<sub>5%</sub>: The temperature for which the weight loss is 5 %. <sup>b</sup> T<sub>10%</sub>: The temperature for which the weight loss is 10 %. <sup>c</sup> T<sub>d max</sub>: Maximum weight loss temperature. <sup>d</sup> Y<sub>c</sub>: Char yield.

#### 4.1.6. Morphology

A transmission electron micrograph of Hs-PI-*b*-PVTMS (Figure 4.1.7 B) block copolymer composed of 80 % randomly hydrosilylated PI block (M<sub>w</sub>=21.6 kg/mol) and PVTMS (M<sub>w</sub>=144.4 kg/mol) is displayed with comparison to the initial PI-*b*-PVTMS from the previous study in Figure 4.1.7 A [10]. In this image, hydrosilylated PI-*b*-PVTMS block copolymer revealed no microphase separation. In the previous study, Rangou et al. reported a strong microphase separation of the polyisoprene (amorphous) and PVTMS (liquid crystalline) blocks. The block copolymers of a liquid crystalline block and an amorphous block tend to form a lamellar structure over larger compositional ranges as compared to block copolymers composed of two amorphous blocks. In the lamellar structure, continuous layers of PI lamellae effectively blocked the permeation of gases [10]. After hydrosilylation of the PI block, the characteristic of this block and the interactions between the blocks were changed. Due to the modification of the PI-block, its electron density is more similar to the one of PVTMS and therefore there is a lack of contrast (Figure 4.1.7 B). Therefore no conclusion about eventual changes of the morphology can be drawn. The observed high increase in the permeation of gases (Table 4.1.4) is due to the improved permeation properties of the hydrosilylated PI-blocks.

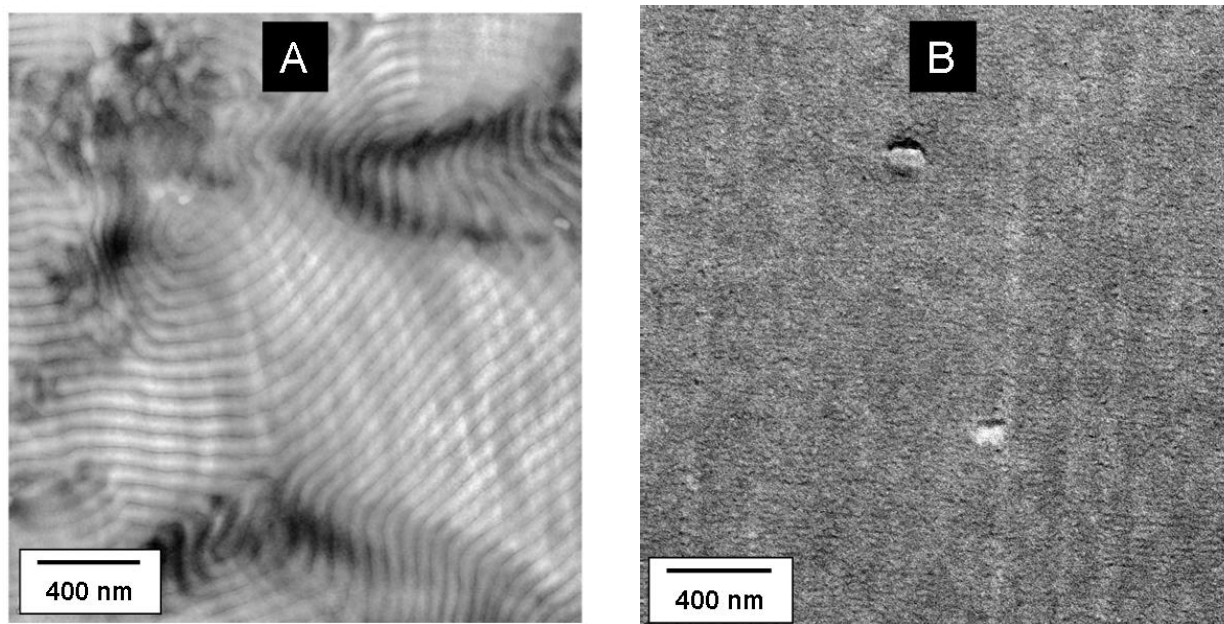


**FIGURE 4.1.7.** TEM micrographs of PI-*b*-PVTMS (A)[10] (Copyright © 2011, Elsevier) and Hs-PI-*b*-PVTMS (B). The scale bar corresponds to 400 nm.

#### 4.1.7. Gas Transport Properties

The results of single gas permeation experiments carried out on the four pristine PI-*b*-PVTMS and their hydrosilylated (Hs-PI-*b*-PVTMS) and hydrogenated (H-PI-*b*-PVTMS) counterparts are reported in Table 4.1.4. The general tendency of permeation rate order of the modified block copolymers is the same as for PI-*b*-PVTMS and pure PVTMS ( $H_2 > CO_2 > O_2 > CH_4 > N_2$ ). The introduction of polyisoprene into the PVTMS matrix leads to a significant drop in gas permeability. Before modification the  $O_2$  and  $H_2$  permeabilities of block copolymers with low isoprene content (10 wt. %, 9.6 kg/mol; 13 wt. %, 21.6 kg/mol) dropped by up to 35 %, compared to PVTMS-ref. while maintaining the  $O_2/N_2$  and  $H_2/N_2$  selectivities. It is clear that polyisoprene with the lower gas transport properties acts as a relatively impermeable additive to PVTMS. However, after hydrosilylation the block copolymers (Hs-PI-*b*-PVTMS) showed increased  $O_2$  and  $H_2$  permeabilities of about 15 to 40 %. Similarly, after hydrogenation the block copolymers (H-PI-*b*-

PVTMS) have increased permeabilities of about 20 to 35 %, compared to initial block copolymers without any significant change in selectivity (Figure 4.1.8). Furthermore, before modification, PI-*b*-PVTMS block copolymers (30 wt. % isoprene, 35.4 kg/mol; 41 wt. % isoprene, 65.6 kg/mol) had up to 65 % decrease in O<sub>2</sub> and H<sub>2</sub> permeabilities compared to PVTMS-ref. On the other hand, after hydrosilylation, block copolymers with high isoprene content (Hs-PI-*b*-PVTMS) had the highest increases (compared to PI-*b*-PVTMS) in O<sub>2</sub> and H<sub>2</sub> permeabilities up to 125 %, and after hydrogenation up to 110 % (Figure 4.1.9). These observations were consistent except for the block copolymer with the highest isoprene content, likely due to degradation (discussed in GPC analysis section) of the polymer main chain during modification. The greatly improved performance of PI-*b*-PVTMS demonstrates the effect of the modifications on gas transport properties. Hydrosilylation of the polyisoprene block introduces triethylsilyl side groups and hydrogenation saturates the double bonds, significantly changing nature and characteristics of the PI block and thus leads to improved interaction between PI and PVTMS blocks. PI is an amorphous polymer with T<sub>g</sub> = -80 °C. After hydrosilylation or hydrogenation the characteristics of the amorphous PI block transformed to that of highly permeable, glassy silicon-containing or olefin polymer, respectively, which positively affects the gas transport properties of PI-*b*-PVTMS, playing an important role in raising of O<sub>2</sub> and H<sub>2</sub> permeability without any negative changes in selectivity. The improved gas transport properties of these modified block copolymers make them potentially useful for industrial applications.

**TABLE 4.1.4.** Gas Permeability Coefficients and Selectivity Values of the Block Copolymers Before and After Modifications. In the brackets is the PI content in wt. % of the block copolymers given.

Polymers	Permeability (Barrer <sup>a</sup> )				Selectivity		
	P(CO <sub>2</sub> )	P(O <sub>2</sub> )	P(N <sub>2</sub> )	P(H <sub>2</sub> )	$\alpha$ (CO <sub>2</sub> /N <sub>2</sub> )	$\alpha$ (O <sub>2</sub> /N <sub>2</sub> )	$\alpha$ (H <sub>2</sub> /N <sub>2</sub> )
<b>(10%b)PI-<i>b</i>-PVTMS-1</b>	126	34.5	9.6	151	13.1	3.6	15.7
Hs-PI- <i>b</i> -PVTMS-1	155	44	12.2	174	12.8	3.6	14.3
H-PI- <i>b</i> -PVTMS-1	139	41	11.7	201	11.8	3.5	17.2
<b>(13%)PI-<i>b</i>-PVTMS-2</b>	114	32	9.4	143	12.1	3.4	15.2
Hs-PI- <i>b</i> -PVTMS-2	149	43	12.2	202	12.2	3.5	16.6
H-PI- <i>b</i> -PVTMS-2	133	38	10.4	182	12.8	3.7	17.5
<b>(30%)PI-<i>b</i>-PVTMS-3</b>	57	16.8	4.6	89	12.5	3.6	19.3
Hs-PI- <i>b</i> -PVTMS-3	130	38	10.3	143	12.6	3.7	13.8
H-PI- <i>b</i> -PVTMS-3	120	35	8.8	173	13.6	4	19.6
<b>(41%)PI-<i>b</i>-PVTMS-4</b>	65	17.3	4.9	95	13	3.5	19.4
Hs-PI- <i>b</i> -PVTMS-4	53	14.5	4.3	78	12.3	3.4	18
H-PI- <i>b</i> -PVTMS-4	57	17.6	4.7	89	12.2	3.8	19
<b>PVTMS ref.</b>	164	48	12.3	219	13.3	3.9	17.8

<sup>a</sup> 1 barrer = 10<sup>-10</sup> cm<sup>3</sup> (STP) cm/(cm<sup>2</sup> s cmHg)



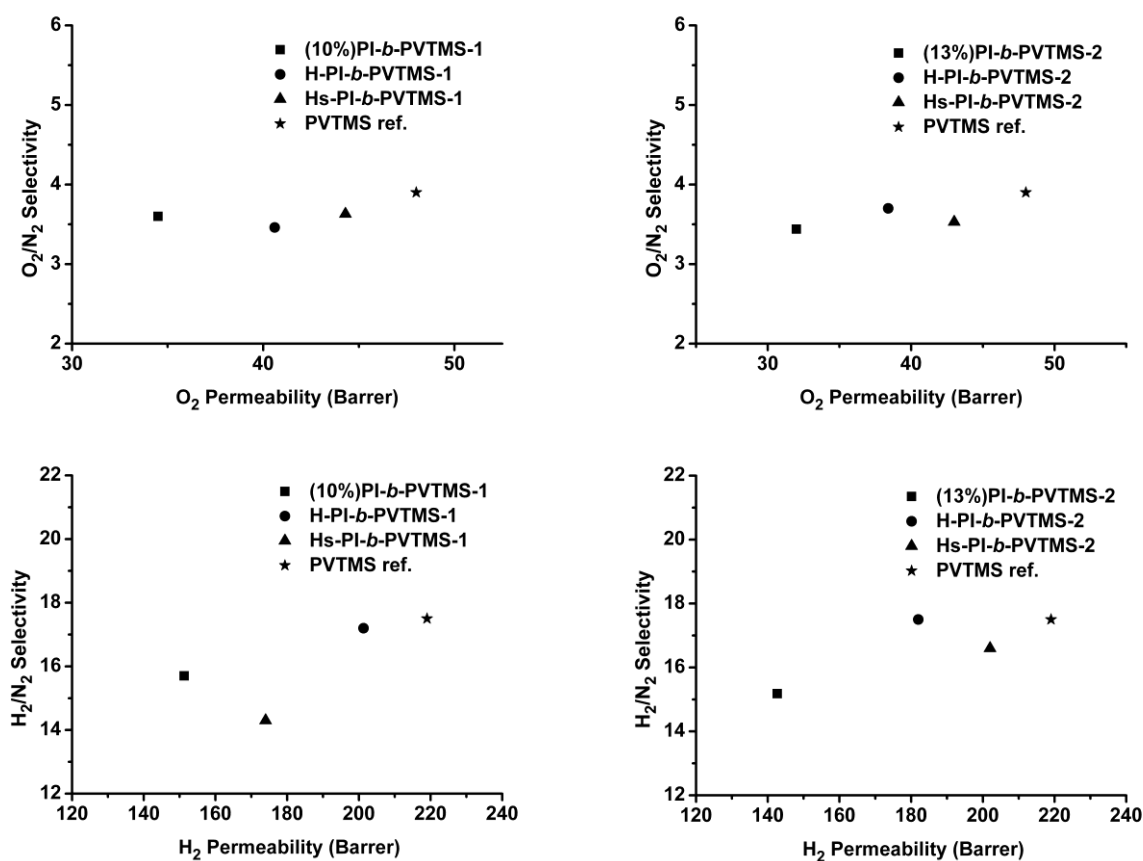


**FIGURE 4.1.8.** Relationship between  $O_2$  and  $H_2$  permeabilities and  $O_2/N_2$  and  $H_2/N_2$  selectivities of low isoprene contents (10 and 13 wt. %) PI-*b*-PVTMS block copolymers and their modified analogues: Hs-PI-*b*-PVTMS and H-PI-*b*-PVTMS.

The initial block copolymers showed advantageous film forming properties. Stable films can be formed with low molecular weight block copolymers (96 kg/mol) while larger molecular weights (> 150 kg/mol) are required for PVTMS [10]. For polymer production and membrane formation it means that the overall molecular weight of the polymer can be relatively low when compared with the one of PVTMS homopolymer used in industrial membrane formation. Lower molecular weights of polymers could lead to the formation of thinner selective layers resulting in high performance membranes. Thinner selective layers ensure lower polymer consumption, as well.

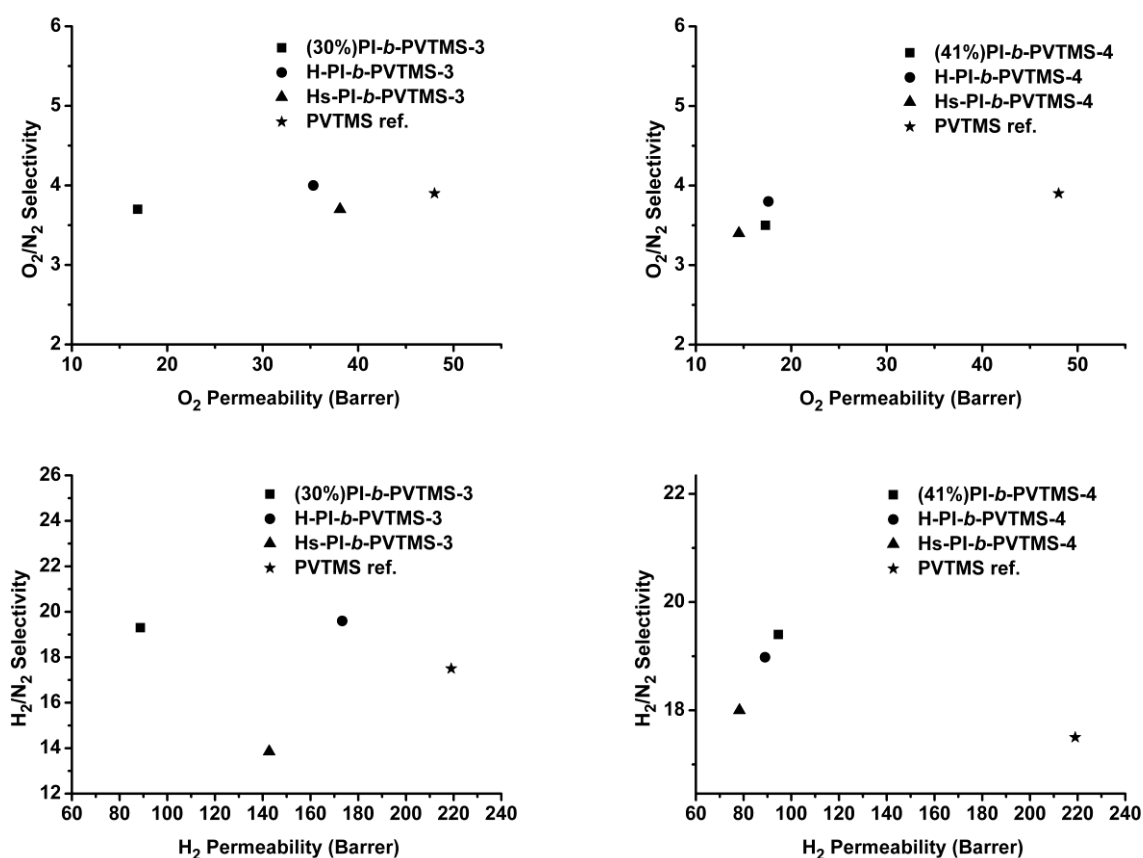


**FIGURE 4.1.9.** Relationship between  $O_2$  and  $H_2$  permeabilities and  $O_2/N_2$  and  $H_2/N_2$  selectivities of high isoprene contents (30 and 41 wt. %) PI-*b*-PVTMS block copolymers and their modifications: Hs-PI-*b*-PVTMS and H-PI-*b*-PVTMS

However, the presence of double bonds on the main chain of the polyisoprene block of the initial block copolymer causes a hindrance on the storage time of the material because of their temperature and light sensitive characteristics. Antioxidant additives or stabilizers have been used in the industry for sensitive natural materials which are not beneficial for the formation of large amounts of thin film composite membranes (TFCM). The absence of double bonds in the modified block copolymers lead to longer storage time without using any stabilizers.

#### 4.1.8. Density and Fractional Free Volume (FFV)

The densities and fractional free volumes of the initial and modified block copolymers at ambient conditions are presented in Table 4.1.5. Introduction of polyisoprene blocks to PVTMS leads to an increase of density depending on the amount of polyisoprene. The densities of polyisoprene and PVTMS are 0.913 g/cm<sup>3</sup> and 0.875 g/cm<sup>3</sup>, respectively [10]. Therefore, the densities of block copolymers are larger than of pure PVTMS. After hydrosilylation of the polyisoprene blocks the densities decreased with changing the polymer characteristics from a rubbery polyisoprene to a glassy silicon-containing block.

**TABLE 4.1.5.** Densities and Fractional Free Volumes of the Block Copolymers Before and After Modifications.

Polymers	$\rho$ (g/cm <sup>3</sup> )	FFV, %	Polymers	$\rho$ (g/cm <sup>3</sup> )	FFV, %
<b>(10%)PI-<i>b</i>-PVTMS-1</b>	0.882	20.1	H-PI- <i>b</i> -PVTMS-2	0.877	20.6
Hs-PI- <i>b</i> -PVTMS-1	0.867	21.1	<b>(30%)PI-<i>b</i>-PVTMS-3</b>	0.906	18.1
H-PI- <i>b</i> -PVTMS-1	0.874	20.8	Hs-PI- <i>b</i> -PVTMS-3	0.876	19.9
<b>(13%)PI-<i>b</i>-PVTMS-2</b>	0.887	19.7	H-PI- <i>b</i> -PVTMS-3	0.891	19.4
Hs-PI- <i>b</i> -PVTMS-2	0.868	21	PVTMS-ref	0.875	21.1

The fractional free volume (FFV) was calculated as discussed in the experimental part. FFV is one of the most important parameters influencing gas transport properties [11]. In the initial block copolymers the FFV decreases with increasing polyisoprene content. Modified block copolymers showed increased FFV compare to initial block copolymers. Especially, hydrosilylated block copolymers showed the highest FFV comparing to the initial and hydrogenated block copolymers and similar to PVTMS-ref. This increased FFV resulted from bulky and symmetrical triethylsilyl

groups attached to the main chain of polyisoprene block [12]. However, the O<sub>2</sub> and H<sub>2</sub> permeability coefficients of hydrosilylated block copolymers were still below the ones of PVTMS-ref. This might arise from the longer linear substituents of triethylsilyl (CH<sub>3</sub>CH<sub>2</sub>-) groups according to trimethylsilyl groups (CH<sub>3</sub>-) of PVTMS, as discussed by Yampolskii [12]. Figure 4.1.10 shows the O<sub>2</sub> permeability coefficients as a function of 1/FFV for the block copolymers and their modifications. The FFV data are in agreement with the permeability data: higher FFV leads to higher permeability.

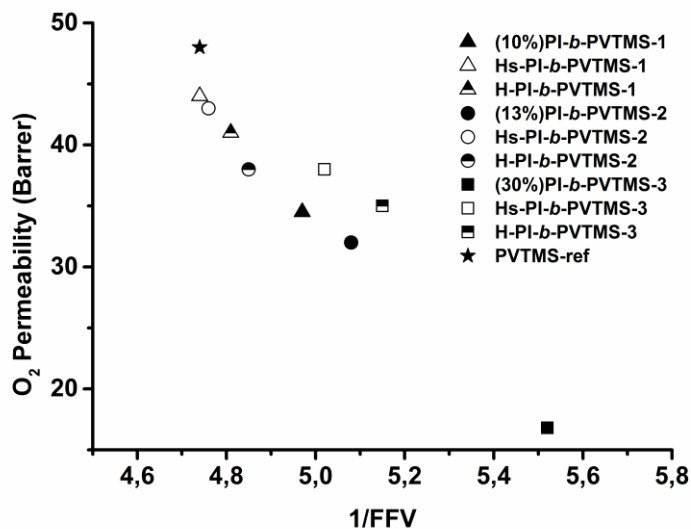


**FIGURE 4.1.10.** O<sub>2</sub> permeability coefficients of (10, 13 and 30 wt. %) PI-*b*-PVTMS block copolymers and their modifications as a function of reciprocal fractional free volume (1/FFV).

#### 4.1.9. Conclusions

It was demonstrated that chemical modification of polyisoprene-*block*-poly(vinyl trimethylsilane) (PI-*b*-PVTMS) block copolymers by hydrosilylation and hydrogenation is a highly effective way to improve the gas transport properties of PI-*b*-PVTMS. The modification processes involve the addition of triethylsilyl pendant groups (hydrosilylation) and hydrogenation of the unsaturated double bonds of the PI main chain. The strategy adopted in this study appears to be entirely

satisfactory in terms of efficiency and simplicity. Successful modification was confirmed by FT-IR,  $^1\text{H}$ -NMR, GPC, and TGA. The products dissolve in conventional solvents such as tetrahydrofuran (THF), toluene and chloroform ( $\text{CHCl}_3$ ) from which membranes can easily be formed. The thermal stability of modified polymers was improved compared to PI-*b*-PVTMS. In the case of gas permeation, membranes made of the modified block copolymers exhibit a significant increase in  $\text{O}_2$  and  $\text{H}_2$  permeabilities reaching the PVTMS-ref level while maintaining the same selectivity. The improvement of  $\text{O}_2$  and  $\text{H}_2$  permeabilities at low isoprene content are up to 40 % and at high isoprene content up to 125 % compared to PI-*b*-PVTMS. The modified block copolymers demonstrate very reasonable gas transport performance while keeping good mechanical stability of the PI-*b*-PVTMS. Successful film formation with low molecular weights of modified block copolymers enables the formation of thinner selective layers in thin film composite membrane (TFCM).

#### 4.1.10. References

- [1] X. Guo, R. Farwaha, G.L. Rempel, Catalytic hydrosilylation of diene-based polymers. 1. Hydrosilylation of polybutadiene, *Macromolecules*, 23 (1990) 5047-5054.
- [2] P. Phinyocheep, S. Pasiri, O. Tavichai, Diimide hydrogenation of isoprene–styrene diblock copolymers, *Journal of Applied Polymer Science*, 87 (2003) 76-82.
- [3] Y. Ren, T.P. Lodge, M.A. Hillmyer, Synthesis, characterization, and interaction strengths of difluorocarbene-modified polystyrene–polyisoprene block copolymers, *Macromolecules*, 33 (2000) 866-876.
- [4] W.J. Koros, B.J. Story, S.M. Jordan, K. O'Brien, G.R. Husk, Material selection considerations for gas separation processes, *Polymer Engineering and Science*, 27 (1987) 603-610.

- [5] F. Ciampelli, D. Morero, M. Cambini, Some remarks on the infrared analysis of polyisoprenes, *Die Makromolekulare Chemie*, 61 (1963) 250-253.
- [6] Y. Tanaka, Y. Takeuchi, M. Kobayashi, H. Tadokoro, Characterization of diene polymers. I. Infrared and NMR studies: Nonadditive behavior of characteristic infrared bands, *Journal of Polymer Science Part B: Polymer Physics*, 9 (1971) 43-57.
- [7] T.J. Crowley, K.Y. Choi, Control of copolymer hydrodynamic volume distribution in a semibatch free radical copolymerization process, *Computers and Chemical Engineering*, 23 (1999) 1153-1165.
- [8] J. Wang, G. Mao, C.K. Ober, E.J. Kramer, Liquid crystalline, semifluorinated side group block copolymers with stable low energy surfaces: Synthesis, liquid crystalline structure, and critical surface tension, *Macromolecules*, 30 (1997) 1906-1914.
- [9] M.A. Hillmyer, F.S. Bates, Synthesis and characterization of model polyalkane-poly(ethylene oxide) block copolymers, *Macromolecules*, 29 (1996) 6994-7002.
- [10] S. Rangou, S. Shishatskiy, V. Filiz, V. Abetz, Poly(vinyl trimethylsilane) and block copolymers of vinyl trimethylsilane with isoprene: Anionic polymerization, morphology and gas transport properties, *European Polymer Journal*, 47 (2011) 723-729.
- [11] H. Li, B.D. Freeman, O.M. Ekiner, Gas permeation properties of poly(urethane-urea)s containing different polyethers, *Journal of Membrane Science*, 369 (2011) 49-58.
- [12] Y. Yampolskii, Polymeric gas separation membranes, *Macromolecules*, 45 (2012) 3298-3311.

## **4.2. Effect of Azidation and UV Cross-linking of Poly(epichlorohydrin) and Poly[(ethylene oxide)-*ran*-(epichlorohydrin)] on Gas Transport Properties**

### **4.2.1. Brief Introduction**

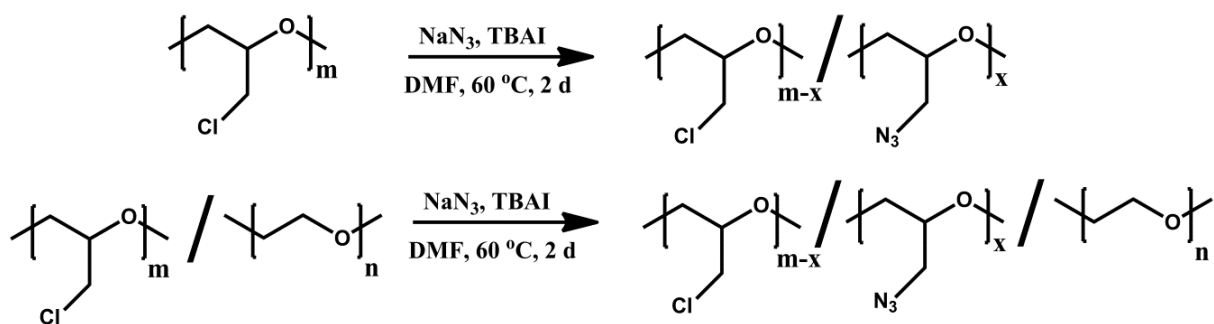
Poly(epichlorohydrin) homopolymer (H-Hydrin) and Poly[(ethylene oxide)-*ran*-(epichlorohydrin)] copolymer (C-Hydrin) are the commercially available thermoplastic elastomers under the trade name Hydrin<sup>®</sup> composed of only hard segment and hard and soft segments, respectively. Especially C-Hydrin is known to exhibit high permeability and selectivity towards CO<sub>2</sub> [1]. In the copolymer system, the use of hard segment is to provide mechanical strength and on the other hand soft segment gives the elastomeric behavior and gas separation property. Additionally, Hydrin polymers have the advantage for further modifications owing to the chloride pendent groups.

This chapter focuses on the modification and UV cross-linking of chlorine-containing H-Hydrin and C-Hydrin polymers via azidation chemistry and nitrene reaction, respectively, and their gas transport properties. Moreover, the correlation between  $T_g$  and gas transport properties after azidation and UV cross-linking is reported. In addition, before and after modification and UV cross-linking the thermal decomposition behaviors of H-Hydrin and C-Hydrin polymers are studied and discussed.

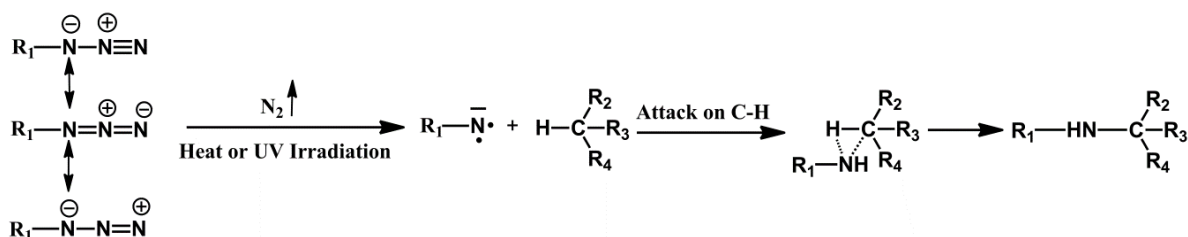
### **4.2.2. Synthesis and Characterization of Azidated Poly(epichlorohydrin) (A-H-Hydrin) and Poly[(ethylene oxide)-*ran*-(epichlorohydrin)] (A-C-Hydrin), and their UV Cross-linked (UV-A-H-Hydrin and UV-A-C-Hydrin) Counterparts**

Poly(epichlorohydrin) is a chlorine-containing polymer and suitable initial material to synthesize new polymers with functional groups enabling easy post-modification. In this study, we report on polymer modification by using the most commonly applied route of azidation chemistry: “Halide

Displacement by Azide Ion” [2]. Azidation was performed H-Hydrin) and C-Hydrin (Scheme 4.2.1). The cross-linking reaction of azidated Hydrin polymers was performed in the presence of UV irradiation. The azide pendent groups of the polymer are 1,3 dipolar structures which can decompose to highly reactive divalent nitrene radicals and molecular nitrogen ( $N_2$ ). The nitrene radicals can attack three types of C-H bonds with the reactivity order of tertiary > secondary > primary [3]. The most probable mechanism is shown in Scheme 4.2.2. The decomposition reaction of azide units cleanly generates the nitrene radical and nitrogen gas without having any other low molecular weight by-products that can lead to contaminations of the polymer network.



**SCHEME 4.2.1.** Azidation of H-Hydrin and C-Hydrin



**SCHEME 4.2.2.** The mechanism of UV cross-linking of azidated Hydrin polymers

The molecular weights of H-Hydrin and C-Hydrin having two different azidation degrees are reported in Table 4.2.1. In the case of H-Hydrin the molecular weight significantly decreases



during the azidation process with increased polydispersity. This might arise from the degradation process on the main chain of the polymer during azidation reaction due to the excess usage of  $\text{NaN}_3$  [5]. On the other hand, the molecular weight of C-Hydrin approximately remains constant with an important decrease in polydispersity. C-Hydrin having low composition of epichlorohydrin (35 wt. %) units results in less usage of  $\text{NaN}_3$  in azidation process compared to H-Hydrin. This provides an azidation reaction without degradation. The significant decrease in polydispersity can be explained by excess precipitation in ethanol leading to removal of low molecular weight copolymers.

**TABLE 4.2.1.** Molecular Weight, Polydispersity and Percentage of Modification of Hydrin Polymers

<b>Polymers</b>	<b><math>M_w^a</math> (kg/mol)</b>	<b><math>M_n</math> (kg/mol)</b>	<b>PDI</b>	<b>Az %<sup>b</sup></b>	<b>Yield (%)<sup>c</sup></b>
<b>H-Hydrin</b>	2178	401	5.4	-	
<b>(33 wt. %)-A-H-Hydrin</b>	1018	181	5.6	33	55
<b>(72 wt. %)-A-H-Hydrin</b>	984	132	7.4	71	51
<b>C-Hydrin</b>	928	79	11.7	-	
<b>(52 wt. %)-A-C-Hydrin</b>	888	219	4.05	52	72
<b>(100 wt. %)-A-C-Hydrin</b>	825	353	2.3	100	69

<sup>a</sup>Molecular weights were determined by GPC; <sup>b</sup>Molar percentage of azidation in terms of chloride moieties was determined by  $^1\text{H}$ -NMR analysis; <sup>c</sup>Gravimetrically calculated values .

The extent of modification was determined using area integration of  $^1\text{H}$ -NMR spectra. The  $^1\text{H}$ -NMR spectrum of H-Hydrin is characterized by a broad signal around 3.7 ppm belongs to chloromethyl ( $-\text{CH}_2\text{Cl}$ ) protons and methylene ( $-\text{OCH}_2-$ ) protons, and a signal at 3.62 ppm that corresponds to methine ( $-\text{O}-\text{CH}_2\text{CH}-$ ) proton. After azidation, in the  $^1\text{H}$ -NMR spectra of azidated H-Hydrin homopolymers the new signal at 3.4 ppm corresponding to azidomethyl ( $-\text{CH}_2\text{N}_3$ )

protons appeared with shifted signal of chloromethyl protons from 3.7 ppm indicates successful modification (Figure 4.2.1). The shifts of the signals of methylene and methine protons from 3.7 to lower ppm can be observed after each degree of modification. The similar effect of modification on shifting of signals was also observed in the  $^1\text{H}$ -NMR spectra of azidated C-Hydrin copolymers (Figure 4.2.2). Additionally, the broad signal at 3.62 ppm belongs to ethylene oxide ( $-\text{CH}_2\text{CH}_2-\text{O}-$ ) protons and methine proton.

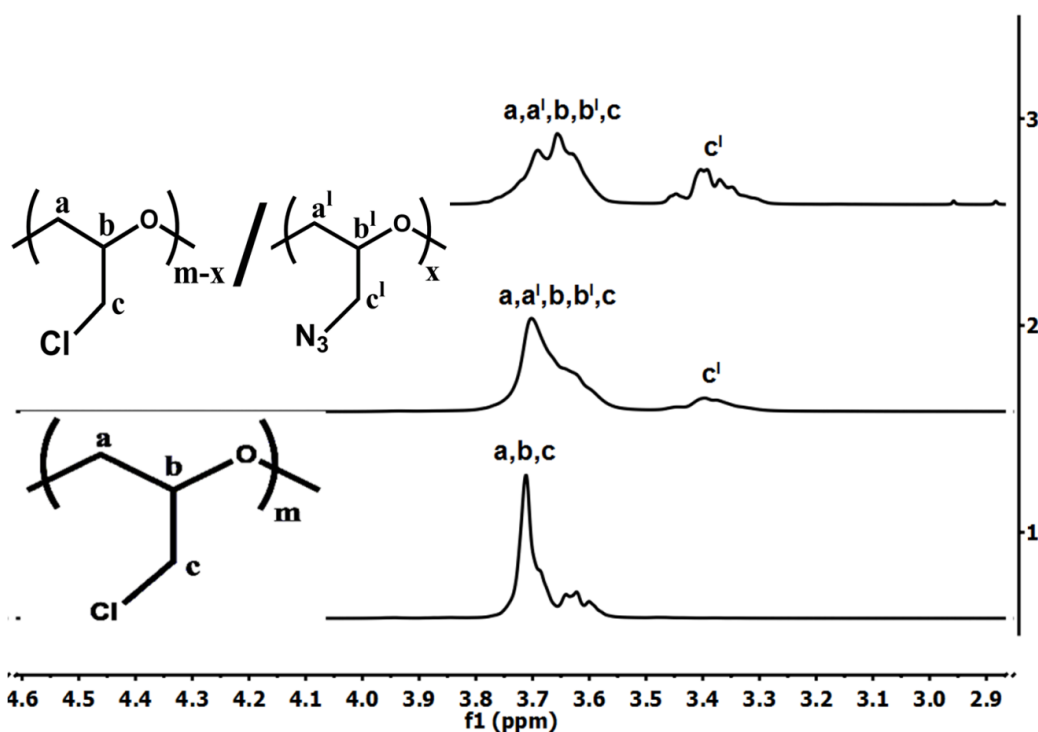


**FIGURE 4.2.1.**  $^1\text{H}$ -NMR spectra of H-Hydrin (1), (33 wt. %)A-H-Hydrin (2) and (71 wt. %)A-H-Hydrin (3) in  $\text{CDCl}_3$ .

The composition of the polymers can be calculated using the following equation:

$$\text{Azide \%} = \frac{5\text{ICH}_2\text{N}_3 100}{2\text{ICH}_2\text{CHCH}_2\text{Cl} + 5\text{ICH}_2\text{N}_3} \quad (4.2.1)$$

where  $ICH_2N_3$  and  $ICH_2CHCH_2Cl$  represent the intensities of the integrals corresponding to the  $CH_2N_3$  and the  $CH_2CHCH_2Cl$  protons, respectively. The percentages of azidation of two types of Hydrin polymers are presented in Table 4.2.1.

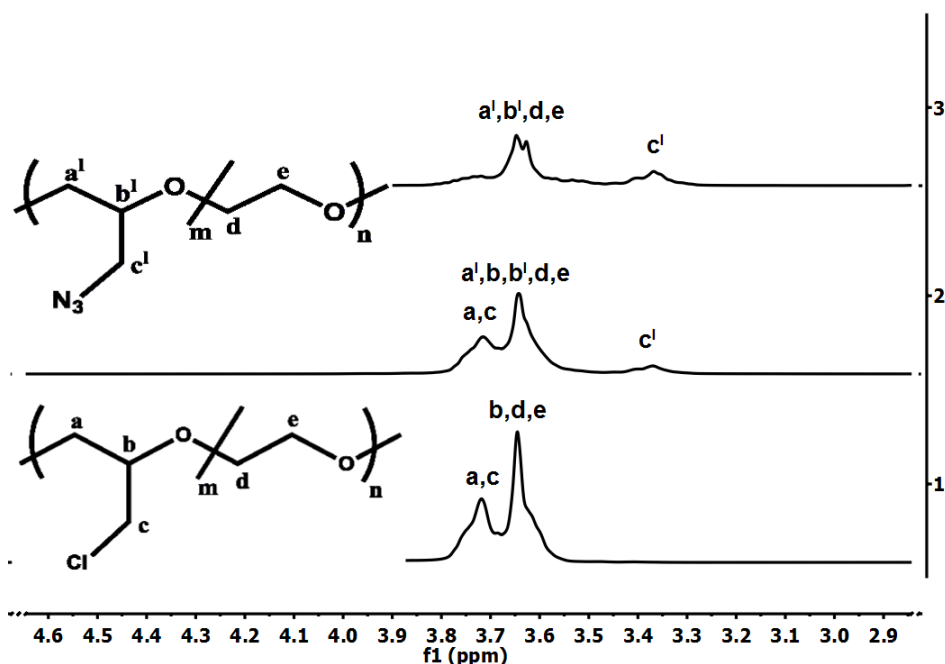


**FIGURE 4.2.2.**  $^1H$ -NMR spectra of C-Hydrin (1), (52 wt. %) A-C-Hydrin (2) and (100 wt. %) A-C-Hydrin (3) in  $CDCl_3$ .

The chemical shifts can also be detected in the  $^{13}C$ -NMR Spectra. In the  $^{13}C$ -NMR spectrum of H-Hydrin the signals at 79.4 ppm, 69.8 ppm and 44.1 ppm which are assigned to the methinic carbon ( $-O-CH_2CH-$ ), methylenic carbon ( $-OCH_2-$ ) on the main chain and chloromethyl carbon ( $-CH_2Cl$ ), respectively. After azidation, in the  $^{13}C$ -NMR spectra of azidated H-Hydrin homopolymers the shifted signal of chloromethyl carbon from 44.1 ppm to 52.2 ppm regarding to azidomethylene carbon prove that modification has taken place (Figure 4.2.3). However, the presence of signal at 44.1 ppm indicates that modification is not complete. Likewise, the  $^{13}C$ -NMR spectra of C-Hydrin

and azidated C-Hydrin copolymers show the same shifting behavior. The disappearance of the signal at 44.1 ppm related to chloromethyl carbon indicates quantitative conversion (Figure 4.2.4).

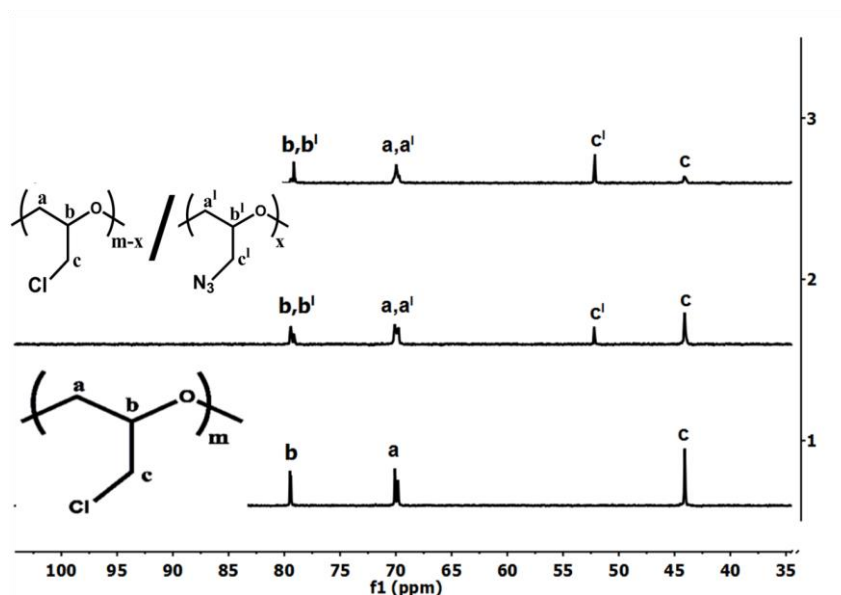


**FIGURE 4.2.3.**  $^{13}\text{C}$ -NMR spectra of H-Hydrin (1), (33 wt. %)A-H-Hydrin (2) and (71 wt. %)A-H-Hydrin (3) in  $\text{CDCl}_3$ .

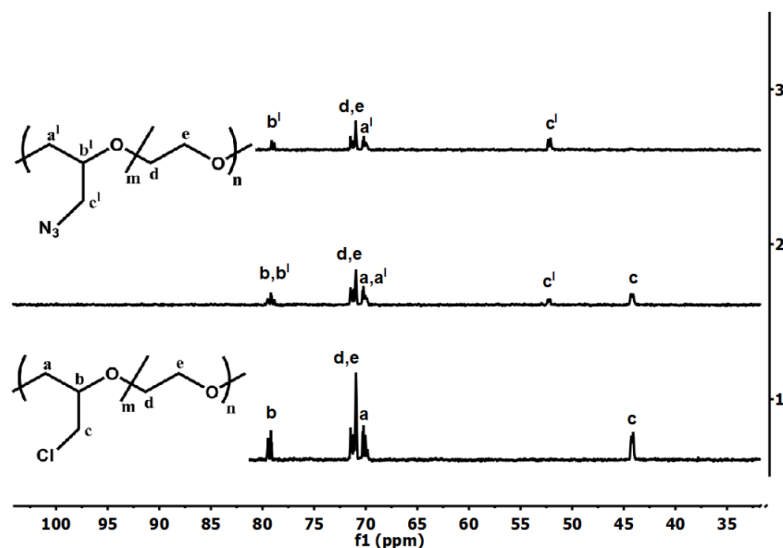


**FIGURE 4.2.4.**  $^{13}\text{C}$ -NMR spectra of C-Hydrin (1), (52 wt. %)A-C-Hydrin (2) and (100 wt. %)A-C-Hydrin (3) in  $\text{CDCl}_3$ .

In the FT-IR spectra of initial and modified H-Hydrin homopolymers, successful azidation was further supported by the observation of the azide stretching band at  $2097\text{ cm}^{-1}$  and  $2091\text{ cm}^{-1}$  corresponding to 33 wt. % and 71 wt. % azidated H-Hydrin, respectively (Figure 4.2.5). Likely, FTIR spectra of C-Hydrin and its modified analogues show the appearance of the azide stretching band at  $2097\text{ cm}^{-1}$  and  $2096\text{ cm}^{-1}$  relevant to 52 wt. % and 100 wt. % azidated C-Hydrin, respectively (Figure 4.2.6). After UV irradiation the decrease in the band areas for both polymers indicate successful cross-linking reaction. This decrease in the stretching band area of azidated H-Hydrin homopolymers is much higher than azidated C-Hydrin copolymers due to the amount of azide pendent groups and tertiary protons which directly increase the reaction reactivity. In addition, the cross-linked polymers were also analysed for their gel content [4]. Initial and modified Hydrin polymers are readily soluble in common solvents such as chloroform, THF, dichloromethane, dichlorobenzene. However, the resulting cross-linked Hydrin films are insoluble in common solvents mentioned above. It was also observed that the cross-linked H-Hydrin films have higher gel content than the cross-linked C-Hydrin films (Table 4.2.2). The conclusions drawn from the FT-IR and gel content analysis is the nitrene reaction generated by azide pendent groups led to an insoluble cross-linked network.

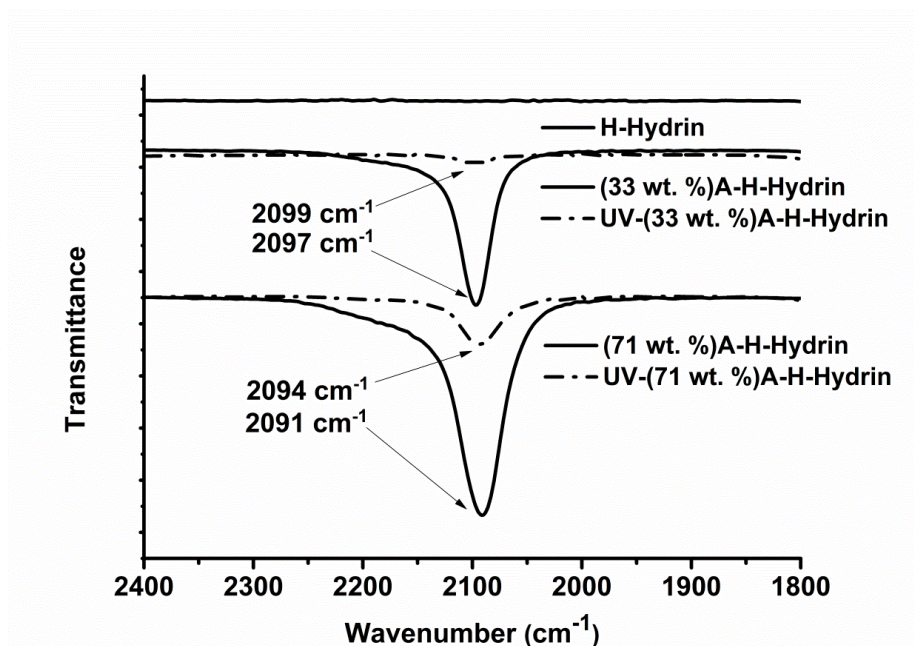


**FIGURE 4.2.5.** FT-IR spectra of H-Hydrin, azidated H-Hydrin homopolymers and their UV cross-linked analogues.

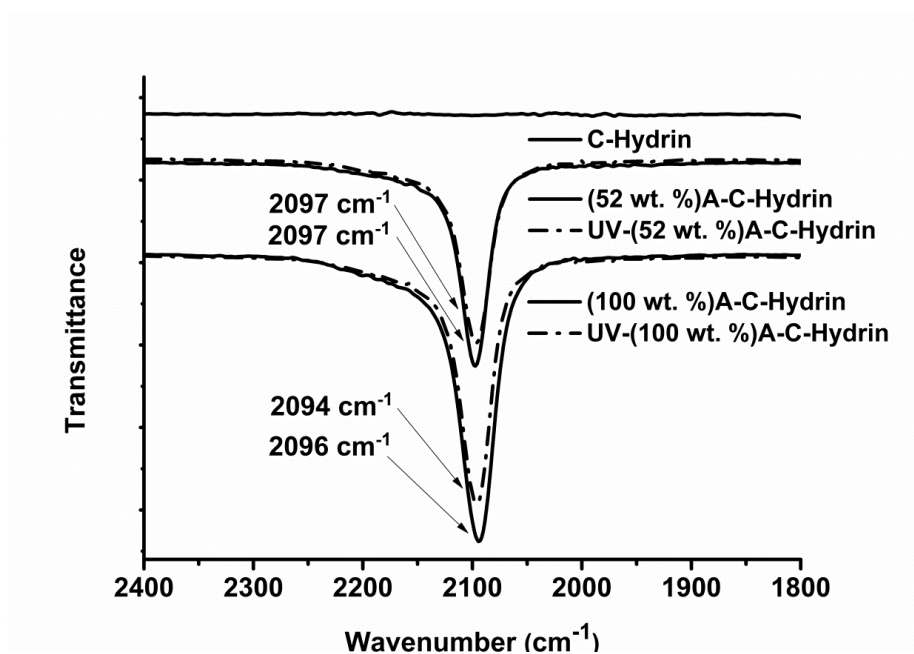


**FIGURE 4.2.6.** FT-IR spectra of C-Hydrin, azidated C-Hydrin copolymers and their UV cross-linked analogues.

**TABLE 4.2.2.** Gel Content Analysis of Cross-Linked Hydrin Polymers as Results from Swelling Experiments (%).

Polymers	Gel Content (Swelling)
UV-(33 wt. %)A-H-Hydrin	91
UV-(71 wt. %)A-H-Hydrin	87.2
UV-(52 wt. %)A-C-Hydrin	88.5
UV-(100 wt. %)A-C-Hydrin	78.2

#### 4.2.3. Thermal Characterization

The glass transition temperatures ( $T_g$ ) of the initial and modified polymers were determined by differential scanning calorimetry (DSC). The degree of azidation indicates the significant impact on the  $T_g$  of the modified polymers [5, 6]. In the case of both type of polymers (H-Hydrin and C-Hydrin) the  $T_g$  crucially decreased with increasing degree of azidation (Figure 4.2.7-8).

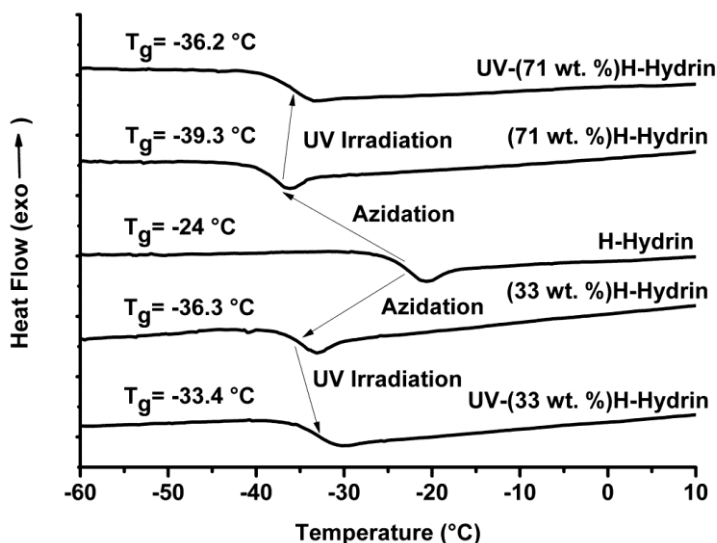


**FIGURE 4.2.7.** DSC thermograms of H-Hydrin, azidated H-Hydrin homopolymers and their UV cross-linked counterparts.

Rapidly decreased  $T_g$  after modification can be explained by increased flexibility of pendent groups influencing the main chain mobility of the polymer [7]. Two main reasons of increased main chain flexibility are: a) newly introduced azide units have longer chain as pendent group compared to chloride which is only one large atom [8] and b)  $R-N^1-N^2-N^3$  and  $R-N^1-N^2-N^3$  conformations of azide units have two different angles which are  $115.2^\circ$  (bent) and  $172.5^\circ$  (linear), respectively, leading them to higher mobility [2]. The glass transition temperature is a practical and sensitive method to follow the UV cross-linking reaction. After cross-linking  $T_g$  of the polymers increases because of reduced flexibility and mobility of chains.

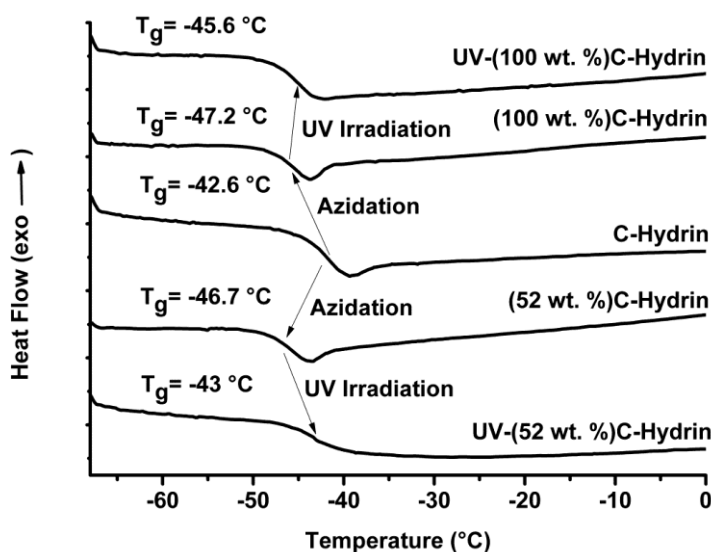


**FIGURE 4.2.8.** DSC thermograms of C-Hydrin, azidated C-Hydrin copolymers and their UV cross-linked counterparts.

Thermogravimetric analysis (TGA) is the technique that is commonly used for having fast evaluation of the thermal stability of various polymeric materials. The thermal stability of the initial Hydrin polymers and their azidated derivatives was further investigated by TGA and derivative thermogravimetry (DTG). TGA curves are presented in Figure 4.2.9 and compared with



DSC decomposition temperatures. The decomposition behaviors and char yields of the species are given in Table 4.2.3. The thermal stability of both types of Hydrin polymers decreased after azidation. Azidated H-Hydrin showed two weight loss steps belonging to azide pendent group decomposition (160 °C-200 °C) which is the starting point of the thermal generation nitrene radicals and polyether main chain decomposition (200 °C-500 °C) (Figure 4.2.9A). Two exothermic peaks in DSC and two degradation peaks in DTG at the similar temperatures are additional proof supporting the two steps decomposition behavior of azidated H-Hydrin (Figure 4.2.9C and Figure 4.2.10). Furthermore, Figure 4.2.9C showed that an increased degree of azidation leads to a higher intensity of the exothermic peak related to azide decomposition. Azidated H-Hydrin homopolymers have much higher char yields compared to initial H-Hydrin because of thermal cross-linking of azide pendent groups, however; they have less char yield than UV cross-linked H-Hydrin (Table 4.2.3). The reason is that polymer main chain decomposition starts before the ending of thermal cross-linking which is the sign of uncompleted curing reaction (Figure 4.2.9A-C). This shows that UV irradiation is the better and more efficient way to obtain successful cross-linking compared to the thermal treatment for Hydrin polymers. After UV irradiation of azidated H-Hydrin one step weight loss in TGA and one exothermic peak in DSC can be observed at the decomposition temperature of polyether main chain that indicates successful cross-linking reaction (Figure 4.2.9A-C) (Figure 4.2.10). Additionally, the increased char yields are another indication for cross-linking with the formation of highly thermal stable permanent polymeric network [9].

**TABLE 4.2.3.** Thermal Properties of Initial Hydrin Polymers and the Counterparts after Modification and UV Cross-linking

Polymers	T <sub>p1</sub> <sup>a</sup> (DSC)	T <sub>p1</sub> <sup>b</sup> (DTG)	T <sub>p2</sub> <sup>c</sup> (DSC)	T <sub>p2</sub> <sup>d</sup> (DTG)	Y <sub>c</sub> <sup>e</sup> at 800 °C (%)
	(°C)	(°C)	(°C)	(°C)	
<b>H-Hydrin</b>	–	–	352	349	8.7
<b>(33 %)A-H-Hydrin</b>	192	188	245	234	21.9
<b>UV-(33 %)A-H-Hydrin</b>	–	–	243	238	25
<b>(71 %)A-H-Hydrin</b>	196	189	242	229	23
<b>UV-(71 %)A-H-Hydrin</b>	–	–	244	233	25.7
<b>C-Hydrin</b>	–	–	346	344	9.3
<b>(52 %)A-C-Hydrin</b>	226	219	226	219	12.6
<b>UV-(52 %)A-C-Hydrin</b>	–	–	226	235	23.8
<b>(100 %)A-C-Hydrin</b>	225	220	225	220	11.7
<b>UV-(100 %)A-C-Hydrin</b>	–	–	230	235	24.9

<sup>a-b</sup> T<sub>p1</sub>: The temperature for azide decomposition and nitrene generation. <sup>c-d</sup> T<sub>p2</sub>: The temperature for polymer main chain decomposition. <sup>e</sup> Y<sub>c</sub>: Char yield

In the case of C-Hydrin copolymers, after azidation the thermal stability of the polymers decreased as well. Azidated C-Hydrin showed one weight loss step which indicates that the decomposition of azide pendent groups and polyether main chain of the polymer rapidly started together (Figure 4.2.9B-D). Therefore, the degradation step (TGA) and the exothermic peak (DSC) are much sharper than azidated H-Hydrin (Figure 4.2.9). An additional indicator of the simultaneous decomposition of azide pendent groups and polymer main chain is the uncompleted curing process that can be observed from the char yields of the polymers. Azidated C-Hydrin copolymers have much less increase in char yields than UV cross-linked C-Hydrin compared to initial C-Hydrin (Table 4.2.3). This showed that thermal cross-linking cannot take place because of the simultaneous starting decomposition of the polymer main chain. After UV cross-linking of azidated C-Hydrin the smoother and larger degradation step and exothermic peak were the proof

of successful cross-linking process (Figure 4.2.9B-D). Moreover, the highly increased char yields are another proof for cross-linking (Table 4.2.3).

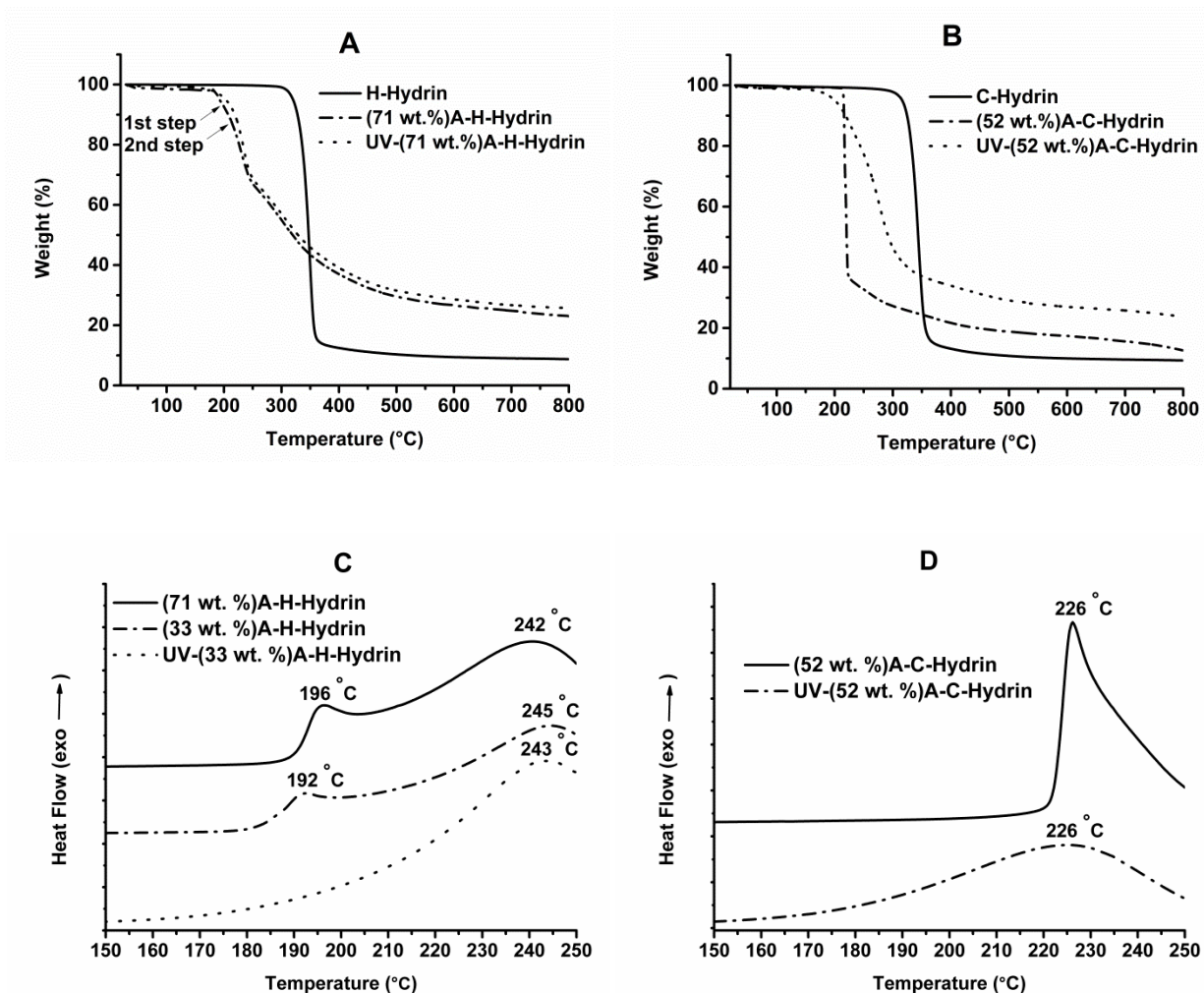


**FIGURE 4.2.9.** TGA analysis of H-Hydrin, 33 wt. % azidated H-Hydrin and after UV cross-linking (A); C-Hydrin, 52 wt. % azidated C-Hydrin and after UV cross-linking (B); DSC exotherms of 33 wt. % azidated H-Hydrin, its UV cross-linked analogue and 71 wt. % azidated H-Hydrin (C); 52 wt. % azidated C-Hydrin and its UV cross-linked analogue (D).

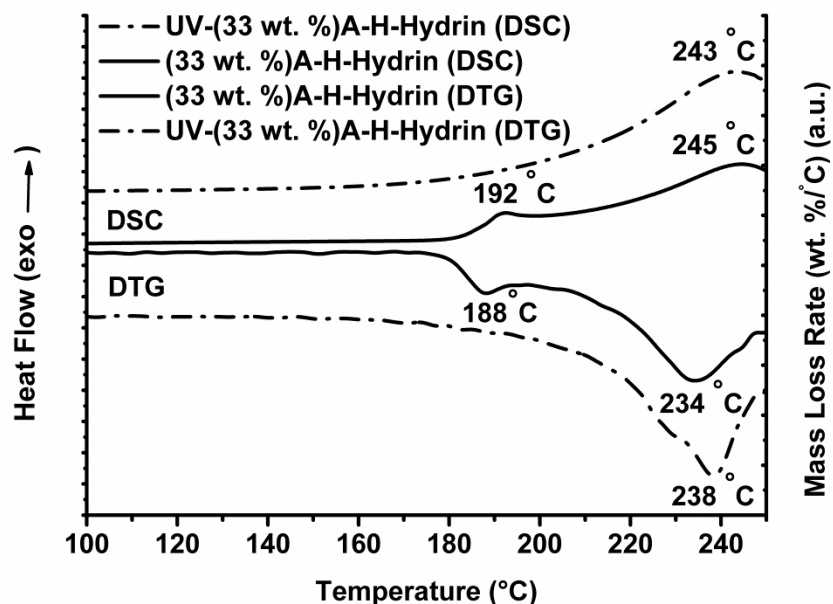


**FIGURE 4.2.10.** DSC and DTG curve comparisons of 33 wt. % azidated H-Hydrin and its UV cross-linked counterpart.

#### 4.2.4. Gas Transport Properties

The results of single gas permeation experiments carried out on poly(epichlorohydrin) homopolymer (H-Hydrin) and poly[(ethylene oxide)-*ran*-(epichlorohydrin)] copolymer (C-Hydrin), their two degrees of azidation ((33 and 71 wt. %)A-H-Hydrin and (51 and 100 wt. %)A-C-Hydrin), and UV irradiated (UV-(51 and 100 wt. %)A-C-Hydrin) counterparts are reported in Table 4.2.4. The general tendency of permeation rate of the modified Hydrin polymers is the same as for H-Hydrin and C-Hydrin ( $\text{CO}_2 > \text{H}_2 > \text{CH}_4 > \text{N}_2$ ). The order is identical to most rubbery polymeric membranes [10]. There is a strong correlation between the order of permeability coefficients and critical temperatures of gases ( $\text{CO}_2$  (304.2 K)  $>$   $\text{CH}_4$  (190.6 K)  $>$   $\text{N}_2$  (126.2 K)  $>$   $\text{H}_2$  (33.2 K)) [10]. The increasing critical temperature generally expresses an increase in gas solubility in polymers. Therefore, the penetrants with higher critical temperature usually have

higher condensability and solubility coefficients [11]. For example, CO<sub>2</sub> often has a higher permeability coefficient than smaller penetrants, such as H<sub>2</sub>, associated with much higher solubility of CO<sub>2</sub>. H<sub>2</sub> with the lowest critical temperature would be expected to have the lowest permeability coefficient, however; the smallest kinetic diameter of H<sub>2</sub> (CH<sub>4</sub> (3.8 Å) > N<sub>2</sub> (3.64 Å) > CO<sub>2</sub> (3.3 Å) > H<sub>2</sub> (2.89 Å)) [10] results in a high diffusion coefficient that makes it more permeable than all other gases except CO<sub>2</sub>. That is, the order of permeability coefficients is based on the competition between solubility favoring the penetrants with higher condensability and diffusivity favoring the gases with smaller kinetic diameter.

**TABLE 4.2.4.** Gas Permeability Coefficients and Selectivity Values of Homo and Copolymers (H-Hydrin and C-Hydrin), and Their Azidated and UV Cross-Linked Counterparts. In the Brackets is the Azidation Degree in wt. % of the Homo and Copolymers Given.

Polymers	P(CO <sub>2</sub> ) <sup>a</sup>	P(N <sub>2</sub> )	P(CH <sub>4</sub> )	P(H <sub>2</sub> )	$\alpha$ (CO <sub>2</sub> /N <sub>2</sub> )	$\alpha$ (CO <sub>2</sub> /CH <sub>4</sub> )	$\alpha$ (CO <sub>2</sub> /H <sub>2</sub> )	$\alpha$ (H <sub>2</sub> /N <sub>2</sub> )
<b>H-Hydrin</b>	6	0.15	0.44	4.6	40	14	1.3	31
<b>(33 %)A-H-Hydrin</b>	21	0.63	1.6	8	33	13	2.6	12.7
<b>(71 %)A-H-Hydrin</b>	32	0.997	2.7	11	32	11.9	2.9	11
<b>C-Hydrin</b>	41	0.97	3.1	9.4	42	13	4.3	9.7
<b>(52 %)A-C-Hydrin</b>	69	1.82	5.2	14.3	38	13.4	4.8	7.9
<b>UV</b>	11.8	0.29	0.51	9.3	41	23	1.3	32
<b>(52 %)A-C-Hydrin</b>								
<b>(100 %)A-C-Hydrin</b>	92	2.3	7.2	16.6	40	14	5.5	7.2
<b>UV</b>	7.1	0.18	0.26	7.05	39	27	1	39
<b>(100 %)A-C-Hydrin</b>								

<sup>a</sup> 1 barrer = 10<sup>-10</sup> cm<sup>3</sup> (STP) cm/(cm<sup>2</sup> s cmHg)

As discussed before, after azidation the glass transition temperatures significantly decreased. This can be explained by higher chain mobility and flexibility which improve the gas permeability

coefficient with the increasing diffusivity of the penetrants. In this direction, azidated H-Hydrin homopolymers have higher gas permeability coefficients with increasing degree of modification (Figure 4.2.11).

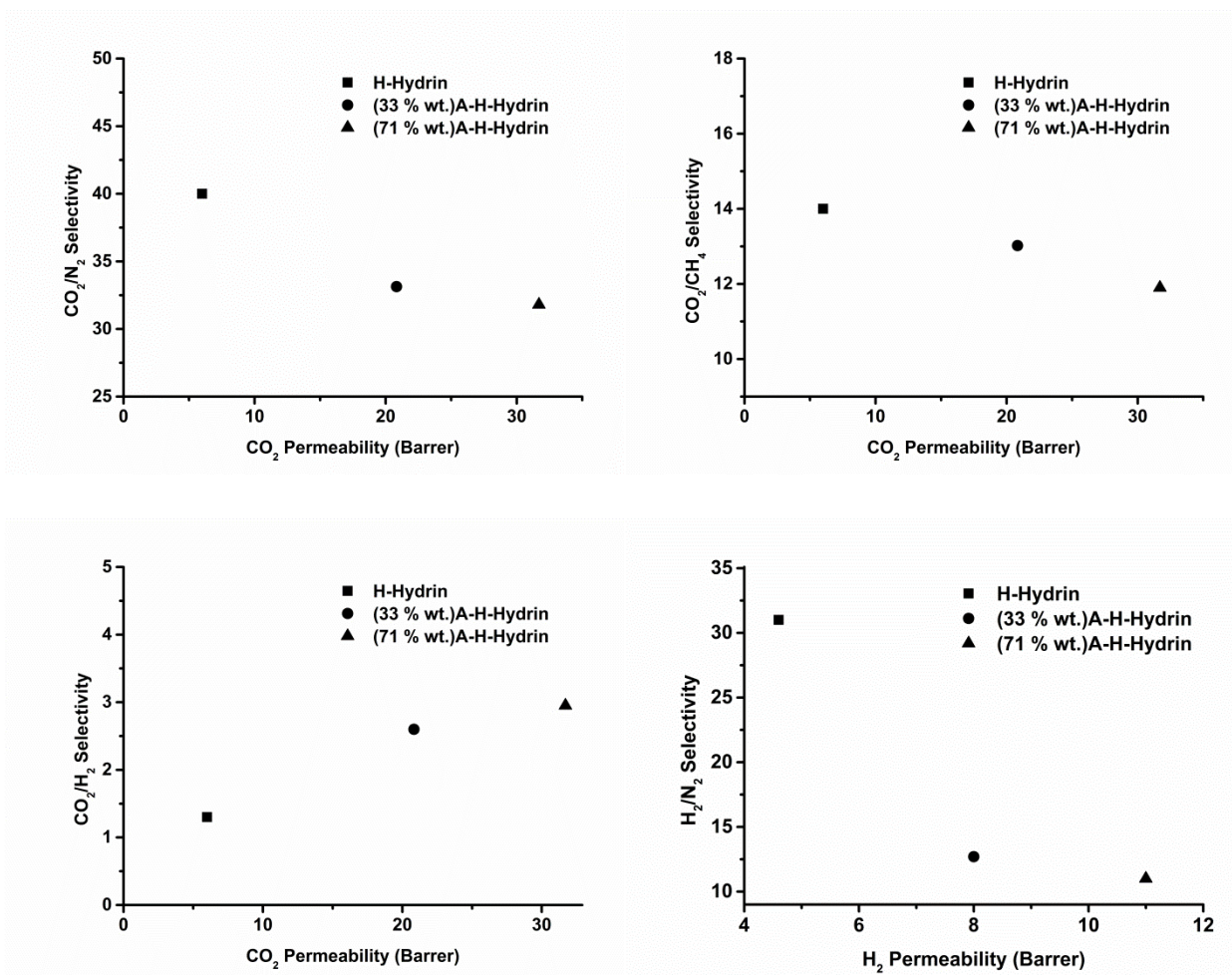


**FIGURE 4.2.11.** Relationship between CO<sub>2</sub> and H<sub>2</sub> permeabilities and CO<sub>2</sub>/N<sub>2</sub>, CO<sub>2</sub>/CH<sub>4</sub>, CO<sub>2</sub>/H<sub>2</sub> and H<sub>2</sub>/N<sub>2</sub> selectivities of H-Hydrin and 33 and 71 wt. % azidated H-Hydrin polymers. The permeability selectivities for the gas pairs are also shown in Table 4.2.4. Azidated H-Hydrin polymers has lower CO<sub>2</sub>/N<sub>2</sub>, CO<sub>2</sub>/CH<sub>4</sub> and H<sub>2</sub>/N<sub>2</sub> selectivities compared to initial H-Hydrin, except CO<sub>2</sub>/H<sub>2</sub> selectivity which arises from the lower kinetic diameter of H<sub>2</sub> (Figure 4.2.11). Diffusion of larger gas molecules is affected more than smaller gas molecules by the increase in chain

mobility leading to significant changes in diffusivity selectivity. As a result, for H-Hydrin homopolymers azidation lead them to have higher permeability coefficients but lower selectivities except  $\text{CO}_2/\text{H}_2$ . In the case of C-Hydrin copolymers after azidation decreased  $T_g$  and after UV irradiation increased  $T_g$  can be observed (Figure 4.2.8). In this direction, similarly, gas permeability coefficients increase after modification and decrease after UV cross-linking (Figure 4.2.12).

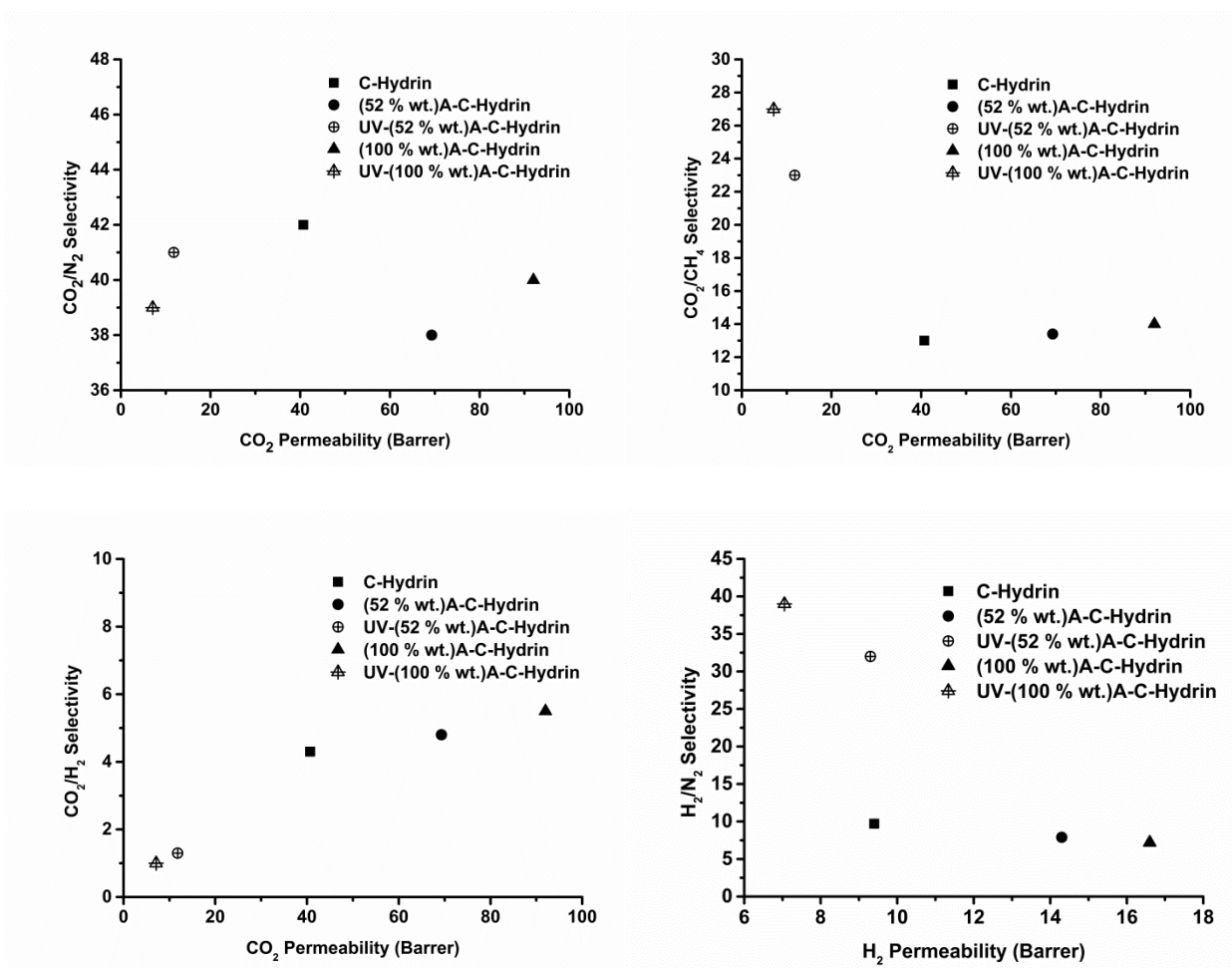


**FIGURE 4.2.12.** Relationship between  $\text{CO}_2$  and  $\text{H}_2$  permeabilities and  $\text{CO}_2/\text{N}_2$ ,  $\text{CO}_2/\text{CH}_4$ ,  $\text{CO}_2/\text{H}_2$  and  $\text{H}_2/\text{N}_2$  selectivities of C-Hydrin, 52 and 100 wt. % azidated C-Hydrin copolymers and their UV cross-linked analogues.

In addition, Figure 4.2.13 shows that an increase in degree of modification of C-Hydrin copolymers leads to higher CO<sub>2</sub> diffusivity while maintaining similar solubility, because the newly introduced azide pendent groups have no influence on solubility. They just reduce the T<sub>g</sub> of polymers and so the diffusivity increases. On contrary, UV cross-linking has a negative effect on chain mobility because of increased T<sub>g</sub> resulting in lower diffusivity (Figure 4.2.13). Azidated C-Hydrin copolymers have maintained CO<sub>2</sub>/N<sub>2</sub> and CO<sub>2</sub>/CH<sub>4</sub> selectivities in contrast to azidated H-Hydrin copolymers. This may be due to the carbon dioxide-philic ethylene oxide units (65 wt. %) which result in enhanced CO<sub>2</sub> solubility selectivity. UV cross-linked A-C-Hydrin polymers have similar CO<sub>2</sub>/N<sub>2</sub> selectivity, much higher CO<sub>2</sub>/CH<sub>4</sub> and H<sub>2</sub>/N<sub>2</sub> selectivities and much less CO<sub>2</sub>/H<sub>2</sub> selectivity in comparison to initial C-Hydrin and azidated C-Hydrin polymers (Figure 4.2.12). The reason is that after UV cross-linking with the limitation of the polymer chain mobility and flexibility the activation energy required for diffusion of a larger molecule increases more than that for smaller molecules [12]. Larger gas molecules (higher kinetic diameter) are affected more than smaller gas molecules by decrease in chain mobility. Additionally, the size difference between CO<sub>2</sub> and N<sub>2</sub> (0.34 Å, as characterized by the difference between their kinetic diameters) is less than that between CO<sub>2</sub> and CH<sub>4</sub> (0.5 Å), and H<sub>2</sub> and N<sub>2</sub> (0.75 Å) [10]. Consequently, the effect of the diffusivity selectivity for CO<sub>2</sub>/N<sub>2</sub> should be less significant compared to CO<sub>2</sub>/CH<sub>4</sub> and H<sub>2</sub>/N<sub>2</sub> separations. This also explains the lower CO<sub>2</sub>/H<sub>2</sub> selectivity in view of the higher kinetic diameter of CO<sub>2</sub> than H<sub>2</sub>. So, CO<sub>2</sub> as the larger gas molecule will be affected more than H<sub>2</sub> by a decrease in the chain mobility resulting in lowering of CO<sub>2</sub>/H<sub>2</sub> selectivity.



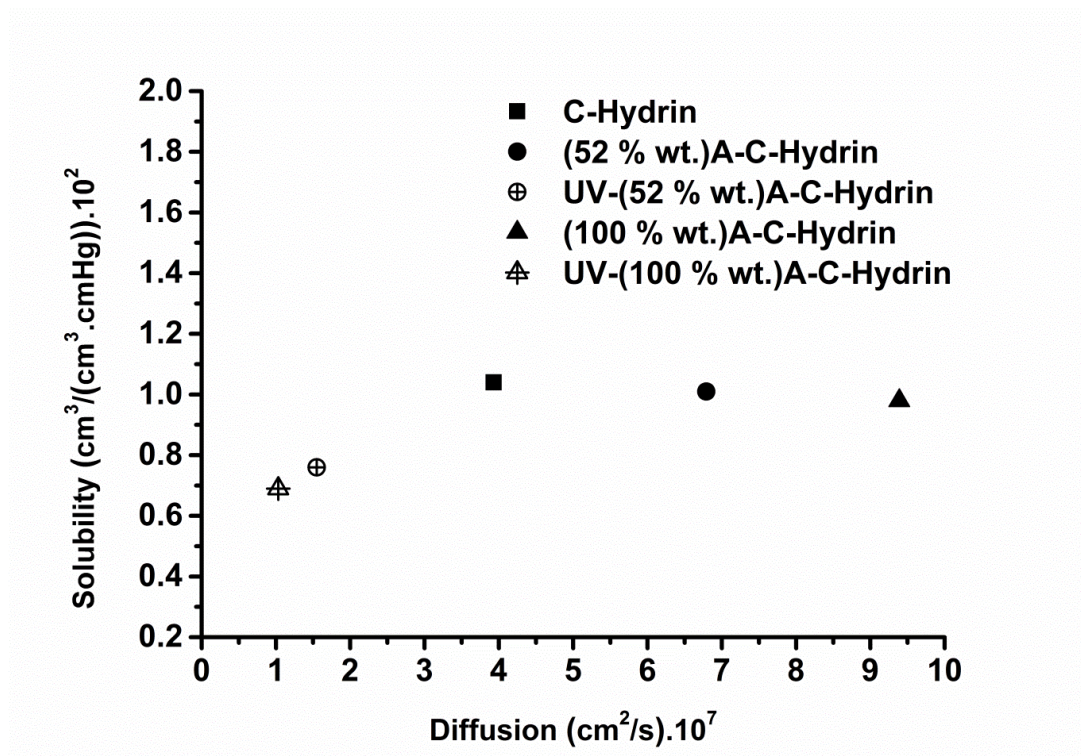


**FIGURE 4.2.13.** Diffusion coefficient and solubility of CO<sub>2</sub> for C-Hydrin, modified C-Hydrin copolymers and their UV cross-linked analogues.

#### 4.2.5. Conclusions

This study examined the effect of chemical modification and UV cross-linking of poly(epichlorohydrin) homopolymer (H-Hydrin) and poly[(ethylene oxide)-*ran*-(epichlorohydrin)] copolymer (C-Hydrin) by azidation chemistry and nitrene reaction, respectively, on gas transport properties. The modification process is based on the chloride side group substitution of poly(epichlorohydrin) with azide ion. UV initiates the decomposition of azide side groups of modified hydrin polymers and generates highly reactive nitrene radicals. This is a self-cross-linking system which does not need any additional cross-linkers. The strategy adopted in this study appears to be entirely satisfactory in terms of efficiency and simplicity. Successful modification was confirmed by <sup>1</sup>H-NMR, <sup>13</sup>C-NMR, FT-IR, GPC, DSC and TGA. The cross-

linked polymers were characterized by FT-IR spectroscopy, DSC, TGA and gel content analysis. The thermal stability of modified polymers was diminished compared to initial Hydrin polymers related to early decomposition of newly introduced energetic azide side groups. However, the high char-yield of modified and cross-linked Hydrin polymers indicate improved thermal stability at high temperatures. After modification the gas permeabilities increase significantly for both H-Hydrin and C-Hydrin with the effect of decreased glass transition temperature which leads them to have high polymer chain mobility and flexibility. The gas selectivities of modified H-Hydrin homopolymers decreased except for CO<sub>2</sub>/H<sub>2</sub> selectivity. In the case of modified C-Hydrin copolymer the gas selectivities were maintained with the effect of CO<sub>2</sub>-philic PEG blocks. After UV cross-linking significantly increased CO<sub>2</sub>/CH<sub>4</sub> and H<sub>2</sub>/N<sub>2</sub> selectivities and decreased CO<sub>2</sub> and H<sub>2</sub> permeabilities were observed.

#### 4.2.6. References

- [1] C. Charmette, J. Sanchez, P. Gramain, N. Masquelez, Structural characterization of poly(ethylene oxide-co-epichlorohydrin) membranes and relation with gas permeation properties, *Journal of Membrane Science*, 344 (2009) 275-280.
- [2] S. Bräse, C. Gil, K. Knepper, V. Zimmermann, Organic azides: an exploding diversity of a unique class of compounds, *Angewandte Chemie International Edition*, 44 (2005) 5188-5240.
- [3] J. Xia, S. Liu, T.-S. Chung, Effect of end groups and grafting on the CO<sub>2</sub> separation performance of poly(ethylene glycol) based membranes, *Macromolecules*, 44 (2011) 7727-7736.
- [4] F.B. Madsen, I. Dimitrov, A.E. Daugaard, S. Hvilsted, A.L. Skov, Novel cross-linkers for PDMS networks for controlled and well distributed grafting of functionalities by click chemistry, *Polymer Chemistry*, 4 (2013) 1700-1707.

- [5] S. Brochu, G. Ampleman, Synthesis and characterization of glycidyl azide polymers using isotactic and chiral poly(epichlorohydrin)s, *Macromolecules*, 29 (1996) 5539-5545.
- [6] B. Jin, J. Shen, R. Peng, Y. Shu, S. Chu, H. Dong, Synthesis, characterization, thermal stability and mechanical sensitivity of polyvinyl azidoacetate as a new energetic binder, *Journal of Polymer Research*, 19 (2012) 1-9.
- [7] Y. Murali Mohan, M. Padmanabha Raju, K. Mohana Raju, Synthesis, spectral and DSC analysis of glycidyl azide polymers containing different initiating diol units, *Journal of Applied Polymer Science*, 93 (2004) 2157-2163.
- [8] K.D. Dorkenoo, P.H. Pfromm, M.E. Rezac, Gas transport properties of a series of high Tg polynorbornenes with aliphatic pendant groups, *Journal of Polymer Science Part B: Polymer Physics*, 36 (1998) 797-803.
- [9] K. Zhang, Q. Zhuang, X. Liu, G. Yang, R. Cai, Z. Han, A new benzoxazine containing benzoxazole-functionalized polyhedral oligomeric silsesquioxane and the corresponding polybenzoxazine nanocomposites, *Macromolecules*, 46 (2013) 2696-2704.
- [10] H. Lin, E.V. Wagner, J.S. Swinnea, B.D. Freeman, S.J. Pas, A.J. Hill, S. Kalakkunnath, D.S. Kalika, Transport and structural characteristics of crosslinked poly(ethylene oxide) rubbers, *Journal of Membrane Science*, 276 (2006) 145-161.
- [11] H. Li, B.D. Freeman, O.M. Ekiner, Gas permeation properties of poly(urethane-urea)s containing different polyethers, *Journal of Membrane Science*, 369 (2011) 49-58.
- [12] V.A. Kusuma, B.D. Freeman, M.A. Borns, D.S. Kalika, Influence of chemical structure of short chain pendant groups on gas transport properties of cross-linked poly(ethylene oxide) copolymers, *Journal of Membrane Science*, 327 (2009) 195-207.

### **4.3. The Synthesis of Poly(ethylene glycol) (PEG) Containing Polymers via Step-Growth Click Coupling Reaction for CO<sub>2</sub> Separation**

#### **4.3.1. Brief Introduction**

The studies about polymers containing PEG as membrane materials have been carried on for especially CO<sub>2</sub> separation, because it has good solubility due to the quadrupole moment favoring the polar groups in polymers such as polar ether oxygens in PEG [1-3]. Similarly, N-containing organic heterocyclic molecules such as triazole and oxazine have good influence on CO<sub>2</sub> separation due to the Lewis acid-Lewis base interactions resulting in hydrogen bonding between heterocyclic molecules and negatively charged oxygen atoms of CO<sub>2</sub>. Therefore, the polymers containing heterocyclic molecules have better interaction with CO<sub>2</sub> leading to higher solubility compared to other gases [4].

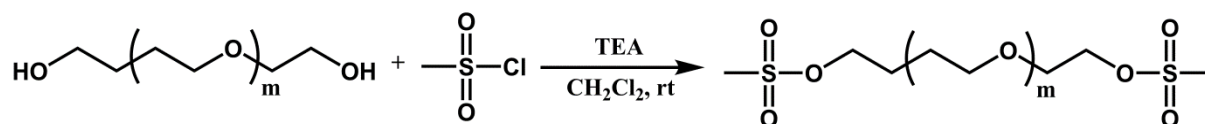
There are several PEG-containing polymers for CO<sub>2</sub> separation such as Pebax<sup>®</sup> [5], Polyactive<sup>®</sup> [6] and Hydrin<sup>®</sup> [7] synthesized by different polycondensation methods. In polycondensation reactions, monomers react with the elimination of small molecules and additional purification is required. However; in polyaddition, reaction happens without the elimination of small molecules. Therefore, step-growth click coupling polymerization (polyaddition) can be a distinctive route to prepare PEG-containing polymers for CO<sub>2</sub> separation.

This chapter focuses on the synthesis of the polymers containing PEG, triazole and benzoxazine heterorings via step-growth click coupling polymerization, and their gas transport properties. Moreover, the influence of the amount of N-containing heterocyclic rings and curing of benzoxazine on thermal properties was studied.

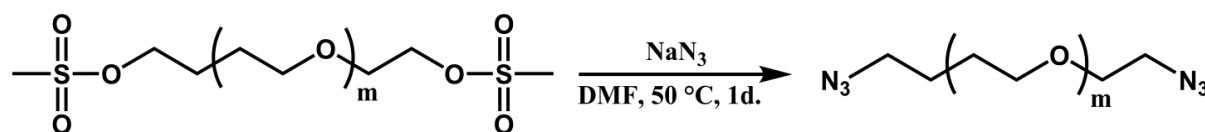
#### 4.3.2. Synthesis and Characterization of Bifunctional PEG-Diazide (N<sub>3</sub>-PEG-N<sub>3</sub>)

In the scope of this study, our main goal was to introduce a “click” chemistry approach to obtain PEG-containing polymers for CO<sub>2</sub> separation. Step-growth click coupling method was used as the polymerization technic. In this direction, the first step is to synthesize the bifunctional suitable click-coupling monomers and the second step is to apply necessary step-growth click reaction conditions to obtain high molecular weight polymers.

In this study, we report on a versatile method which allows converting end hydroxyl groups into azide functionality by a simple two-step reaction performed on PEG-dihydroxyl (HO-PEG-OH). For this purpose, mesylation of HO-PEG-OH with methanesulfonyl chloride (MsCl; 1:4; in terms of OH-moieties) was conducted as described in the experimental section to obtain PEG with mesyl end groups (Ms-PEG-Ms) (Scheme 4.3.1). The resulting Ms-PEG-Ms was then converted into N<sub>3</sub>-PEG-N<sub>3</sub> in the presence of NaN<sub>3</sub>/DMF at 50 °C (Scheme 4.3.2).



**Scheme 4.3.1.** Synthesis of PEG-dimesyl.



**Scheme 4.3.2.** Synthesis of PEG-diazide.

The extent of the modification was determined using area integration of <sup>13</sup>C-NMR spectra. The signal of neighbouring methylenic carbons (HO-CH<sub>2</sub>-PEG-CH<sub>2</sub>-OH) of end hydroxyl groups appeared at 61.89 ppm. After mesylation, this signal moves to the signal area PEG carbons and a new signal appears at 38.03 ppm belonging to methylic carbon (CH<sub>3</sub>-S(=O)<sub>2</sub>-PEG-(O)<sub>2</sub>S-CH<sub>3</sub>). After azidation, the migration of the signal of methylenic carbons to 50.62 ppm give reliable

evidence about the successful reaction (Figure 4.3.1). The effective mesylation and azidation were further supported by the disappearance of the hydroxyl stretching band at  $3456\text{ cm}^{-1}$  and the appearance of the azide stretching band at  $2098\text{ cm}^{-1}$ , respectively, in the FT-IR spectra of HO-PEG-OH, Ms-PEG-Ms, and N<sub>3</sub>-PEG-N<sub>3</sub> (Figure 4.3.2).

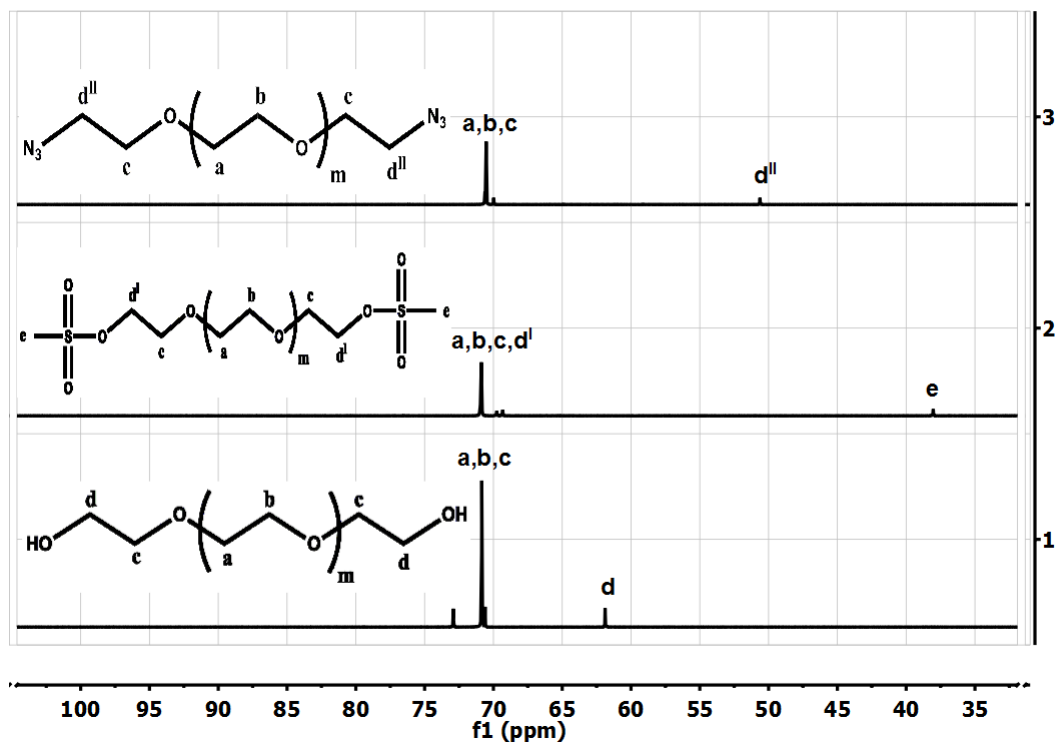


**FIGURE 4.3.1.** <sup>13</sup>C-NMR spectra of HO-PEG-OH (1), Ms-PEG-Ms (2), and N<sub>3</sub>-PEG-N<sub>3</sub> (3) in CDCl<sub>3</sub>.

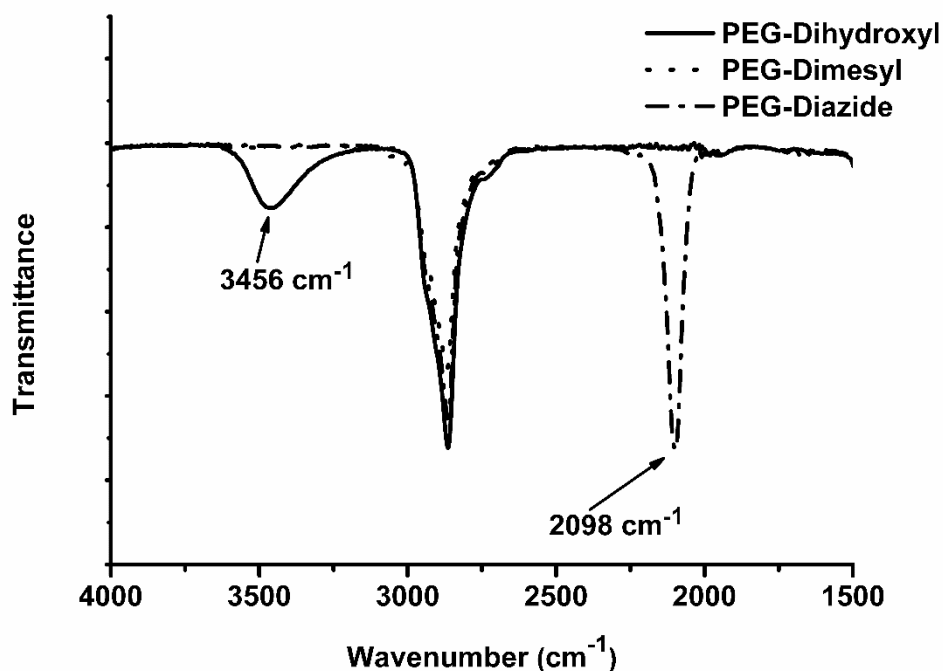
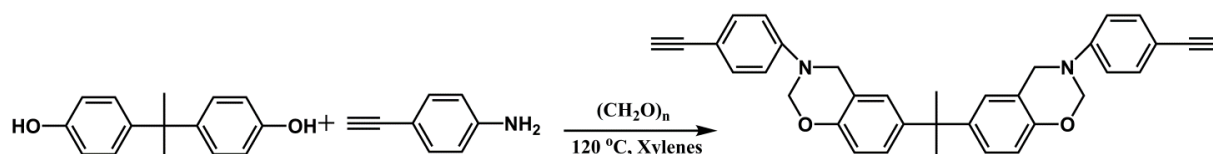


**FIGURE 4.3.2.** FT-IR spectra of HO-PEG-OH, Ms-PEG-Ms, and N<sub>3</sub>-PEG-N<sub>3</sub>.

#### 4.3.3. Synthesis and Characterization of Bifunctional Benzoxazine-Diacetylene Click Monomer

Bifunctional benzoxazine-diacetylene, possessing click functional group, was prepared according to the following reaction (Scheme 4.3.3).



**Scheme 4.3.3.** Synthesis of benzoxazine-diacetylene.

The chemical structure of benzoxazine-diacetylene was confirmed by both <sup>1</sup>H-NMR and FTIR. <sup>1</sup>H-NMR spectrum of benzoxazine click monomer showed two signals at 4.64 ppm and 5.43 ppm which are assigned to CH<sub>2</sub> protons of the newly formed oxazine ring. Notably, H-C≡C proton of acetylene moiety appears at 3.97 ppm. In the <sup>1</sup>H-NMR spectrum of bisphenol A, two different

signals belonging to two different aromatic protons can be observed. However, in the case of the  $^1\text{H}$ -NMR spectrum of benzoxazine-diacetylene click monomer, with the addition of new aromatic units and the formation of the oxazine ring 5 different aromatic protons were detectable at 6.58-7.39 ppm (Figure 4.3.3). In the FTIR spectrum, acetylene group was evidenced by appearing characteristic bands of  $\text{H}-\text{C}\equiv\text{C}$  and  $-\text{C}\equiv\text{C}-$  at  $3275$  and  $2098\text{ cm}^{-1}$ , respectively. Additionally, the reduction of the large hydroxyl ( $-\text{OH}$ ) stretching band at  $3294\text{ cm}^{-1}$  was another proof for modification (Figure 4.3.4).

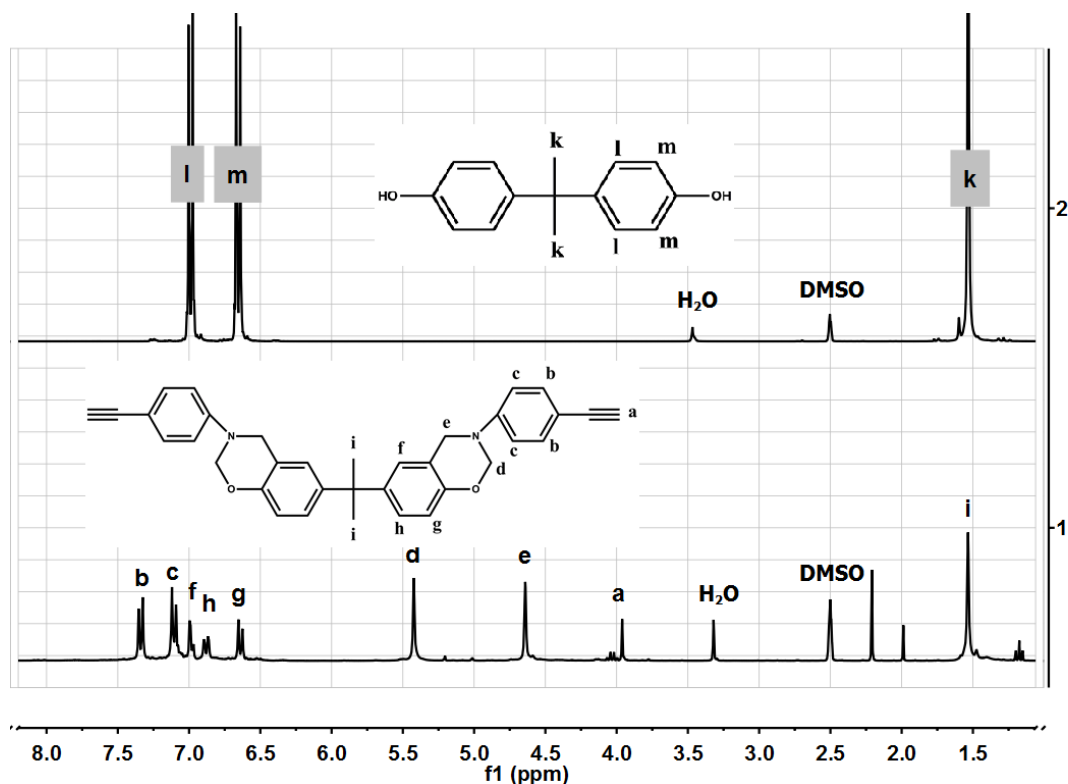


**FIGURE 4.3.3.**  $^1\text{H}$ -NMR spectra of benzoxazine-diacetylene monomer (1) and Bisphenol A (2) in DMSO.



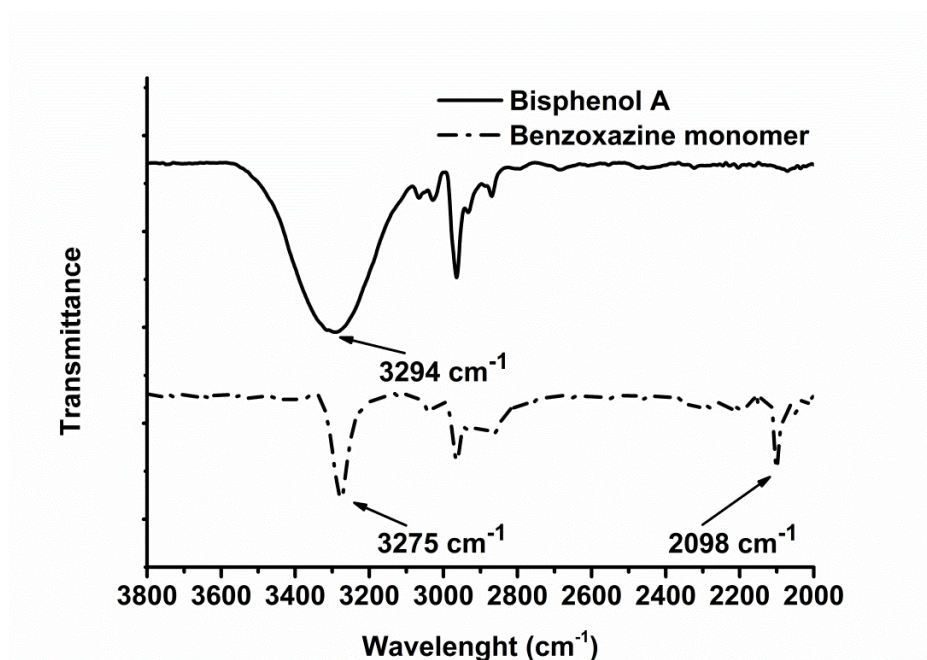


**FIGURE 4.3.4.** FT-IR spectra of Bisphenol A and benzoxazine-diacetylene monomer.

#### 4.3.4. Synthesis and Characterization of Step-Growth Polymers

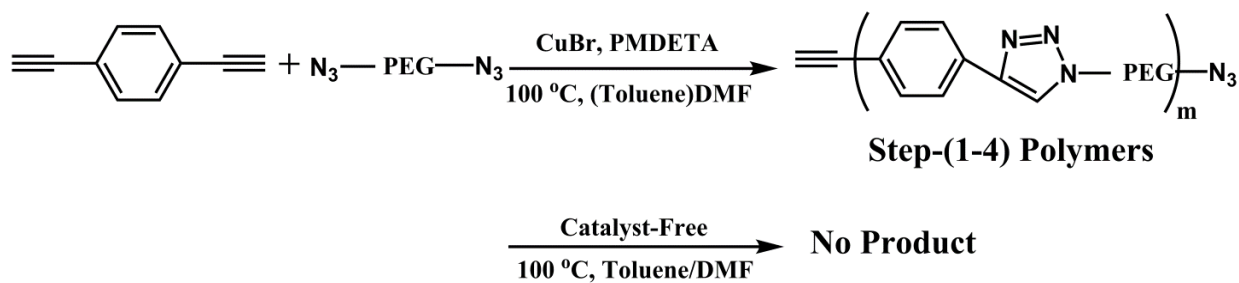
For desired step-growth coupling click process, PEG-diazide (400 g/mol or 600 g/mol) ( $N_3$ -PEG- $N_3$ ), diethynylbenzene or benzoxazine-diacetylene monomer were dissolved in DMF or Toluene/DMF (1:1) in different combinations (Table 4.3.1). Reaction was performed in the presence of *N,N,N',N'',N''*-Pentamethyldiethylenetriamine (PMDETA) and copper(I) bromide (CuBr) at 100 °C (Scheme 4.3.4-5) (Table 4.3.1). Catalyst-free step-growth click coupling reaction did not give any product (Scheme 4.3.4). There are two different types of triazole ring formation (1,4-triazole and 1,5-triazole) (Table 4.3.1). In fact, in the presence of a catalytic amount of  $Cu^I$  complexes, 1,4-disubstituted triazoles are obtained exclusively. However, the high temperature conditions in order to get high molecular weight polymers led the triazoles to form in two types and to lose the regioselectivity of the copper catalysed click reaction. The molecular fraction of 1,4 triazole was between 71 and 74 % depending on solvent system. The reaction which was

performed in DMF had 2-3 % more 1,4 triazole formation compared to toluene/DMF (1:1) solvent system.

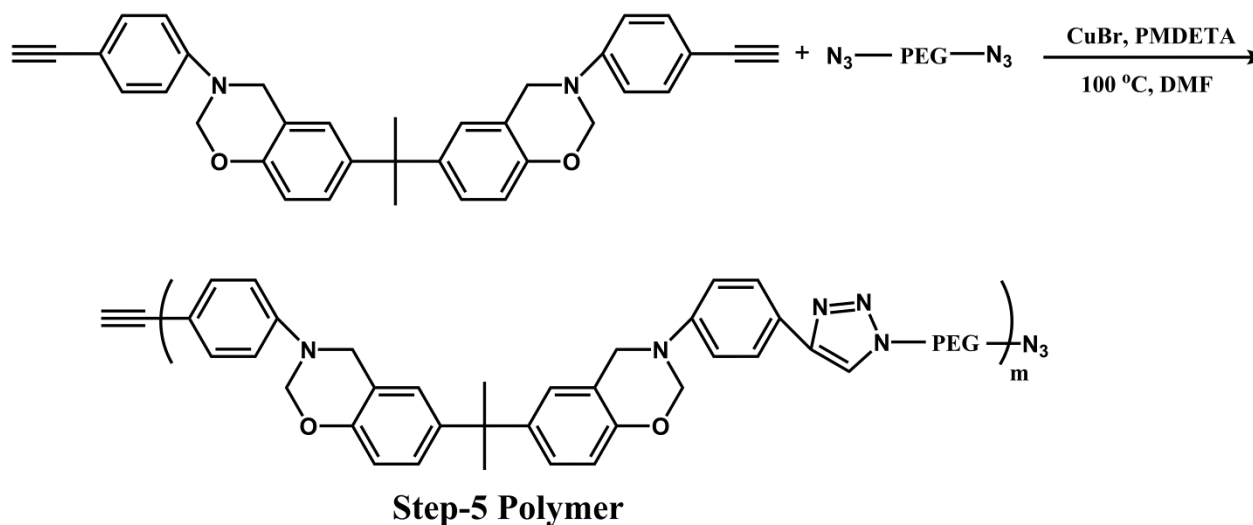
**TABLE 4.3.1.** Step-Growth Click Coupling Polyaddition Conditions.

polymer	catalyst	solvent	monomer-1	monomer-2 <sup>c</sup>	Time (d)	F <sub>1,4</sub> (%) <sup>d</sup>
<b>Step-1</b>	CuBr/PMDETA	DMF	diethynylbenzene	PEG(600)	5	73
<b>Step-2</b>	CuBr/PMDETA	Toluene/DMF	diethynylbenzene	PEG(600)	5	71
<b>Step-3</b>	CuBr/PMDETA	Toluene/DMF	diethynylbenzene	PEG(600)	10	71
<b>Step-4</b>	CuBr/PMDETA	DMF	diethynylbenzene	PEG(400)	10	73
<b>Step-5</b>	CuBr/PMDETA	DMF	benzoxazine <sup>b</sup>	PEG(600)	10	74
<b>Step-6<sup>a</sup></b>	—	Toluene/DMF	diethynylbenzene	PEG(600)	10	—

<sup>a</sup> Polymerization did not take place in the absence of catalyst. <sup>b</sup> Bifunctional benzoxazine-diacetylene. <sup>c</sup> Bifunctional PEG-diazide (N<sub>3</sub>-PEG-N<sub>3</sub>) <sup>d</sup> Molar fraction of 1,4-disubstituted 1,2,3-triazole repeating units was determined by <sup>1</sup>H-NMR analysis



**Scheme 4.3.4.** Step-growth click coupling polyaddition of diethynylbenzene and PEG-diazide in the catalyst and catalyst-free conditions.



**Scheme 4.3.5.** Step-growth click coupling polyaddition of benzoxazine-diacetylene and PEG-diazide in the presence of catalyst.

The click reaction was characterized by  $^1\text{H-NMR}$  and FTIR spectroscopy. The extent of conversion of the end diazide and diacetylene moieties to triazoles was monitored by observing the appearance of new methylene protons adjacent to the triazole and PEG at 3.86 and 4.57 ppm (triazole- $\text{CH}_2\text{CH}_2\text{-O-PEG}$ ), and 1,4 and 1,5 triazole protons at 8.57 and 8.64 ppm, respectively. The characteristic peaks for aromatic protons of benzene between 7.63 and 8.03 ppm also noted (Figure 4.3.5). Similarly, for Step-5 polymer the same new methylene protons adjacent to triazole and PEG were observed in the  $^1\text{H-NMR}$  spectrum (Figure 4.3.6). Additionally, the peaks belonging to protons of oxazine ring at 4.62 ppm (benzene- $\text{CH}_2\text{-N-}$ ) and 5.37 ppm ( $\text{-O-CH}_2\text{-N-}$ ) gave the evidence of protected benzoxazine rings during step-growth click coupling reaction (Figure 4.3.6). Moreover, in the FTIR spectrum, the band corresponding to  $\text{-N}_3$  group at  $2098\text{ cm}^{-1}$  completely disappeared (Figure 4.3.7). These spectral characterizations clearly indicate the triazole formation and efficient step-growth click coupling reaction.

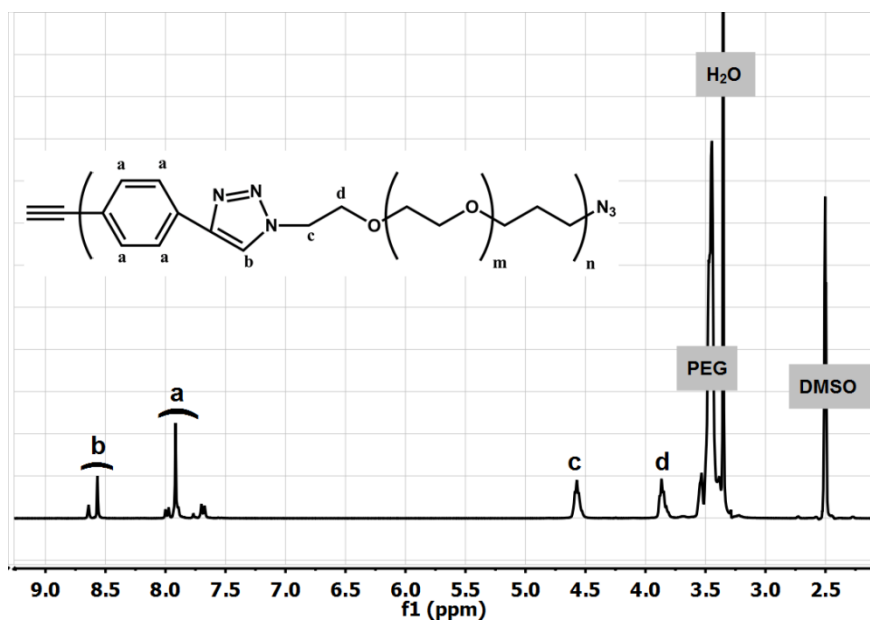


**FIGURE 4.3.5.**  $^1\text{H}$ -NMR spectra of Step-3 in DMSO.

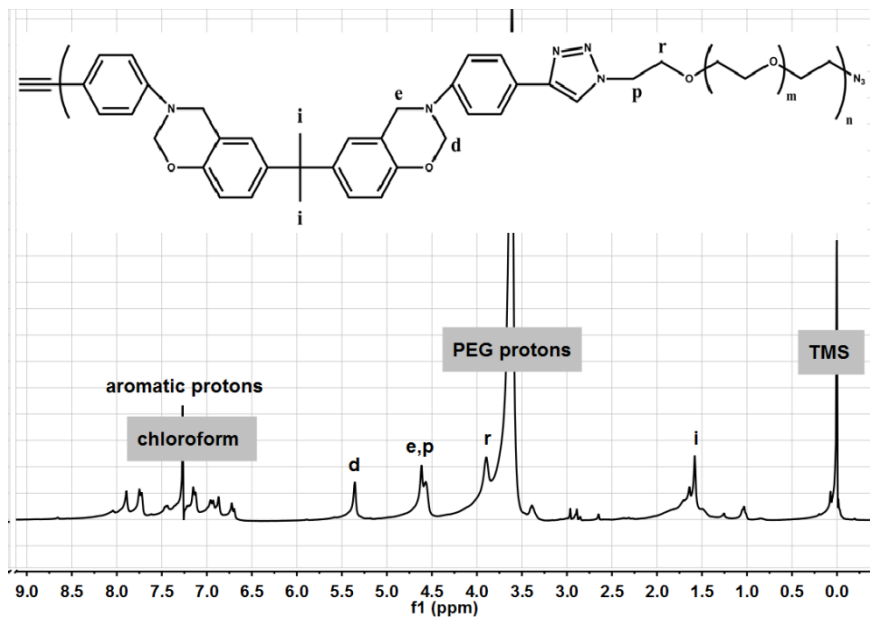


**FIGURE 4.3.6.**  $^1\text{H}$ -NMR spectra of Step-5 in  $\text{CDCl}_3$ .

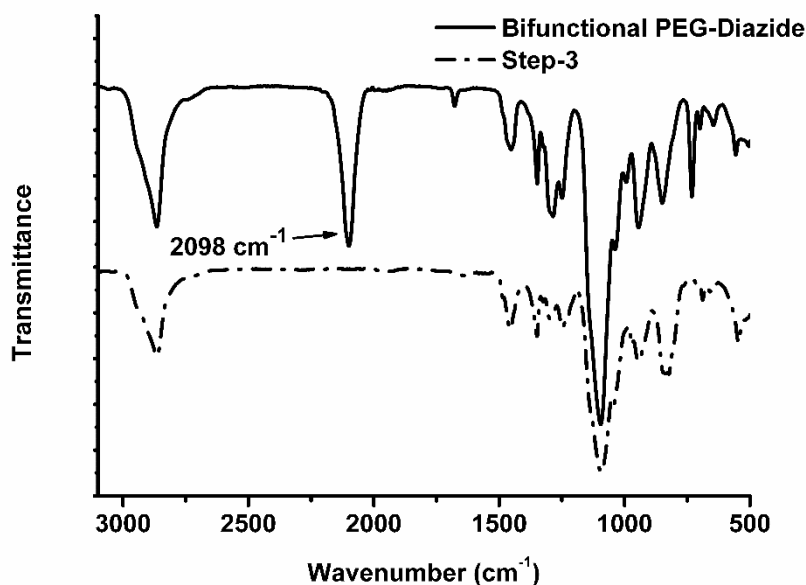


**FIGURE 4.3.7.** FT-IR spectra of PEG-diazone and Step-3.

#### 4.3.5. Gel Permeation Chromatography (GPC) Analysis

GPC results of Step-(1-5) step-growth polymers are shown in Table 4.3.2 and Figure 4.3.8. The click coupling of parent bifunctional monomers resulted in a polymer of high molecular weight and relatively broad molecular weight distribution, as expected for a step-growth process. In the same catalyst system, temperature and time (5 days), Step-1 had higher molecular weight and narrower molecular weight distribution (lower polydispersity (PDI)) compared to Step-2. The only difference between two reaction conditions was the solvent that was for Step-1 DMF and for Step-2 toluene/DMF (1:1) mixture (Table 4.3.1). This indicated that DMF is better solvent for step-growth click coupling reaction under the high temperature conditions with respect to toluene/DMF (1:1) mixture. With increased reaction time (from 5 to 10 days), Step-3 polymer exhibited a much higher molecular weight but broader molecular weight distribution compared to Step-2. In the case of Step-4 polymer, the lower molecular weight possibly indicates the solubility problem during the reaction due to the low molecular weight PEG (400 g/mol) click coupling monomer resulting

in increased amount of aromatic triazole units on the mainchain. Lastly, Step-5 polymer had the lowest molecular weight among the other step-growth polymers because of the bulky and geometrically nonlinear benzoxazine-diacetylene click coupling monomer.

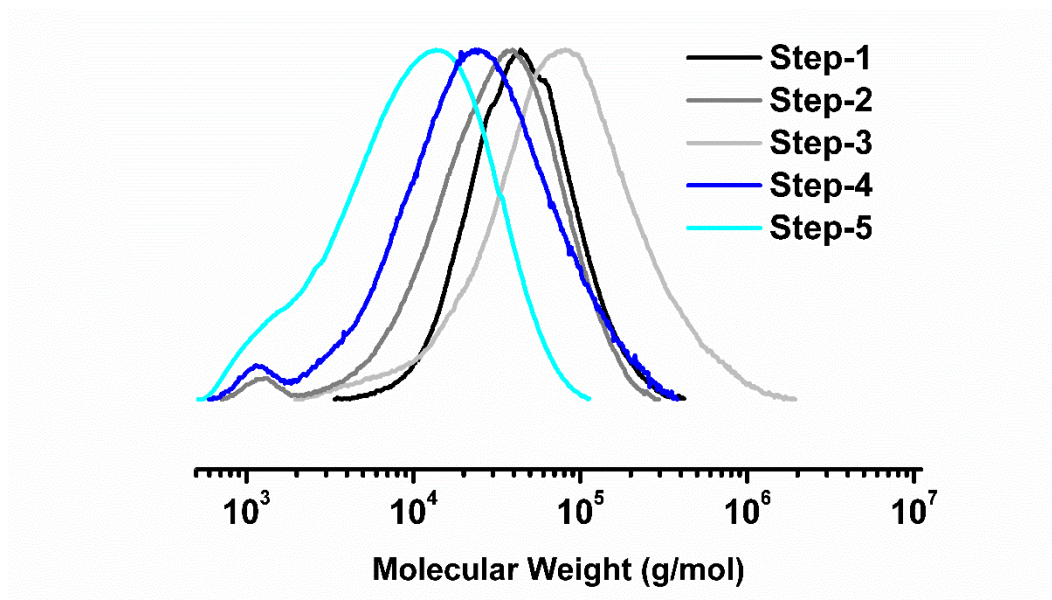


**FIGURE 4.3.8.** Gel permeation chromatograms of Step-Polymers.

**TABLE 4.3.2.** Molecular Weight, Polydispersity (PDI) and Glass Transition Temperature ( $T_g$ ) of Step-(1-5) Step-Growth Polymers.

Polymer	$M_w$ (kg/mol) <sup>a</sup>	PDI ( $M_w/M_n$ )	$T_g$ (°C)
Step-1	56	1.6	-23
Step-2	43	2.5	-18
Step-3	130	3	-19
Step-4	38	3.2	4
Step-5	18	2.9	16(24) <sup>b</sup>

<sup>a</sup> Molecular weights and polydispersities were determined with GPC. <sup>b</sup> Glass transition temperature after curing.

#### 4.3.6. Thermal Characterization

The glass transition temperatures ( $T_g$ ) of Step-(1-5) polymers were determined by differential scanning calorimetry (DSC) (Table 4.3.2). Step-(1-3) multiblock copolymers containing the same click-coupling monomers had nearly similar  $T_g$  between -17 and -24 °C. However, in the case of Step-4,  $T_g$  increased to 4 °C due to the shorter chain PEG (400 g/mol) click-coupling monomer resulting in increased amount of aromatic triazole groups on the main-chain of the polymer. Step-5 had the highest  $T_g$  compared to other polymers owing to long and bulky benzoxazine-diacetylene click monomer that leads the polymer chains to have less mobility and flexibility. Furthermore, the well-known characteristic of benzoxazines is to give thermally induced ring opening polymerization (ROP). This is an exothermic process which shows a peak at around 180-270 °C depending on functionalities and amount of the benzoxazines [8]. The DSC thermograms exhibit the ROP temperatures for benzoxazine-diacetylene monomer and its polymer “Step-5” at 206 °C with total 61 and 20 cal/g exotherms, respectively (Figure 4.3.9). The disappearance of the exothermic effect in the third runs was the evidence of complete curing process resulting in increased  $T_g$  for Step-5 due to the decrease in chain mobility and flexibility (Table 4.3.2).

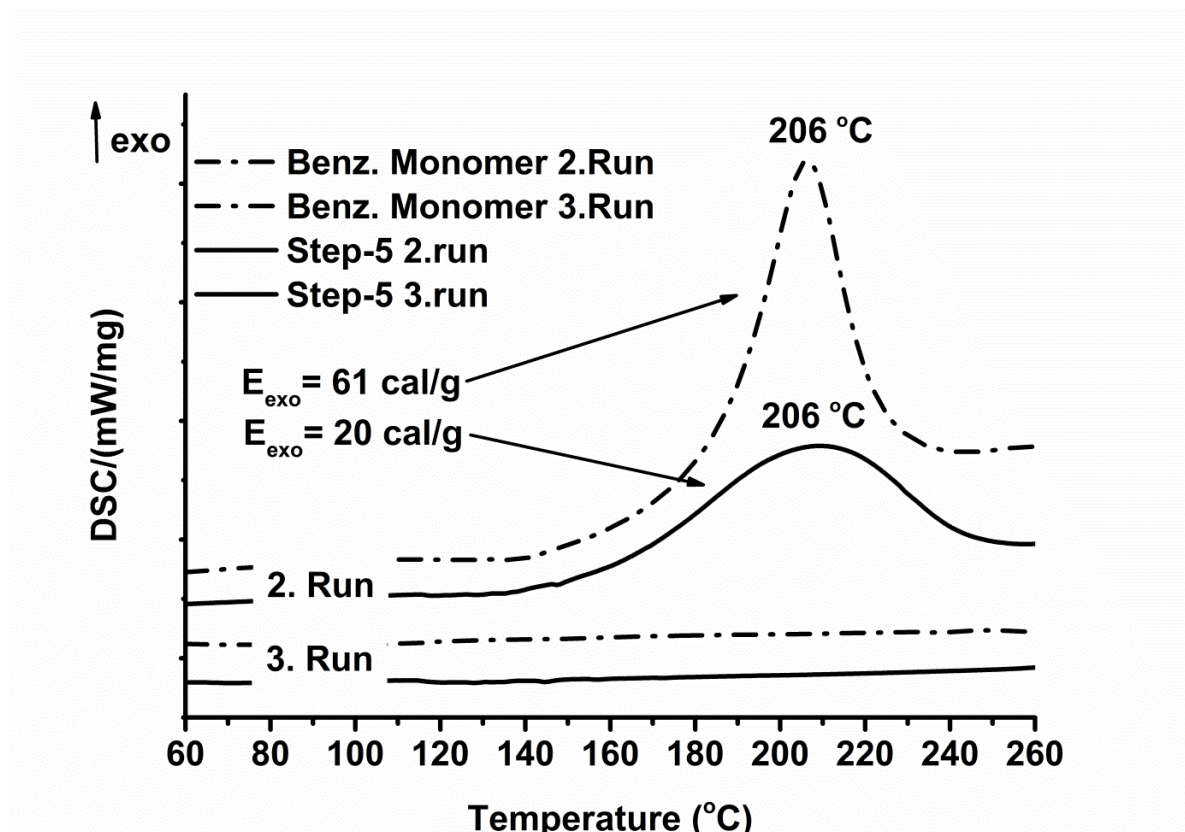


**FIGURE 4.3.9.** DSC thermograms of benzoxazine-diacetylene monomer and its polymer (Step-5) before and after ring opening polymerization.

Thermogravimetric analysis (TGA) is the technique that is commonly used for having fast evaluation of the thermal stability of various polymeric materials. The thermal stability of the Step-(1-5), thermally cured Step-5 (Step-5-XL) and benzoxazine-diacetylene monomer (Benz-XL) was further investigated by TGA. The TGA curves are presented in Figure 4.3.10 and weight loss behaviours of the species are given in Table 4.3.3.



**TABLE 4.3.3.** Thermal Properties of Step-(1-5), thermally crosslinked Step-5 (Step-5-XL) and benzoxazine-diacetylene monomer (Benz-XL).

<b>Polymer</b>	<b>T<sub>5%</sub><sup>a</sup></b> (°C)	<b>T<sub>10%</sub><sup>b</sup></b> (°C)	<b>T<sub>d max</sub><sup>c</sup></b> (°C)	<b>Y<sub>c</sub><sup>d</sup> at</b> <b>800 °C</b> (%)
<b>Step-1</b>	313	338	350	15
<b>Step-2</b>	254	325	349	19
<b>Step-3</b>	328	342	343	16
<b>Step-4</b>	349	371	376	29.5
<b>Step-5</b>	250	324	353	35
<b>Step-5-XL<sup>e</sup></b>	310	342	349	37
<b>Benz-XL<sup>f</sup></b>	401	419	388	55

<sup>a</sup> T<sub>5%</sub>: The temperature for which the weight loss is 5 %. <sup>b</sup> T<sub>10%</sub>: The temperature for which the weight loss is 10 %. <sup>c</sup> T<sub>d max</sub>: Maximum weight loss temperature. <sup>d</sup> Y<sub>c</sub>: Char yield. <sup>e</sup> Thermally crosslinked Step-5 copolymer <sup>f</sup> Thermally crosslinked benzoxazine-diacetylene monomer

Step-(1-3) polymers have similar thermal stabilities. However, Step-4 polymer containing low molecular weight PEG (400 g/mol) showed much higher thermal stability among the other polymers in terms of the starting temperatures of 5 %, 10 % and maximum weight losses, and char yield. The reason of enhanced thermal stability is the high amount of aromatic triazole units on the main chain of the polymer. Heteroaromatic rings such as triazole and oxadiazole are well-known structures having high thermal stabilities [9-11]. In the case of Step 5, the thermal stability was similar to Step-(1-3) polymers according to the temperatures of 5 %, 10 % and maximum weight losses. However, it has much higher char yield compared to other polymers which is one of the most important parameters of thermal stability. This arises from the curing process of benzoxazine rings of Step-5 resulting in the formation of highly thermal stable polymeric network. After thermal treatment of Step-5, Step-5-XL has higher temperatures for 5-10 % weight losses which indicate enhanced thermal stability. Benz-XL has the highest thermal stability compared to Step-

(1-5) and Step-5-XL due to having the largest amount of benzoxazine units and crosslinking density.

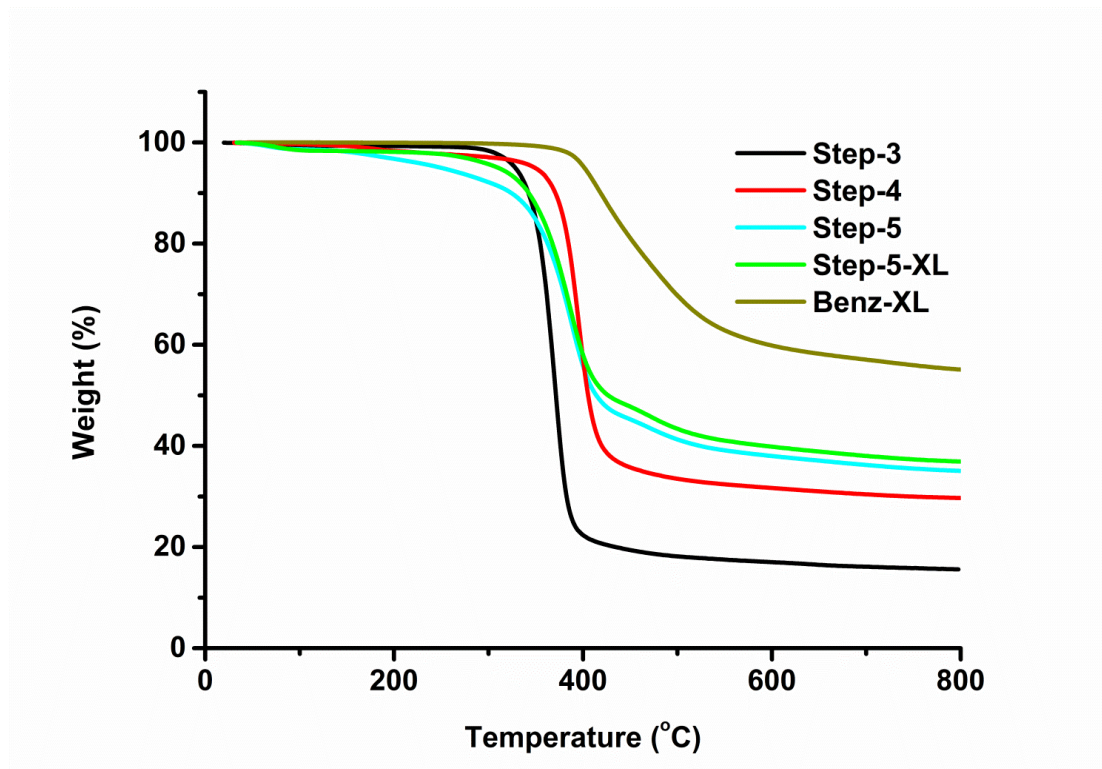


**FIGURE 4.3.10.** TGA curves of Step-(3-5) copolymers, crosslinked Step-5-XL and benzoxazine-diacetylene monomer (Benz-XL)

#### 4.3.7. Gas Transport Properties

The results of single gas permeation experiments carried out on Step 5 polymer as function of temperature ranging from 30 °C to 90 °C are reported in Table 4.3.4.

**Table 4.3.4.** Gas Permeability Coefficients and Selectivity Values of Step-5 Polymer in the Temperatures Ranging from 30 to 90 °C.

Polymer	P(CO <sub>2</sub> ) <sup>a</sup>	P(N <sub>2</sub> )	P(CH <sub>4</sub> )	P(H <sub>2</sub> )	P(O <sub>2</sub> )	$\alpha$ (CO <sub>2</sub> /N <sub>2</sub> )	$\alpha$ (CO <sub>2</sub> /CH <sub>4</sub> )	$\alpha$ (CO <sub>2</sub> /O <sub>2</sub> )	$\alpha$ (H <sub>2</sub> /N <sub>2</sub> )	$\alpha$ (O <sub>2</sub> /N <sub>2</sub> )
30 °C	2	0.054	0.098	1.87	0.18	40	22.3	11.35	37.4	3.5
40 °C	4.02	0.117	0.22	3.56	0.379	36	19	10.8	31	3.3
50 °C	6.9	0.24	0.47	5.7	0.72	30.6	15.7	10.1	22.7	3
60 °C	12.83	0.56	1.127	9.25	1.44	23.7	11.9	8.85	16	2.7
70 °C	20	1.06	1.83	10.95	2.73	20.2	10.85	7.55	12.3	2.66
80 °C	30	1.84	2.79	16.1	4.64	16.8	9.7	6.95	10.2	2.4
90 °C	43.1	4.07	5.74	24.7	7.69	10.7	6.9	5.5	6.8	1.95

The general tendency of permeation rate is CO<sub>2</sub> > H<sub>2</sub> > O<sub>2</sub> > CH<sub>4</sub> > N<sub>2</sub>. This order is the same as for most rubbery polymer membranes [2]. Step 5 polymer is a rubbery polymer; therefore the solution-diffusion mechanism is the base of the gas permeation. In this direction, the most important parameter determining the permeability coefficient is critical temperature of gases (CO<sub>2</sub> (304.2 K) > CH<sub>4</sub> (190.6 K) > O<sub>2</sub> (154.4 K) > N<sub>2</sub> (126.2 K) > H<sub>2</sub> (33.2 K)) [2]. The gases with higher critical temperature generally have higher condensability and solubility coefficients [12]. H<sub>2</sub> with the lowest critical temperature would be expected to have the lowest permeability coefficient, however; the smallest kinetic diameter of H<sub>2</sub> (CH<sub>4</sub> (3.8 Å) > N<sub>2</sub> (3.64 Å) > O<sub>2</sub> (3.46 Å) > CO<sub>2</sub> (3.3 Å) > H<sub>2</sub> (2.89 Å)) [2] leads to a high diffusion coefficient that makes it more permeable than all other gases except CO<sub>2</sub>. Due to the much higher solubility of CO<sub>2</sub>, it often has a higher permeability coefficient than the gases with smaller kinetic diameters such as H<sub>2</sub>. So the order of permeability coefficients bases on the competition between solubility favoring the penetrants with higher condensability and diffusion favoring the penetrants with smaller kinetic diameter.

In rubbery polymer membranes, one of the most important parameters affecting the permeability coefficient is glass transition temperature ( $T_g$ ). A decreasing  $T_g$  generally expresses an increase in gas permeability. This can be explained by higher chain mobility and flexibility resulting in the increasing diffusivity of the penetrants. Therefore, the rubbery polymer membranes with low  $T_g$  usually have high permeability coefficients. Step-5 polymer has 16 °C of  $T_g$  which is significantly higher compared to other rubbery polymer membranes for gas separation such as Pebax® (-77 °C,  $P(\text{CO}_2) = 221$  Barrer,  $\alpha(\text{CO}_2/\text{N}_2) = 23.4$ ) [13], Hydrin® (-42.6 °C,  $P(\text{CO}_2) = 41$  Barrer,  $\alpha(\text{CO}_2/\text{N}_2) = 42$ ) and natural rubber ( -70 °C,  $P(\text{CO}_2) = 131$  Barrer,  $\alpha(\text{CO}_2/\text{N}_2) = 16.1$ ) [13]. Therefore, its permeability coefficients are fairly low, however; it has significantly high  $\text{CO}_2$  separation with the effect of PEG and N-containing heterocyclic rings favoring  $\text{CO}_2$  with higher solubility compared to other gases (Figure 4.3.11). In the case of the diffusivity selectivity, the effect for  $\text{CO}_2/\text{N}_2$  should be less significant compared to  $\text{CO}_2/\text{CH}_4$  and  $\text{H}_2/\text{N}_2$  separations because the size difference between  $\text{CO}_2$  and  $\text{N}_2$  (0.34 Å, as characterized by the difference between their kinetic diameters) is less than that between  $\text{CO}_2$  and  $\text{CO}_4$  (0.5 Å), and  $\text{H}_2$  and  $\text{N}_2$  (0.75 Å) [2]. The increasing temperature leads to an increase in the permeability coefficients and a decrease in selectivities (Figure 4.3.11).

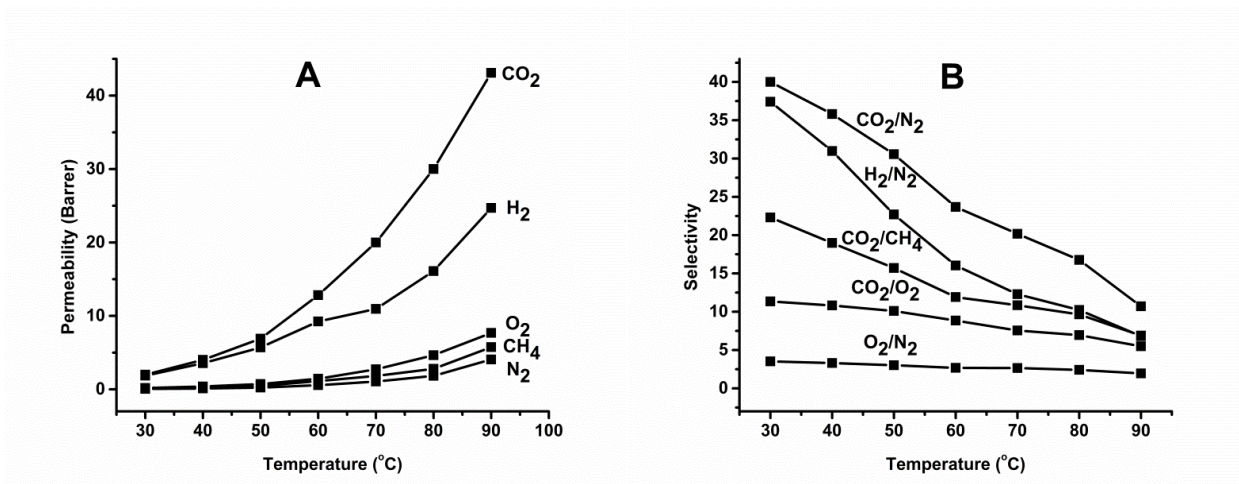


**FIGURE 4.3.11.** CO<sub>2</sub>, H<sub>2</sub>, O<sub>2</sub>, CH<sub>4</sub> and N<sub>2</sub> permeabilities, and CO<sub>2</sub>/N<sub>2</sub>, H<sub>2</sub>/N<sub>2</sub>, CO<sub>2</sub>/CH<sub>4</sub>, CO<sub>2</sub>/O<sub>2</sub> and O<sub>2</sub>/N<sub>2</sub> selectivities as a function of temperature for Step-5 polymer.

Moreover, heating permeability coefficients of Step-5 polymer membrane were compared with the cooling one to understand the effect of the temperature on the polymer because Step-5 has benzoxazine rings on the main-chain which can thermally be induced to ring opening polymerization and curing. Eventually, Figure 4.3.12 shows that there is no significant change on the permeability coefficients of heating and cooling cycle.

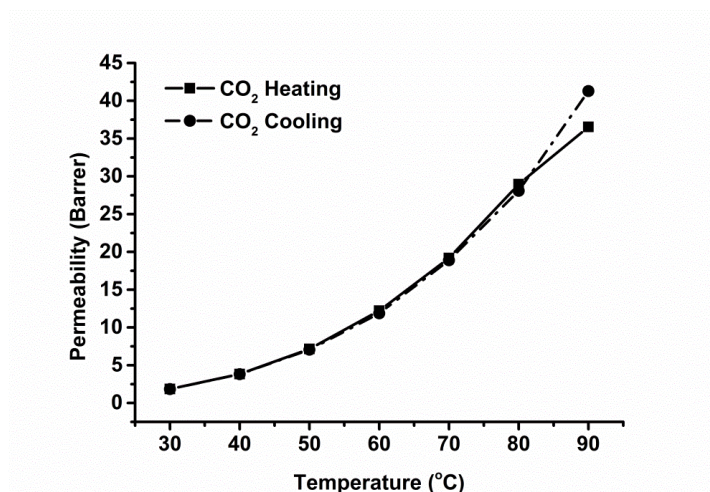


**FIGURE 4.3.12.** CO<sub>2</sub> permeability in the heating and cooling cycle as a function of temperature for Step-5 polymer.

So the increasing temperature until 90 °C did not result in decomposition, ring opening polymerization or curing in the Step-5 polymer. That is, the Step-5 polymer membrane is stable during the gas permeation experiments at the temperature ranging from 30 °C to 90 °C.

#### **4.3.8. Conclusions**

This study examined the synthesis of high molecular weight PEG-containing polymers via step-growth click coupling polymerization for efficient CO<sub>2</sub> separation. The monomers and step-growth polymers were characterized by <sup>1</sup>H-NMR, <sup>13</sup>C-NMR, FT-IR, GPC, DSC and TGA. Step-5 polymer has low permeability coefficients due to the high glass transition temperature (T<sub>g</sub>) resulting in low chain mobility, but high selectivity owing to CO<sub>2</sub>-philic groups such as PEG and triazole. Step-5 polymer membrane had chemical stability during the gas permeation experiment with the temperature ranging from 30 °C to 90 °C. There were no significant differences between the permeability coefficients of heating and cooling cycle. The thermal stability of Step-(1-5) polymers depended on the molecular weight of the PEG monomer determining the amount of the highly thermal stable triazole groups. Higher amount of triazole in polymer results in enhanced thermal stability. Additionally, Step-5 polymer having benzoxazine groups had improved thermal stability at high temperature due to the ring opening polymerization of benzoxazine groups leading to the formation of permanent network.

#### **4.3.9. References**

[1] K. Ghosal, R.T. Chern, B.D. Freeman, W.H. Daly, I.I. Negulescu, Effect of basic substituents on gas sorption and permeation in polysulfone, *Macromolecules*, 29 (1996) 4360-4369.

- [2] H. Lin, E.V. Wagner, J.S. Swinnea, B.D. Freeman, S.J. Pas, A.J. Hill, S. Kalakkunnath, D.S. Kalika, Transport and structural characteristics of crosslinked poly(ethylene oxide) rubbers, *Journal of Membrane Science*, 276 (2006) 145-161.
- [3] A.C. Comer, D.S. Kalika, V.A. Kusuma, B.D. Freeman, Glass-transition and gas-transport characteristics of polymer nanocomposites based on crosslinked poly(ethylene oxide), *Journal of Applied Polymer Science*, 117 (2010) 2395-2405.
- [4] N. Du, H.B. Park, G.P. Robertson, M.M. Dal-Cin, T. Visser, L. Scoles, M.D. Guiver, Polymer nanosieve membranes for CO<sub>2</sub>-capture applications, *Nature Materials*, 10 (2011) 372-375.
- [5] J.R. Flesher Jr, Pebax<sup>®</sup> Polyether block amide: A new family of engineering thermoplastic elastomers, in: *High performance polymers: Their origin and development*, Springer, 1987, pp. 401-408.
- [6] J. Djonlagic, M.S. Nikolic, Thermoplastic copolyester elastomers, *Handbook of engineering and speciality thermoplastics: Volume 3: Polyethers and polyesters*, 63 (2011) 377.
- [7] Y. Ikeda, Elastomeric poly (oxyethylene) matrixes for ion conduction, *Journal of Applied Polymer Science*, 78 (2000) 1530-1540.
- [8] K.D. Demir, B. Kiskan, S.S. Latthe, A.L. Demirel, Y. Yagci, Thermally curable fluorinated main chain benzoxazine polyethers via Ullmann coupling, *Polymer Chemistry*, 4 (2013) 2106-2114.
- [9] B. Gebben, M.H.V. Mulder, C.A. Smolders, Gas separation properties of a thermally stable and chemically resistant polytriazole membrane, *Journal of Membrane Science*, 46 (1989) 29-41.
- [10] H. Maab, S. Pereira Nunes, Porous polyoxadiazole membranes for harsh environment, *Journal of Membrane Science*, 445 (2013) 127-134.

- [11] B. Bae, S. Kawamura, K. Miyatake, M. Watanabe, Synthesis and properties of sulfonated poly(arylene ether)s containing azole groups, *Journal of Polymer Science Part A: Polymer Chemistry*, 49 (2011) 3863-3873.
- [12] H. Li, B.D. Freeman, O.M. Ekiner, Gas permeation properties of poly(urethane-urea)s containing different polyethers, *Journal of Membrane Science*, 369 (2011) 49-58.
- [13] V. Bondar, B. Freeman, I. Pinnau, Gas transport properties of poly (ether-b-amide) segmented block copolymers, *Journal of Polymer Science Part B: Polymer Physics*, 38 (2000) 2051-2062.



## Chapter 5

### Summary and Outlook

#### 5.1. Summary and Outlook

The main motivation of the present work had two issues focused on enhancing the gas transport properties of selected polymers with different appropriate chemical modification methods; and synthesizing poly(ethylene glycol) (PEG) containing polymers via step-growth click coupling reaction for efficient CO<sub>2</sub> separation.

Hydrosilylation (Hs-PI-*b*-PVTMS) and hydrogenation (H-PI-*b*-PVTMS) chemistries were preferred as chemical modification methods for polyisoprene block of poly(isoprene)-*block*-poly(vinyl trimethylsilane) (PI-*b*-PVTMS) block copolymers to alter the thermodynamic and repulsive interactions between blocks, resulting in different morphologies, which are directly related to the gas transport properties of the modified block copolymers. The morphology of PI-*b*-PVTMS and Hs-PI-*b*-PVTMS block copolymers was examined by transmission electron micrographs (TEM). PI-*b*-PVTMS had a strong microphase separation between amorphous polyisoprene and liquid crystalline PVTMS leading to form a lamellar structure over larger compositional ranges as compared to block copolymers composed of two amorphous blocks. Continuous layers of PI lamellae significantly blocked the permeation of gases. Hs-PI-*b*-PVTMS revealed no microphase separation. Membranes made of the modified block copolymers exhibit a significant increase in O<sub>2</sub> and H<sub>2</sub> permeabilities reaching the PVTMS-ref level while maintaining

the same selectivity. Apart from altering the morphology of modified block copolymers, another reason of enhanced gas transport properties was the increasing fractional free volume (FFV). FFV is one of the most important parameters influencing the gas transport properties. The modified block copolymers showed improved FFV compared to PI-*b*-PVTMS. Particularly, hydrosilylated block copolymers showed the highest increase in FFV due to the bulky and symmetrical triethylsilyl groups attached to the main chain of polyisoprene block. The thermal stability of modified block copolymers was investigated by thermogravimetric analysis (TGA) and compared to PI-*b*-PVTMS. The modified block copolymers exhibited better thermal stability than PI-*b*-PVTMS due to the saturation of double bonds of polyisoprene resulting in early decomposition.

Azidation chemistry was used as another chemical modification method for poly(epichlorohydrin) homopolymer (H-Hydrin) and poly[(ethylene oxide)-*ran*-(epichlorohydrin)] random copolymer (C-Hydrin). Afterwards UV-crosslinking of azidated hydrin polymers (A-H-Hydrin and A-C-Hydrin) was performed via nitrene reaction. The goal of this study was to examine the effect of azidation and UV cross-linking of H-Hydrin and C-Hydrin on gas transport properties. The mechanistic aspect of the modification was based on the chloride pendent group substitution of poly(epichlorohydrin) with azide ions. UV initiates the decomposition of azide side groups of hydrin polymers resulting in generation of highly reactive nitrene radical and gives the opportunity for self-cross-linking without any additional cross-linkers. Azidated hydrin polymers exhibited a decrease in glass transition temperature ( $T_g$ ) due to longer chain of azide units as a pendent group compared to chloride which is only one large atom. Moreover, bent and linear conformations of azide units also have an influence on the decreasing  $T_g$ . Therefore, azidated Hydrin polymers have higher chain mobility and flexibility resulting in enhanced gas diffusivity and permeability. The gas selectivities of modified Hydrin homopolymers decreased except for CO<sub>2</sub>/H<sub>2</sub>. In the case of

modified Hydrin copolymer the gas selectivities were maintained with the effect of CO<sub>2</sub>-philic PEG blocks. After UV cross-linking significantly increased CO<sub>2</sub>/CH<sub>4</sub> and H<sub>2</sub>/N<sub>2</sub> selectivities and decreased CO<sub>2</sub> and H<sub>2</sub> permeabilities were observed. The study also examined the detailed thermal properties of initial and resulting polymers. The thermal stability of modified polymers was diminished compared to initial hydrin polymers related to early decomposition of newly introduced energetic azide side groups. A-H-Hydrin had two weight loss steps associated with azide pendent group decomposition which is the starting point of thermal generation of nitrene radicals and polyether main chain decomposition. On contrary, A-C-Hydrin showed one weight loss step which indicates simultaneous decomposition of azide pendent groups and polyether main chain of the polymer. UV-cross-linked Hydrin polymers had higher char-yields compared to initial and azidated Hydrin polymers pointing out improved thermal stability at high temperatures.

Besides of chemical modification methods, step-growth click coupling reaction was performed to obtain PEG containing polymers for CO<sub>2</sub> separation. The step-growth process is based on the copper(I)-catalyzed azide alkyne cycloaddition (CuAAC) reaction. With different reaction times and monomers, various polymers were synthesized and characterized by <sup>1</sup>H-NMR, <sup>13</sup>C-NMR, FT-IR, GPC, DSC and TGA. Although, there are several types of polycondensation reactions to synthesize the polymers for gas separation, step-growth click coupling reaction applied the first time for this purpose. Step-growth click coupling reaction is a polyaddition which monomers react without the elimination of small molecules. However, mostly commercial PEG-containing polymers for CO<sub>2</sub> separation such as Pebax<sup>®</sup> and Polyactive<sup>®</sup> are synthesized by different polycondensation methods that monomers react with the elimination of small molecules requiring additional purification step. Therefore, step-growth click coupling reaction can be a distinctive route to synthesis PEG-containing polymers for CO<sub>2</sub> separation. The strategy adopted in this study

appears to be entirely satisfactory in terms of efficiency and simplicity. The resulting step-growth polymer exhibited low permeabilities due to its high glass transition temperature leading to low chain mobility and flexibility. On the other hand, it had high gas selectivities with the effect of CO<sub>2</sub>-philic groups such as PEG, triazole and benzoxazine resulting in good CO<sub>2</sub> solubility compared to other gases. The low gas permeabilities can be improved to increase the composition of PEG units in the polymer. Additionally, the thermal stability of the step-growth polymers was studied. The amount of composition of the PEG and triazole units in polymers was the most important parameter for thermal stability. Increasing amount of the PEG units decreases the amount of highly thermal stable triazole groups in polymer resulting in lowering of thermal stability. Moreover, the benzoxazine ring gave better thermal stability to the polymer at high temperatures owing to curing property resulting in high char-yield. Cured benzoxazine monomer had the highest thermal properties due to the high amount of benzoxazine rings and cross-linking density.

## **5.2 Zusammenfassung und Ausblick**

Die gezielte Trennung von Gasen in technischen Prozessen oder zur CO<sub>2</sub>-Abtrennung ist eine bedeutende Herausforderung der heutigen Zeit. In diesem Zusammenhang zeigen Polymermembranen ein hohes Potential zur energieeffizienten Gastrennung.

Die Motivation der vorliegenden Arbeit war insbesondere die Verbesserung der Gastransporteigenschaften von ausgewählten Polymeren mit unterschiedlichen chemischen Modifizierungsverfahren. Weiterhin sollten neuen Poly (Ethylenglycol) (PEG) haltige Polymere über eine auf einer Klick-Kupplungsreaktion basierenden Stufenwachstumspolymerisation (Polyaddition) synthetisiert werden. Im Weiteren sollte das Potential der Polymere in der effizienten CO<sub>2</sub>-Abtrennung ausgemacht werden.

Die chemischen Modifikation des Polyisoprenblocks von Poly(Isopren)-block-poly (Vinyltrimethylsilan) (PI-*b*-PVTMS)-Blockcopolymeren erfolgte mittels Hydrosilylierung (Hs-PI-*b*-PVTMS) und Hydrierung-Reaktionen (H-PI-*b*-PVTMS). Das Ziel der Modifizierung war die Änderung der thermodynamischen Wechselwirkungen zwischen den Blöcken. Auf diesem Weg sollte die Morphologie der Polymere verändert werden, die wiederum direkt mit den Gastransporteigenschaften der Membran verbunden sind. Die Bulkmorphologien der Blockcopolymere PI-*b*-PVTMS und Hs-PI-*b*-PVTMS wurden mittels Transmissionelektronenmikroskop-Aufnahmen (TEM) untersucht. PI-*b*-PVTMS im Bulk wies eine starke Mikrophasenseparation zwischen dem amorphen Polyisopren- und flüssigkristallinen PVTMS-block auf, welche zu einer lamellaren Struktur führt. Hierdurch wird die Permeation durch kontinuierliche Schichten aus Polyisopren signifikant behindert. Hs-PI-*b*-PVTMS Polymer zeigte keine Mikrophasenseparation im Bulk. Die aus den modifizierten Blockcopolymeren hergestellten Membranen zeigten im Vergleich zu PVTMS-ref. einen deutlichen Anstieg der O<sub>2</sub>- und H<sub>2</sub>-Permeabilitäten bei Erreichen der gleichen Selektivität. Die Verbesserung der Gastransporteigenschaften konnte neben der morphologischen Änderung der modifizierten Blockcopolymermembranen auf das zunehmende Freivolumen (FFV) zurückgeführt werden. Dieses ist einer der wichtigsten Parameter für die Gastransporteigenschaften von Polymermembranen. Membranen der hydrosilylierten Blockcopolymere zeigten die höchste Zunahme des FFV. Dies kann auf die sperrigen und symmetrischen Triethylsilyl-Gruppen an der Hauptkette des Polyisopren-Blocks zurückgeführt werden. Die thermische Stabilität der modifizierten Blockcopolymeren wurde durch thermogravimetrische Analyse (TGA) untersucht und mit PI-*b*-PVTMS verglichen. Die modifizierten Blockcopolymere wiesen aufgrund der

Sättigung der Doppelbindungen von Polyisopren eine bessere thermische Stabilität als PI-*b*-PVTMS auf.

Die chemischen Modifizierung von Poly (epichlorhydrin)-Homopolymer (H-Hydrin) und Poly (ethylenoxid-*co*-epichlorhydrin)-Copolymer (C-Hydrin) erfolgte mittels Azidierungsreaktionen. Die Polymere (AH-Hydrin-und AC-Hydrin) wurden über eine UV-induzierte Nitren-Reaktion quervernetzt. Das Ziel dieser Studie war die Untersuchung der Wirkung von Azidierung und UV-Vernetzung von H- und C-Hydrin auf die Gastransporteigenschaften der Polymermembranen. Die Modifizierung erfolgte mit Azid-Ionen und verlief über das substituierte Chlorid in der Seitengruppe von Poly (Epichlorhydrin). UV initiiert die Zersetzung des Azids in den Seitengruppen der Polymere was zur Erzeugung von hochreaktiven Nitrenradikalen führt und ermöglicht somit die Selbstvernetzung ohne zusätzliche Vernetzungsmittel. Azidierte Hydrin Polymere zeigten eine Abnahme der Glasübergangstemperatur ( $T_g$ ). Dies basiert auf der Zunahme der Länge der Seitengruppe im Falle der azidierten Polymeren im Vergleich zu Chlorid. Darüber hinaus hat auch die Konformationen der Azideinheiten einen Einfluss auf die Abnahme des  $T_g$ . Hierbei zeigt sich für azidierte Hydrin Polymere mit einer höheren Kettenmobilität und -flexibilität eine erhöhte Gasdiffusion und Durchlässigkeit. Die Gasselektivitäten von modifizierten Homopolymer Hydrin verringert außerdem noch die Selektivität für  $\text{CO}_2/\text{H}_2$ . Im Fall von modifizierten Hydrin-Copolymer wurden die Gasselektivitäten mit  $\text{CO}_2$ -philen PEO-Blöcken erhalten. Nach der UV-Vernetzung wurde die Selektivität für  $\text{CO}_2/\text{CH}_4$  und  $\text{H}_2/\text{N}_2$  deutlich erhöht und verringerte  $\text{CO}_2$ - und  $\text{H}_2$ -Pemeabilitäten beobachtet. Weiterhin wurden in dieser Studie ebenfalls die thermischen Eigenschaften der unfunktionalisierten und der funktionalisierten Polymere detailliert untersucht. Das unfunktionalisierte gummiartige Hydrin Polymer zersetzt sich früh. Durch die Einführung der Azid-Seitengruppen konnte die thermische Stabilität erhöht

werden. A-H-Hydrin zeigte in TGA-Untersuchungen zwei Gewichtsverluste. Diese hängen mit der Zersetzung der Azidseitengruppe zusammen, welche durch die thermischen Erzeugung von Nitrinradikalen resultiert. Auch AC-Hydrin zeigte in TGA-Untersuchungen eine Gewichtsabnahme. Dieser zeigt die gleichzeitige Zersetzung des Azids und Polyether-Seitengruppen der Hauptkette des Polymers. UV-vernetzte Hydrin Polymere hatten höhere char- Erträge im Vergleich zum unvernetztem Polymer. Dies ist ein Hinweis auf verbesserte thermische Stabilität bei hohen Temperaturen.

Neben chemischen Modifizierungen wurde eine Stufenwachstums-Klick-Kupplungsreaktion durchgeführt, um PEG-haltige Polymere für den Einsatz als Membranmaterial zur CO<sub>2</sub>-Abscheidung zu erhalten. Der Stufenwachstumsmechanismus basiert auf einer Kupfer(I)-katalysierten Azid-Alkin-Cycloaddition (CuAAC). Auf Basis von unterschiedlichen Reaktionszeiten und der Verwendung verschiedener Monomeren als Edukte konnten verschiedene Polymere erfolgreich synthetisiert werden. Die Charakterisierung der Polymere erfolgte mittels <sup>1</sup>H-NMR, <sup>13</sup>C-NMR, FT-IR, GPC, DSC und TGA. Auf diese Weise konnte erstmals eine Stufenwachstums-Klick-Kupplungsreaktion zur Synthese von Polymeren für die Verwendung als Membranmaterial zur Gastrennung verwendet werden. Bei der Klick-Kupplungsreaktion handelt es sich um eine Polyaddition, bei der Monomere ohne den Austritt von kleinen Molekülen reagieren. In der Synthese der meisten kommerziellen PEG-haltigen Polymere die in der CO<sub>2</sub>-Abtrennung Anwendung finden, wie z.B. Pebax<sup>®</sup> und Polyactive<sup>™</sup>, erfolgt die Reaktion der Monomere unter Abspaltung kleiner Moleküle. Hierdurch ist eine zusätzliche Reinigung des Produktes erforderlich. Daher ermöglicht die Stufenwachstums-Klick-Kupplungsreaktion einen neuartiger und verbesserten Weg zur Sythese von PEG-haltige Polymeren. Die in dieser Studie gewählte Strategie kombiniert Effizienz und Simplizität.

Die Membranen, die aus den erzeugten Stufenwachstumspolymeren hergestellt wurden, zeigten geringe Gasdurchlässigkeiten aufgrund ihrer hohen Glasübergangstemperatur, die zu einer geringen Mobilität und Flexibilität der Polymerkette führt. Auf der anderen Seite wiesen die neuen Polymere hohe Gasselektivitäten auf, die auf die CO<sub>2</sub>-philen Gruppen wie PEG, Triazol und Benzoxazin zurückgeführt werden. Dies führt zu einer guten Löslichkeit von CO<sub>2</sub> im Membranmaterial im Vergleich zu anderen Gasen. Die Gasdurchlässigkeiten konnten verbessert werden durch Erhöhung des Anteils an PEG-Einheiten. Weiterhin wurde die thermische Stabilität der Stufenwachstumspolymere untersucht. Hierbei ist die Zusammensetzung von PEG- und Triazol-Einheiten im Polymer der bedeutenste Parameter für die thermische Stabilität. Mit zunehmender Menge der PEG-Einheiten nimmt die Menge der thermisch hochstabilen Triazol-Gruppen im Polymer ab. Dies führt zu einer Verringerung der thermischen Stabilität des Polymers. Außerdem konnte durch den Einsatz des Benzoxazinmonomers eine bessere thermische Stabilität des resultierenden Polymers erreicht werden.



## Acknowledgement

First of all, I would like to thank Prof. Dr. Volker Abetz for giving me the opportunity to carry out my PhD work in his group. I am deeply indebted to him for his kind guidance, valuable criticism, support, understanding and help in all possible ways throughout this work. He has always been quite friendly and kind during the discussions.

I express my thanks to Dr. Volkan Filiz, Head of PMS department, for his guidance and support during the work.

I would like to thank Dr. Sergey Shishatskiy for his valuable comments and help during gas separation measurements, Dr. Sofia Rangou for kind support during the synthesis of the polymers, Silvio Neumann for helpful discussions on DSC and TGA results, Clarissa Abetz for TEM analysis, Maren Brinkmann for GPC analysis and all the past and present members of the group for their help, friendship and nice environment. Particularly, Dr. Shahid Majeed (Mario, my former office mate for 2 years), Dr. Rakibul Kabir (my first office mate for 1 year), Dr. Gisela Bengtson, Brigitte Lademann, Jan Wind, Muntazim Munir Khan, Md. Mushfequr Rahman, Dr. Propokios Georgopanos, Silke Dargel, Dr. Markus Gallei, Dr. Juliana Clodt, Damla Keskin, Dr. Adina Jung, Janina Hahn, Judith Grünauer, Petra Merten, Dirk Lüdke, Dr. Thomas Emmmler, Hong Xie, Dr. Bing Du, Ivonne Ternes, Dr. Alberto Tena, Heiko Notzke, Jan Pohlmann, Wiebke Junior, Dr. Shahin Homaeigohar, Dr. Maryam Radjabian, Carsten Scholles and Ilona Zillich for being helpful coworkers.

I also would like to thank my friends in the institute of coastal research: Dr. Monika Barcikowska, Dr. Hasan Örek and Nusret Sevinc for their support outside.

I wish to express my warm thanks to my best friend Hakan Bildirir (Duke).

I am deeply grateful to my mother Gürsel Gacal, my father Adnan Gacal and the deepest color of my life, my sister, Burçin Gacal for their endless love, care, faith, support and understanding throughout my life.

Finally, I would like to dedicate this thesis to my sister, Burçin Gacal, my mother Gürsel Gacal and my father Adnan Gacal.

## Appendix

### Toxicity of Chemicals

In the following Table, all used chemicals with H- and P-data are given.

Substances	GHS Symbol	Hazard Statements	Precautionary Statements
p-Toluenesulfonyl hydrazide	GHS02, GHS06	H242-H301-H319	P301 + P310-P305 + P351 + P338
Tris(triphenylphosphine)rhodium(I) chloride	–	–	–
Triethylsilane	GHS02	H225-H412	P210-P273
Toluene	GHS02, GHS07, GHS08	H225-H304-H315-H336-H361d-H373	P210-P261-P281-P301 + P310-P331
Ethanol	GHS02, GHS07, GHS08	H225-H302-H371	P210-P260
o-Xylene	GHS02, GHS07	H226-H312-H315-H332	P280
Poly(epichlorohydrin)	–	–	–
Poly[(ethylene oxide)- <i>ran</i> -(epichlorohydrin)]	–	–	–
Sodium azide	GHS06, GHS09	H300-H410	P264-P273-P301 + P310-P501

Tetrabutylammonium iodide	GHS07	H302-H315-H319-H335	P261-P305 + P351 + P338
<i>N,N</i> -Dimethylformamide	GHS02, GHS07, GHS08	H226-H312 + H332-H319-H360D	P201-P280-P305 + P351 + P338-P308 + P313
Poly(ethylene glycol)	–	–	–
Methanesulfonyl chloride	GHS05, GHS06	H300 + H310 + H330-H314-H335	P260-P264-P280-P284-P301 + P310-P302 + P350
Dichloromethane	GHS07, GHS08	H315-H319-H335-H336-H351-H373	P261-P281-P305 + P351 + P338
Magnesium sulfate	–	–	–
Triethylamine	GHS02, GHS05, GHS07	H225-H302-H312-H314-H332	P210-P280-P305 + P351 + P338-P310
Hydrochloric acid	GHS05, GHS07	H314-H335	P261-P280-P305 + P351 + P338-P310
Sodium hydroxide	GHS05	H314	P280-P305 + P351 + P338-P310
Sodium chloride	–	–	–
1,4-Diethynylbenzene	GHS07	H317	P280
Copper(I) bromide	GHS07	H315-H319-H335	P261-P305 + P351 + P338
4-Ethynylaniline	GHS07	H315-H319-H335	P261-P305 + P351 + P338
Bisphenol A	GHS05, GHS07, GHS08	H317-H318-H361	P280-P305 + P351 + P338
<i>N,N,N',N'',N'''</i> -Pentamethyldiethylenetriamine	GHS05, GHS06	H302-H311-H314	P280-P305 + P351 + P338-P310
Paraformaldehyde	GHS02, GHS05, GHS07, GHS08	H228-H302 + H332-H315-H317-H318-H335-H351	P210-P261-P280-P305 + P351 + P338
Xylenes	GHS02, GHS07	H226-H312-H315-H332	P280

Tetrahydrofuran	–	–	–
Diethyl ether	GHS02, GHS07	H224-H302-H336	P210-P261

## List of Publications

1. **Gacal, B. N.**, Koz, B., Gacal, B., Kiskan, B., Erdogan, M., Yagci, Y., "Pyrene Functional Poly(vinyl alcohol) by "Click" Chemistry", Journal of Polymer Science Part A: Polymer Chemistry, **2009**, 47, 5, 1317-1326.
2. Odaci, D., **Gacal, B. N.**, Gacal, B., Timur, S., Yagci, Y., "Fluorescence Sensing of Glucose Using Glucose Oxidase Modified by PVA-Pyrene Prepared via "Click" Chemistry" Biomacromolecules, **2009**, 10, 2928-2934.
3. Karagoz, B., Durmaz, Y. Y., **Gacal, B. N.**, Bıcak, N., Yagci, Y., "Functionalization of Poly(divinylbenzene) Microspheres by Click Chemistry", Designed Mon. & Polm., **2009**, 12, 511-522.
4. Medine, E. I., Odaci, D., **Gacal B. N.**, Gacal, B., Sakarya, S., Unak P., Timur, S., Yagci. Y., "Anti-Metadherin Targeted PVA-Pyrene Prepared by "Click Chemistry": A New Approach for *in vitro* Imaging of Breast Cancer Cells", Macromolecular Bioscience, **2010**, 10, 657-663.
5. Ervithayasuporn, V., Wang, X., Gacal, B., **Gacal, B. N.**, Yagci, Y., Kawakami, Y., "Formation of trimethylsilylated open-cage oligomeric azidophenyl silsesquioxanes", Journal of Organometallic Chemistry, **2011**, 696, 2193-2198.
6. **Gacal, B. N.**, Shishatskiy, S., Rangou, S., Neumann S., Filiz, V., Abetz V., "Modification of polyisoprene-*block*-poly(vinyl trimethylsilane) block copolymers via hydrosilylation and hydrogenation, and their gas transport properties", Journal of Polymer Science Part B: Polymer Physics, **2013**, 51, 1252-1261.
7. Khan, M. M., Bengtson, G., Shishatskiy, S., **Gacal, B. N.**, Rahman, M. M., Neumann, S., Filiz, V., Abetz, V., "Cross-linking of Polymer of Intrinsic Microporosity (PIM-1) via nitrene reaction and its effect on gas transport property", European Polymer Journal, **2013**, 49, 4157-4166.

8. **Gacal, B. N.**, Filiz, V., Shishatskiy, S., Neumann S., Wind, J., Abetz V., “Effect of azidation and UV cross-linking of poly(epichlorohydrin) and poly[(ethylene oxide)-*ran*-(epichlorohydrin)] on gas transport properties”, Journal of Membrane Science, **2014**, 467, 126-135.
9. Rahman M. M., Filiz V., Khan M. M., **Gacal B. N.**, Abetz V., “Functionalization of POSS nanoparticles and fabrication of block copolymer nanocomposite membranes for CO<sub>2</sub> separation”, Reactive and Functional Polymer, DOI: 10.1016/j.reactfunctpolym.2014.07.006.

## Curriculum Vitae

Ph. D. in Polymer Synthesis For Membrane Technology, Helmholtz-

**2009 - present** Zentrum Geesthacht.

Research Area: ‘Modification of Polyisoprene-*block*-PVTMS Block Copolymers and Epichlorohydrin Based Homo and Random Copolymers via Hydrosilylation, Hydrogenation, Epoxidation and Azidation, and Their Gas Transport Properties; To Synthesize High Molecular Weight PEG Main-Chain Polymers and Poly(Ionic Liquid)s via Step-Growth Click Chemistry and Their Gas Transport Properties ’, Advisor: Prof. Dr. Volker Abetz.

**2008 - 2009** M.Sc. in Organic Chemistry, Istanbul Technical University.

Final Year Project: ‘Functional Poly(Vinyl Alcohol) as Precursor for Bioapplications’, Advisor: Prof. Dr. Yusuf Yağcı.

**2004 - 2008** B.Sc. in Chemistry, Istanbul Technical University

Final Year Project: ‘Pyrene Functional Poly(vinyl alcohol) by

“Click Chemistry”, Advisor: Prof. Dr. Yusuf YAĞCI

**1998 - 2003** High School, Istanbul Lisesi, Turkey

### **Meetings Attended**

1. Participant at 1st. Polymeric Composite, November 2006, Izmir, Turkey.
2. Poster Presentation at 21st. National Chemistry Conference, August 2007, Malatya, Turkey.
3. Participant at 4th National Nanoscience and Nanotechnology Conference, June 2008, Istanbul, Turkey.
4. Poster Presentation at 8th International Conference on Advanced Polymers via Macromolecular Engineering, October 2009, Dresden, Germany.
5. Poster Presentation at the International Congress on Membranes and Membrane Processes (ICOM), July 2011, Amsterdam, The Netherlands.
6. Poster Presentation at the European Polymer Congress, June 16-21, Pisa, Italy.
7. Oral Presentation at the European Polymer Congress, June 16-21, Pisa, Italy.